SANDIA REPORT
SAND2019-15428

Printed

Sandia National Laboratories

Advanced WEC Dynamics and Controls MASK3 Test

Ryan G. Coe, Giorgio Bacelli, Steven J. Spencer, Dominic Forbush, Kevin Dullea

Prepared by
Sandia National Laboratories
Albuquerque, New Mexico 87185
Livermore, California 94550

Issued by Sandia National Laboratories, operated for the United States Department of Energy by National Technology & Engineering Solutions of Sandia, LLC.

Printed in the United States of America. This report has been reproduced directly from the best available copy.

Available to DOE and DOE contractors from

U.S. Department of Energy
Office of Scientific and Technical Information
P.O. Box 62
Oak Ridge, TN 37831

Telephone:	(865) 576-8401
Facsimile:	(865) 576-5728
E-Mail:	reports@osti.gov
Online ordering:	http://www.osti.gov/scitech

Available to the public from

U.S. Department of Commerce
National Technical Information Service
5301 Shawnee Road
Alexandria, VA 22312

Telephone:	(800) 553-6847
Facsimile:	(703) 605-6900
E-Mail:	orders@ntis.gov
Online order:	https://classic.ntis.gov/help/order-methods

ABSTRACT

This report outlines the “MASK3” wave tank test within the Advanced WEC Dynamics and Controls (AWDC) project. This test represents the final test in the AWDC project. The focus of the MASK3 test was to consider coordinated 3-degree-of-freedom (3DOF) control of a WEC in a realistic ocean environment. A key aspect of this test was the inclusion of a “self-tuning” mechanism which uses an optimization algorithm to update controller gains based on a changing sea state. The successful implementation of the self-tuning mechanism is the last crucial step required for such a controller to be implemented in real ocean environments.

CONTENTS

LIST OF FIGURES

LIST OF TABLES

NOMENCLATURE

Abbreviation	Definition
AC	alternating current
DC	direct current
DOE	Department of Energy
DOF	degree of freedom
CDIP	Coastal Data Information Program
NSWCCD	Naval Surface Warfare Center Carderock Division
MASK	Maneuvering and Sea Keeping Basin
MIMO	multi-input multi-output
PTO	power take-off
PI	proportional, integral
SID	system identification
WEC	wave energy converter
WETS	Wave Energy Test Site

1. INTRODUCTION

Sandia National Laboratories and the Department of Energy (DOE) have completed on a multi-year program to examine the effects of control theory on increasing power produced by resonant wave energy conversion (WEC) devices. The tank tests have been conducted at the Naval Surface Warfare Center Carderock Division (NSWCCD) Maneuvering and Sea Keeping Basin (MASK) in West Bethesda, MD. The tests within this effort and their respective focuses are shown in Table 1-1 [8].

This report presents the results from the "MASK3" test. Expanding on the goals of the MASK3 test, these are as follows:

- **Predictionless control** - Further assess the ability of predictionless controllers to provide comparable performance to optimal WEC control
  - **Self-tuning control** - Test the ability to create a self-tuning feedback controller based on estimates of incoming waves during changing sea states
  - **Real sea states** - Test both idealized spectra and waves recorded in the ocean to determine whether any factors important to WEC control performance are not captured by realizations from idealized spectra
  - **Bimodal sea states** - Test controller performance in both idealized and real bimodal sea states
  - **Wave groupyness** - Assess the extent to which wave groupyness affects WEC dynamics and controller performance
- **Mechanical power vs. electrical power** - Better understand the differences between controller design for mechanical power vs. electrical power
- **Multi-input, multi-output control** - Model the WaveBot as a multi-input, multi-output (MIMO) system, design controllers for the coupled system, and assess their performance
- **Secondary goals**
  - **Focused waves** - Perform experiments and collect data in focused waves to support future high-fidelity modeling work.

Table 1-1. MASK testing phases.

MASK1	MASK2A	MASK2B	MASK3
1DOF SID [7, 2, 1, 4]	Study/verification of basic 1DOF closed-loop performance [3]	1DOF control [8] & 3DOF SID	Autonomous (self-tuning) 1DOF & 3DOF control

Parameter	Value
Displaced volume, $\forall$ [m^3]	0.858
Water density, ρ [kg/m^3]	1000
Inertia, heave [kg]	858
Inertia, surge [kg]	1420
Inertia, pitch [kg m^2]	84

$$m_{RB} = \begin{bmatrix} 1420 & & & & & \\ & NaN & & & & \\ & & 858 & & & \\ & & & NaN & & \\ & & & & 84 & \\ & & & & & NaN \end{bmatrix}$$

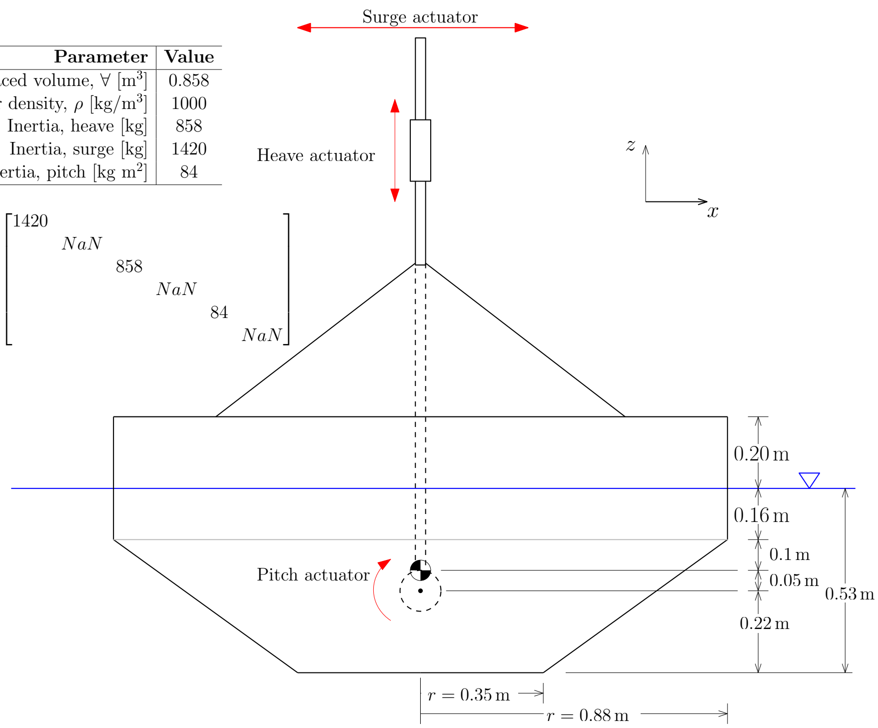

Figure 1-1. Test device diagram.

– **Statistically significant experiments** - Perform experiments with long non-repeating waves to support future fatigue and extreme response work.

This report provides an overview of testing and a high-level summary of results. Additionally, this report provides guidance to using the open-source dataset, available on `https://mhkdr.openei.org`.

1.1. EXPERIMENTAL SET UP

The "MASK3" test builds lessons learned from the the first two tests in this series [7, 8] and generally makes use of the same hardware and test procedures.

All data acquisition and hardware are the same as used in previous tests of this series, as described in [8]. Figure 1-1 shows a diagram of the "WaveBot" device tested. Table 1-2 provides important device parameters. Wave probe locations within the basin are shown in Figure 1-2. For calibration tests, in which the WaveBot was not present, Figure 1-3 shows the locations of wave probes near the average location of the device. A more complete summary of data acquisition, hardware, and the open-source dataset is provided in [6].

Table 1-2. Model-scale WEC physical parameters.

Parameter	Value
Surge rigid-body inertia, m_1 [kg]	1420
Heave rigid-body inertia, m_3 [kg]	893
Pitch rigid-body inertia, m_5 [kg m^2]	84
Displaced volume, $\forall$ [m^3]	0.858
Float radius, r [m]	0.88
Float draft, T [m]	0.53
Water density, ρ [kg/m^3]	1000
Water depth, h [m]	6.1
Linear hydrostatic stiffness, G [kN/m]	23.9
Infinite-frequency added mass, A_∞ [kg]	822
Max vertical travel, $\lvert z_{\text{max}}\rvert$ [m]	0.6

1.2. WAVE CASES

A number of wave types were used to create experimental tests. These cases are summarized in the subsequent sections. A summary listing of wave cases is presented in Table 1-3 in Appendix B. Unless otherwise noted, all waves propagate at an angle of 70° (as shown by the arrow in Figure 1-2). A complete description of the different wave cases considered in provided in Appendix B. The naming convention for JONSWAP and regular waves with the parametric is factors shown in Table 1-3.

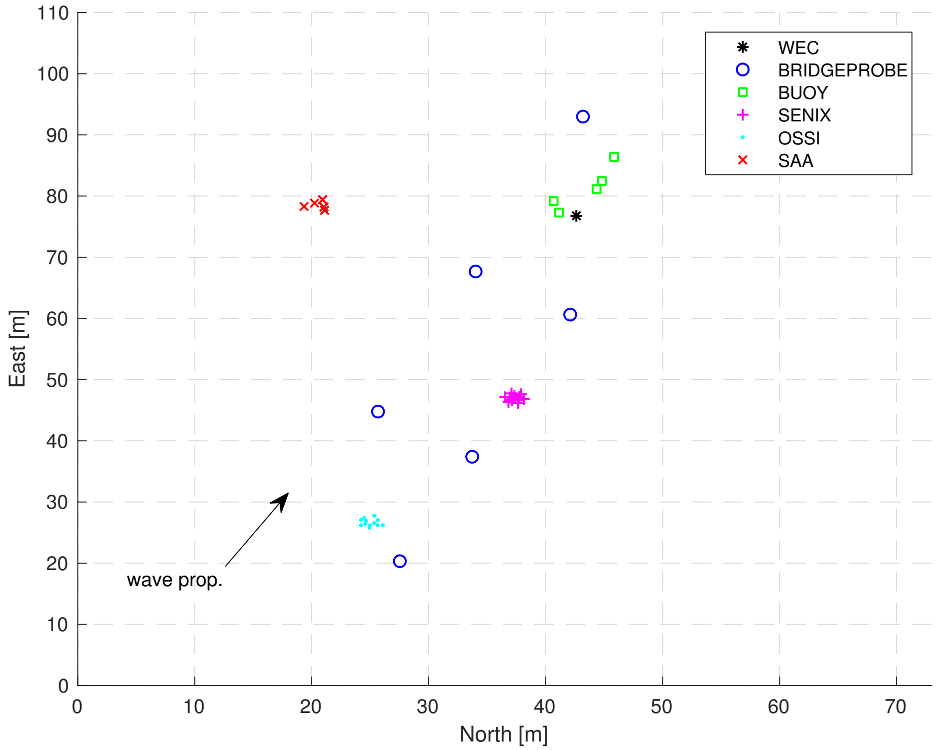

Figure 1-2. Wave basin layout. See [8] for complete listing.

Table 1-3. Wave cases considered.

ID	Peak period, T_p [s]	Sig. wave height, H_s [m]	Peak factor, γ []
1	1.58	0.127	1
2	1.58	0.127	3.3
3	2.5	0.127	1
4	2.5	0.127	3.3
5	2.5	0.254	1
6	2.5	0.254	3.3
7	3.5	0.127	1
8	3.5	0.127	3.3
9	3.5	0.254	1
10	3.5	0.254	3.3
11	3.5	0.381	3.3
12	2.5	0.381	3.3
13	1.58	0.254	3.3

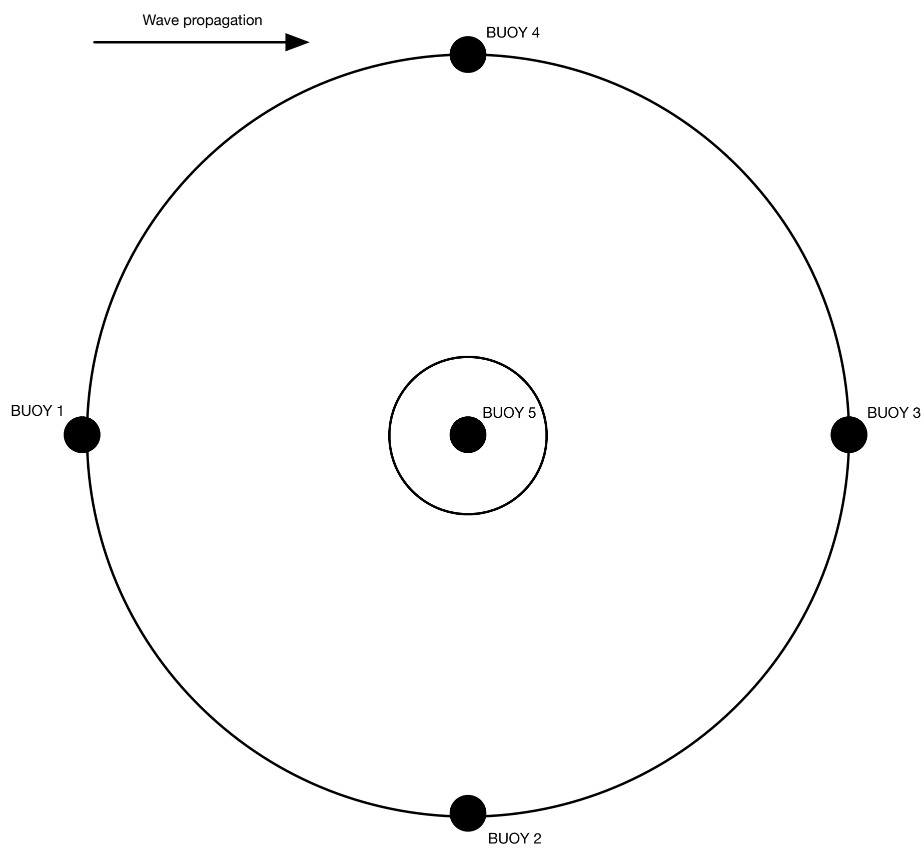

Figure 1-3. Layout of wave probes at WEC location. The probes BUOY02, BUOY04, and BUOY05 are all in line with the center of the WEC with respect to the wave front. BUOY05 is located close to the center of the WEC.

2. CONTROL SYSTEM DESIGN

2.1. CONTROLLER DESIGN

This section describes the control system design for the maximization of the electrical power absorbed by the device using a "model-based design" approach, which involves three main steps:

- Definition of the objective
- Derivation of a reduced order model of the system for control design
- Synthesis of the control system

The WaveBot device is capable of being independently actuated in 3 degrees of freedom, namely: heave, surge and pitch. Each degree of freedom is controlled through by a rotary motor/generator, which applies a force to the buoy by means of a belt transmission system for heave and surge, and by means of a drive shaft and gearhead for pitch (full detailed description is provided in [8]). The objective is to design a control system that maximizes the overall electrical power generated by the device is all three degrees of freedom, which is equal to the sum of the power dissipated on the three electrical loads Z_L^h, Z_L^s and Z_L^p, as illustrated in Figure 2-1.

In order to design a controller that can take into account the entire dynamics of the device (including efficiency), it is necessary to derive a coupled model that includes the hydrodynamic, mechanic and electrical systems. Models used for controller synthesis are known as "controller models". These models are generally simplified models of the system, hence the term "reduced order models" that is generally used in the literature, which still retain a good trade-off between accuracy and complexity.

A convenient approach to formulate a controller model for WECs is to abstract the problem and consider multi-port circuit theory, which allows a unified description of the multi-physics problem using impedance and admittance matrices. Since the problem of maximizing the absorbed power for a WEC is

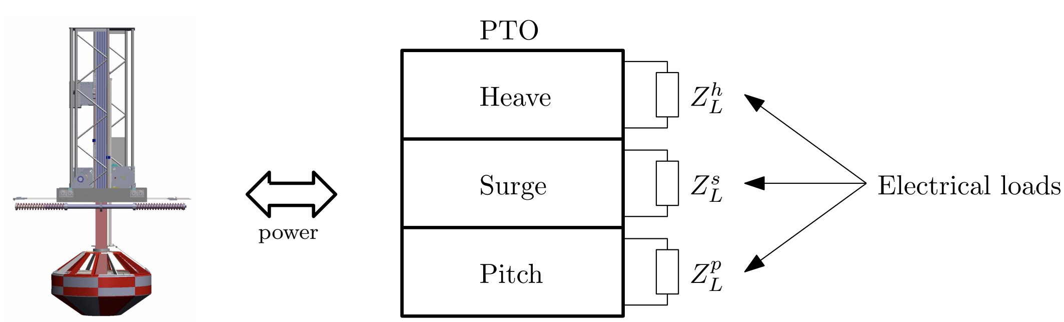

Figure 2-1. Caption here

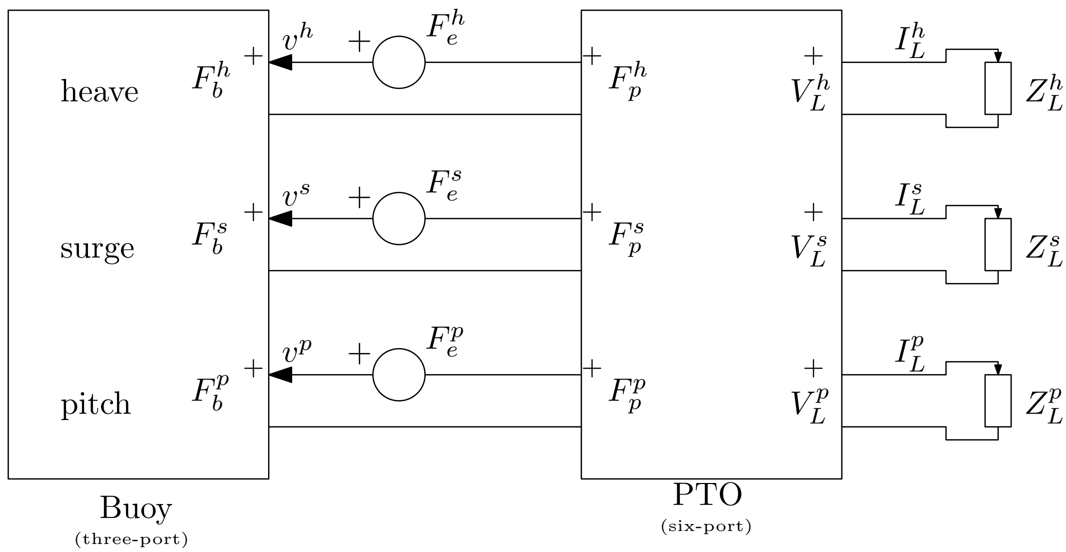

Figure 2-2. Multi-Port representation on the WaveBot

essentially an impedance matching problem, the availability of a controller model in this form is convenient for control design.

By using this formulation, the WaveBot device can be described in terms of two multi-ports as illustrated in Figure 2-2: a three-port block describing the hydro-mechanical part (wave-body interaction and drive-train) and a six-port describing the generator.

The three-port block describing the hydro-mechanical response of the device is the classical well known impedance/admittance model, where the quantities on the input ports are the forces and velocities in the three degrees of freedom. The generators F_e^h, F_e^s and F_e^p describe the wave excitation forces. The six-port block that describes the PTO has forces and velocities on the three ports on the left-hand-side connected to the buoy, whereas the quantities on the right-hand-side ports are voltage and current on the DC bus output of each motor drive.

The intrinsic impedance model Z_i of the three coupled three degrees-of-freedom device is obtained by means of system identification, using the multiple experiment approach for the identification of MIMO systems described in [9]. For each experiment, the device has been excited using multisine, with same magnitude but with different phase realizations for each degree of freedom. In general, for an N degree of freedom system, at least N experiments are required for the identification. The Bode plot of the resulting impedance Z_i is shown in Figure 2-3.

Since each degree of freedom has an independent PTO, the coupling between different degrees of freedom is only occurring through the intrinsic impedance Z_i. Therefore, the six-port model for the PTO becomes diagonal, and each block can be described by a two-port. Additionally, all the PTOs have the same generator, motor drive and electrical load, therefore the tow-port models are identical. In particular, the two-port model for the i-th degree-of-freedom between the motor force/velocity and quadrature voltage/current, in transmission form, is:

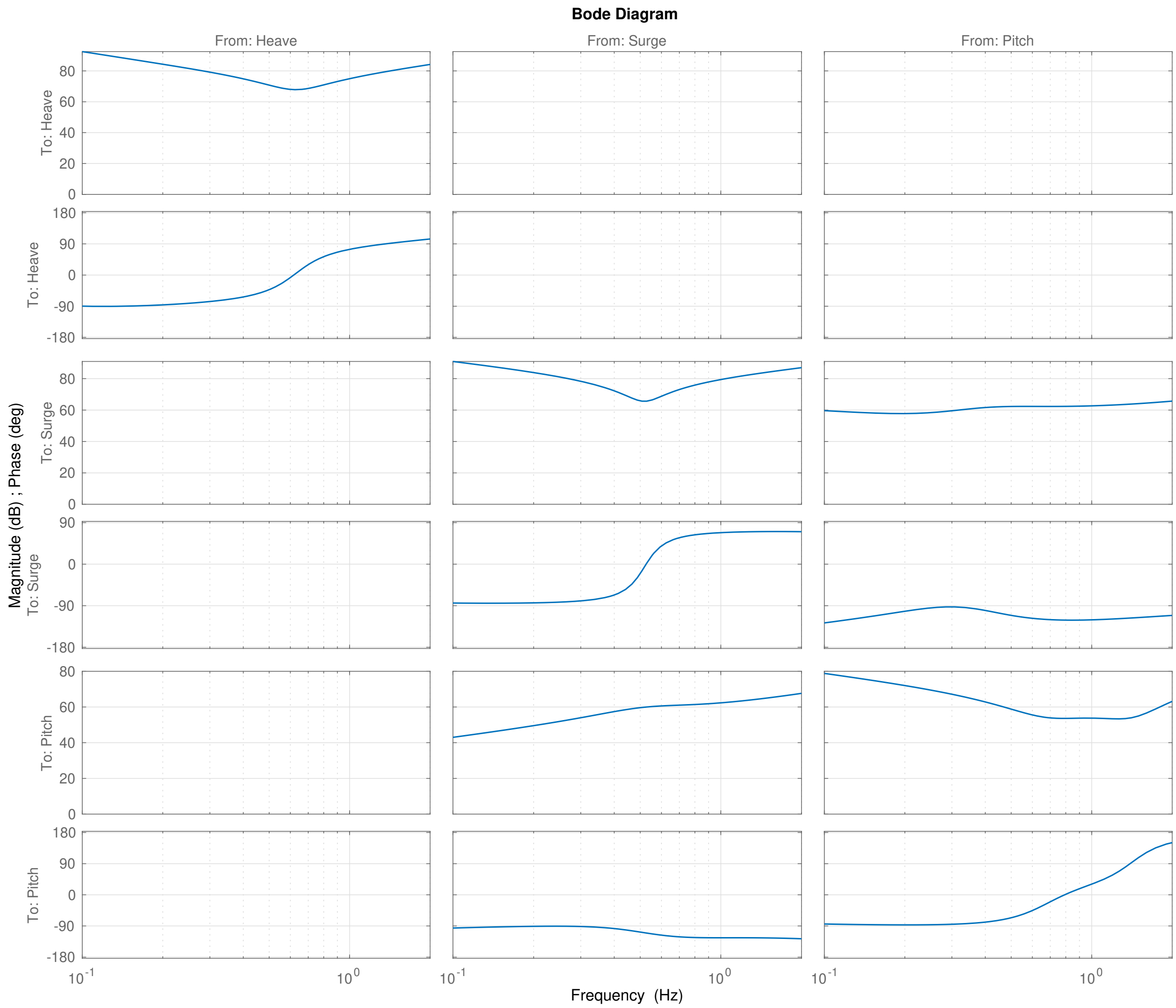

Figure 2-3. Multi-input, multi-output (MIMO) impedance system for WaveBot.

$$\begin{bmatrix} I_q^i \\ V_q^i \end{bmatrix} = \begin{bmatrix} 0 & k_t^i N^i)^{-1} \\ k_e^i N^i & R(k_t^i N^i)^{-1} \end{bmatrix} \begin{bmatrix} v^i \\ F_p^i \end{bmatrix}, \tag{2.1}$$

where the parameters K_t^i, K_e^i, N^i and R are defined in Table 2-1.

It should be noted that the variables describing the electrical quantities on the output ports of the PTO in eq. (2.1) are the quadrature current I_q^i and the quadrature voltage V_q^i, instead of the load voltage and current, V_L^i and I_L^i, respectively. The reason is that the problem of designing a controller that maximizes the electrical power dissipated on the loads Z_l^i can be further simplified by considering that the maximum power transferred to the load occurs when the controller also maximizes the power on the q-axis is also being maximized. This can be seen by considering the simplified model for the motor drive and the equivalent circuit for q-axis of the generator described in Figure 2-4. In particular, the generator drive is

Table 2-1. WaveBot drivetrain motor parameters

Parameter	Heave	Surge	Pitch
Gear ratio, N	12.4666	12.4666	3
Torque constant, k_τ [Nm/A]	6.1745	6.1745	6.1745
Electrical constant, k_e [Vs/rad]	4.116	4.116	4.116
Winding resistance, R [Ω]	0.5	0.5	0.5

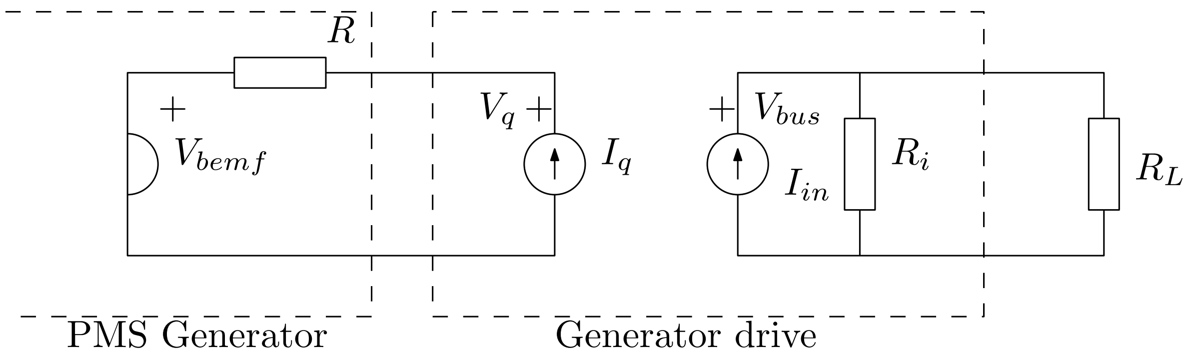

Figure 2-4. Simplified diagram of the generator and motor drive

being modeled with a Norton equivalent circuit, where the losses are described by the resistor R_i. The input power to the drive from the generator on the q-axis

$$P_{in} = \frac{3}{2} V_q I_q, \tag{2.2}$$

while the dissipated power is

$$P_d = \frac{V_{bus}^2}{R_i}, \tag{2.3}$$

and the output power on the load resistance is

$$P_{out} = \frac{V_{bus}^2}{R_L}. \tag{2.4}$$

With simple manipulation it can be seen that the efficiency of the system is

$$\frac{P_{out}}{P_{in}} = \frac{1}{1 + \frac{R_i}{R_L}}, \tag{2.5}$$

which depends only on the load and internal resistance of the drive. In this case, the maximum power dissipated on the load occurs when the input power to the drive is maximized; thus the control problem can be formulated as the maximization of the electrical power on the q-axis.

The controller is then implemented as in the block diagram in Figure 2-5, where the control input is the desired force on the buoy F_{des} and the measured quantity is the velocity of the buoy, as:

$$F_{des} = C\ \Omega; \tag{2.6}$$

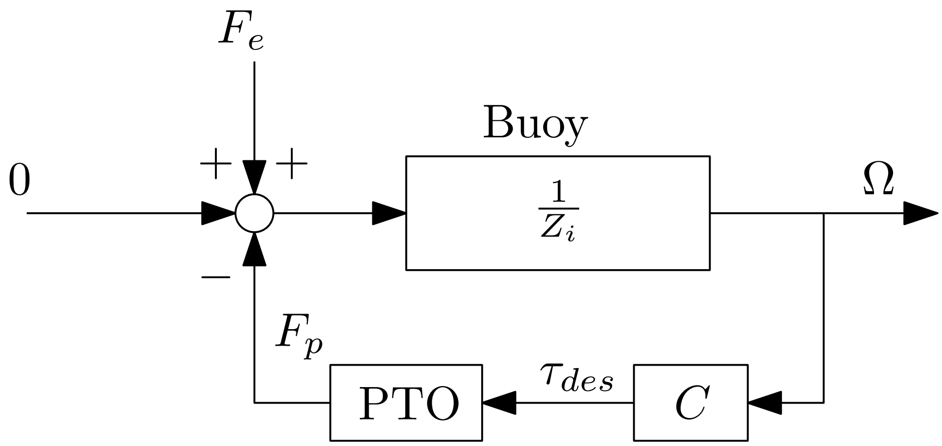

Figure 2-5. WaveBot controller structure block diagram

where the C is the MIMO controller defined as a 3×3 transfer function matrix, and Ω is the vector of the buoy velocity:

$$\Omega = \left[v^h, v^s, v^p\right]^T . \tag{2.7}$$

By mean of simple derivations using block diagram algebra it is possible to express the velocity of the buoy as function of the excitation force vector F_e as

$$\Omega = (Z_i - C)^{-1} F_e. \tag{2.8}$$

Additionally, by using the definition of the controller in (2.6) and the model of the generator in (2.1) , the matrix expression for current and voltage in the quadrature axis can be written as

$$\begin{bmatrix} I_q \\ V_q \end{bmatrix} = \begin{bmatrix} 0 & (NK_t)^{-1} \\ K_e N & R(NK_t)^{-1} \end{bmatrix} \begin{bmatrix} I_q \\ V_q \end{bmatrix}, \tag{2.9}$$

where:

$$I_q = [I_q^h, I_q^s, I_q^p]^T, \qquad V_q = [V_q^h, V_q^s, V_q^p]^T, \tag{2.10}$$

$$K_e = \begin{bmatrix} k_e^h & 0 & 0 \\ 0 & k_e^s & 0 \\ 0 & 0 & k_e^p \end{bmatrix} \qquad K_t = \begin{bmatrix} k_t^h & 0 & 0 \\ 0 & k_t^s & 0 \\ 0 & 0 & k_t^p \end{bmatrix} \tag{2.11}$$

$$R = \begin{bmatrix} R^h & 0 & 0 \\ 0 & R^s & 0 \\ 0 & 0 & R^p \end{bmatrix} \qquad K_t = \begin{bmatrix} N^h & 0 & 0 \\ 0 & N^s & 0 \\ 0 & 0 & N^p \end{bmatrix}. \tag{2.12}$$

The total electrical power on the q-axis is then

$$P_{abs} = \frac{1}{2}\mathrm{Re}\left[\frac{3}{2}\, I_q^+\, V_q\right] = \left((NK_t)^{-1}C\Omega\right)^+ \left(\left(K_e\, N + R(NK_t)^{-1}C\right)\Omega\right) \tag{2.13}$$

where the velocity vector Ω is defined in eq. (2.8).

A simple structure for the controller is a diagonal PI, defined as

$$C = \begin{bmatrix} K_p^h + \dfrac{K_i^h}{s} & 0 & 0 \\ 0 & K_p^s + \dfrac{K_i^s}{s} & 0 \\ 0 & 0 & K_p^p + \dfrac{K_i^p}{s} \end{bmatrix}. \tag{2.14}$$

The synthesis of the controller consists to find the parameters $\eta = \{K_p^h, K_i^h, K_p^s, K_i^s, K_p^p, K_i^p\}$ of the controller in eq. (2.14) that maximize the electrical power absorbed by the device. This task can be carried out, for any given seas state defined by the excitation force F_e, by solving the following optimization problem:

$$\eta_{opt} = \arg\max_{\eta} P_{abs}(\eta, F_e). \tag{2.15}$$

2.2. EXPERIMENTAL RESULTS

The controller was tested by first generating a sequence of random parameters η using a Latin Hypercube Sampling for each sea state. The wave profile time series, for each profile, repeats every 300 s and the controller's parameters are also updated every 300 s. The time profiles of the power absorbed by each PTO are plotted in Figure 2-6 through Figure 2-29. The top plot shown the time series of the mechanical power, the electrical power at the generator and the power dissipated by the winding resistance. The middle plot shows the mechanical and electrical average power for each 300 s interval, whereas the bottom plot shows the controller parameters. It can be immediately observed that the maximization of the mechanical power does not correspond to the maximization of the electrical power. In particular, in some situation, the controller gains that provide maximum mechanical power results in a negative absorbed power (net power flow from the grid to the device). See for example intervals 14-16 in Figure 2-9, where large values of the K_i^h provides large amount of mechanical power and negative average electrical power.

The experimental results are shown from a different perspective in Figure 2-30 throughFigure 2-56. The left contour plot in each figure shows the electrical power as function of the controller's parameters, whereas the plot on the right shows the mechanical power as function of the controllers parameters. It is immediately obvious also from these plots that the optimal tuning for electrical power maximization does not correspond to the optimal tuning for mechanical power maximization. It is also evident that, in every test case, the electrical power is much smaller than the mechanical power.

In order to improve and facilitate the understanding of the results, a 4-D second order polynomial has been used to fit the surge+pitch absorbed power, as function of the surge and pitch controller parameters. This is illustrated in Figure 2-57 through Figure 2-70. The same plots also show with a red mark the tuning provided by the optimizer described in Section 2.1. It can be seen that the power absorbed is not very sensitive to the controller tuning in the neighborhood of the optimum, and the optimizer provides tuning parameters that provide good performance (close to optimum).

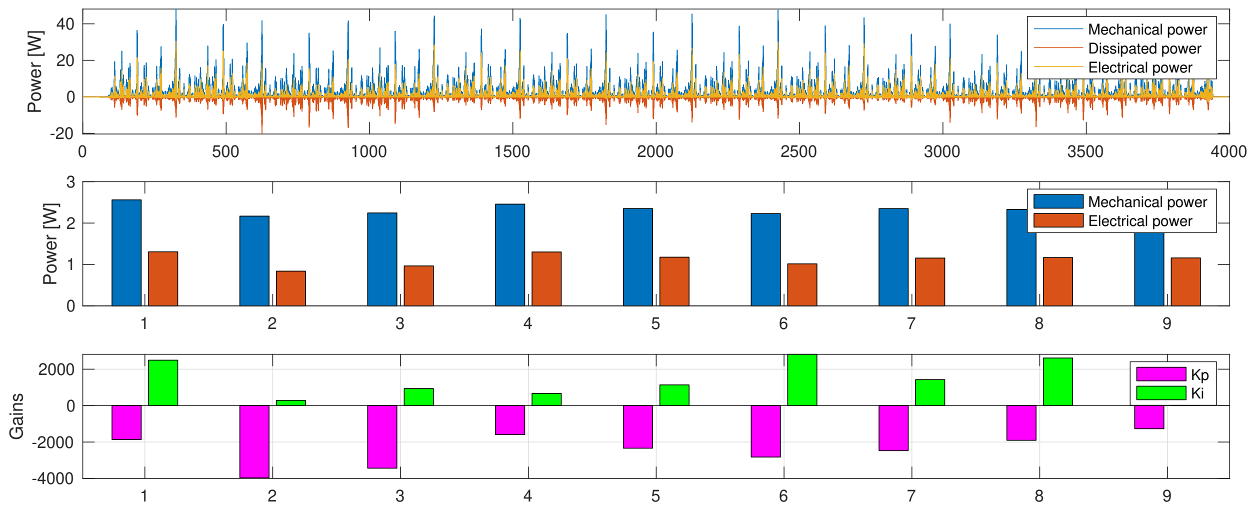

Figure 2-6. Test Case 2 - Power absorption and dissipation profiles for heave PTO.

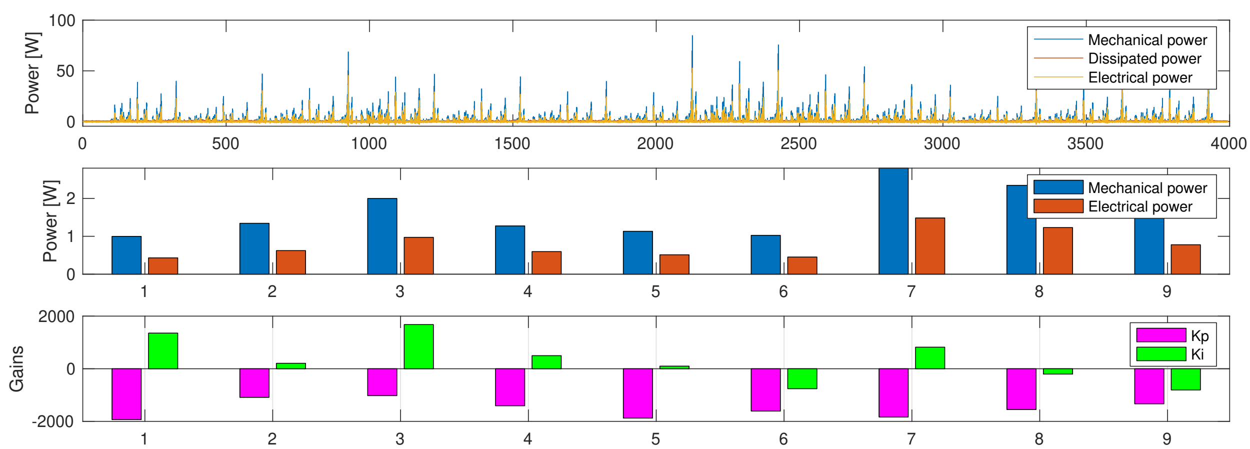

Figure 2-7. Test Case 2 - Power absorption and dissipation profiles for surge PTO.

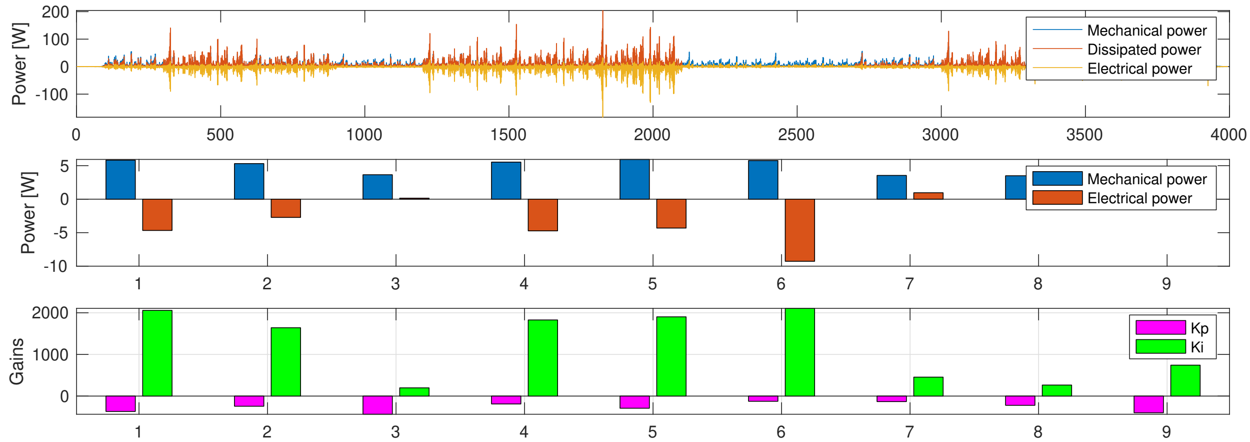

Figure 2-8. Test Case 2 - Power absorption and dissipation profiles for pitch PTO.

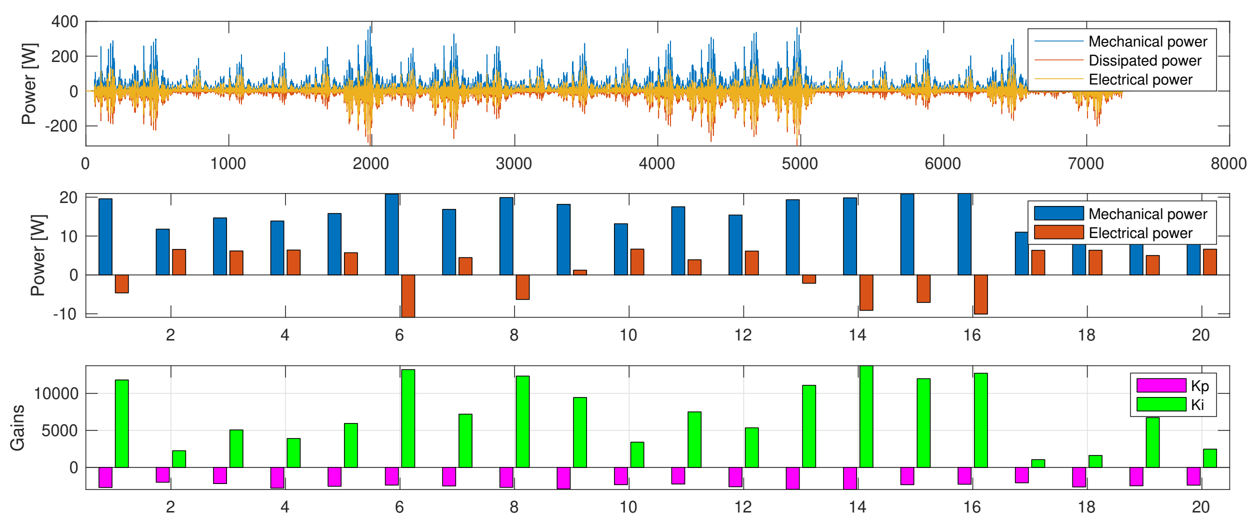

Figure 2-9. Test Case 4 - Power absorption and dissipation profiles for heave PTO.

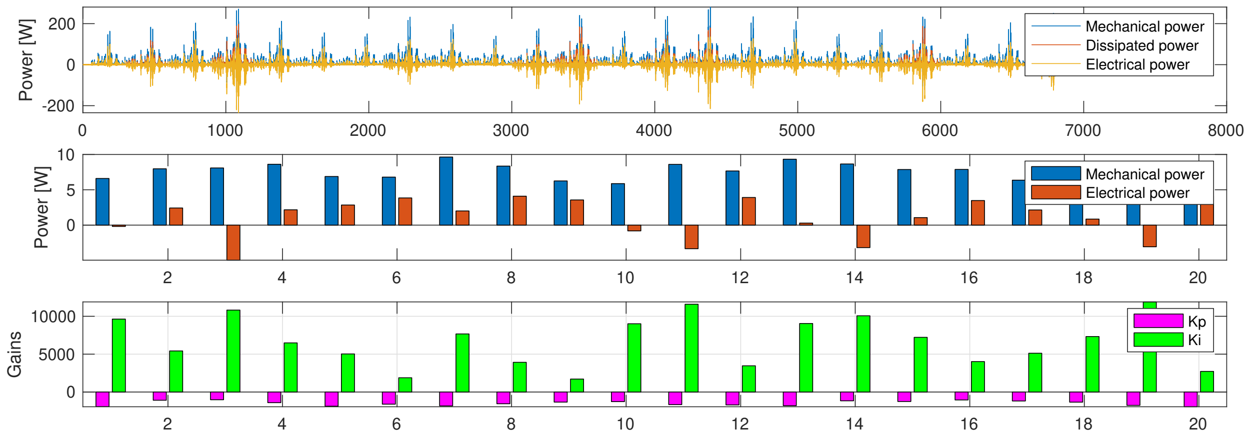

Figure 2-10. Test Case 4 - Power absorption and dissipation profiles for surge PTO.

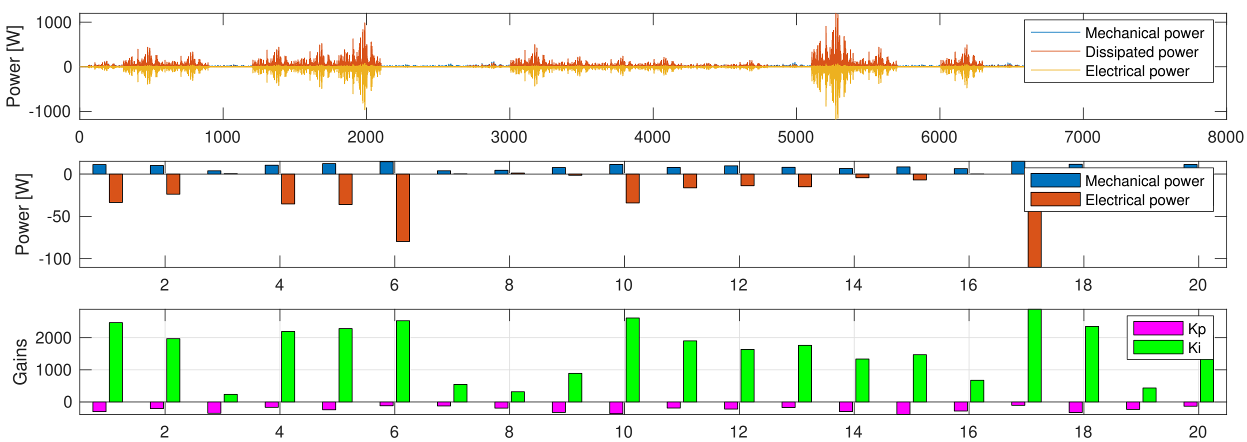

Figure 2-11. Test Case 4 - Power absorption and dissipation profiles for pitch PTO.

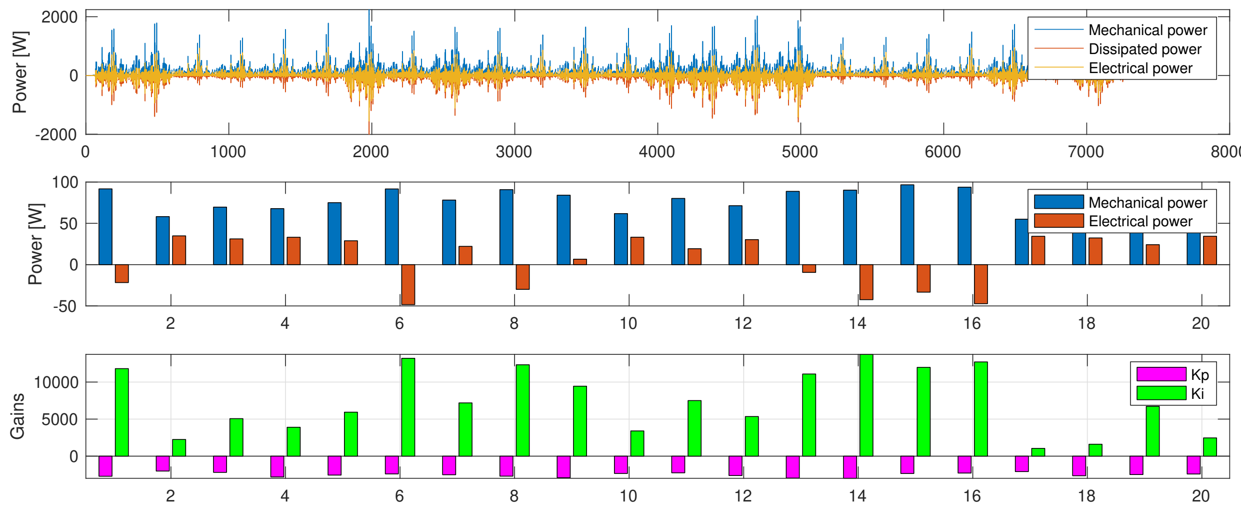

Figure 2-12. Test Case 6 - Power absorption and dissipation profiles for heave PTO.

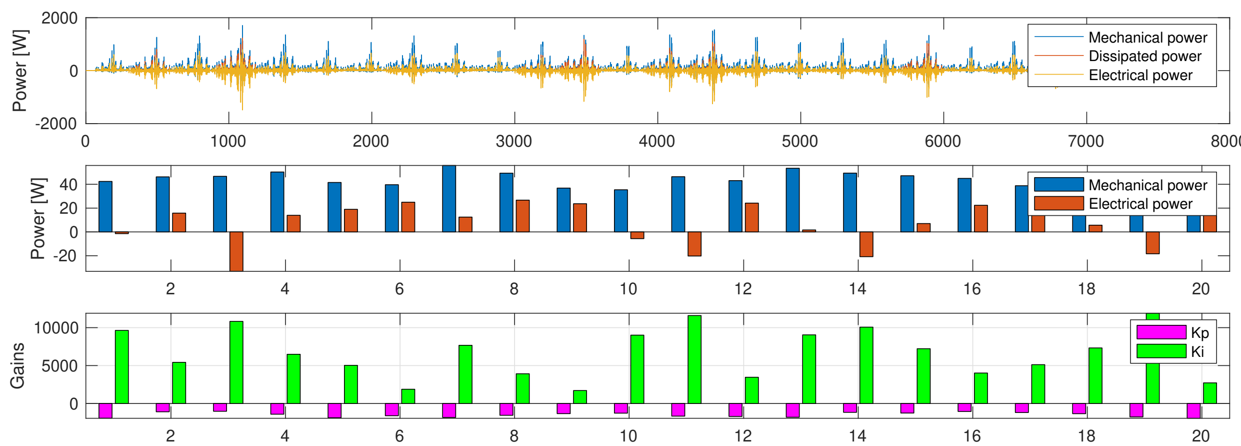

Figure 2-13. Test Case 6 - Power absorption and dissipation profiles for surge PTO.

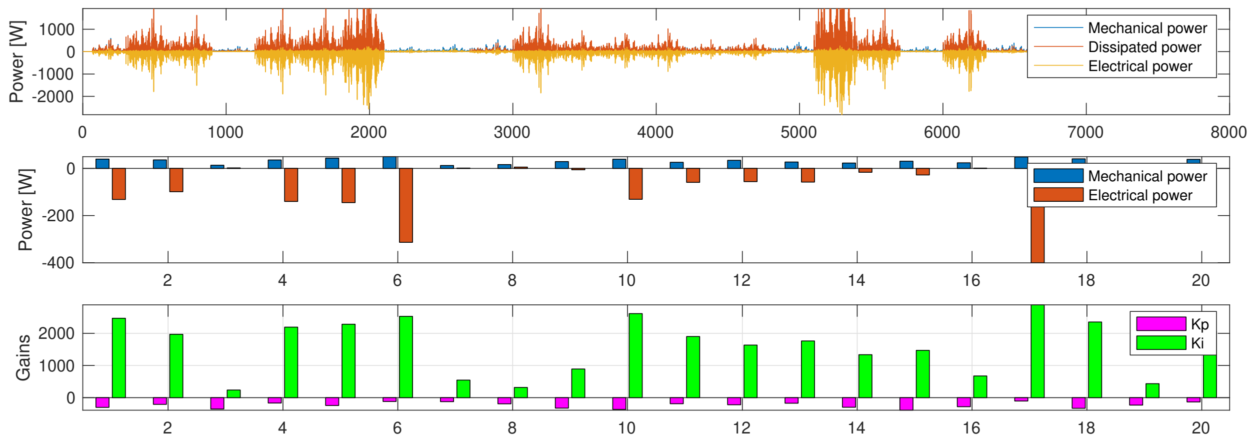

Figure 2-14. Test Case 6 - Power absorption and dissipation profiles for pitch PTO.

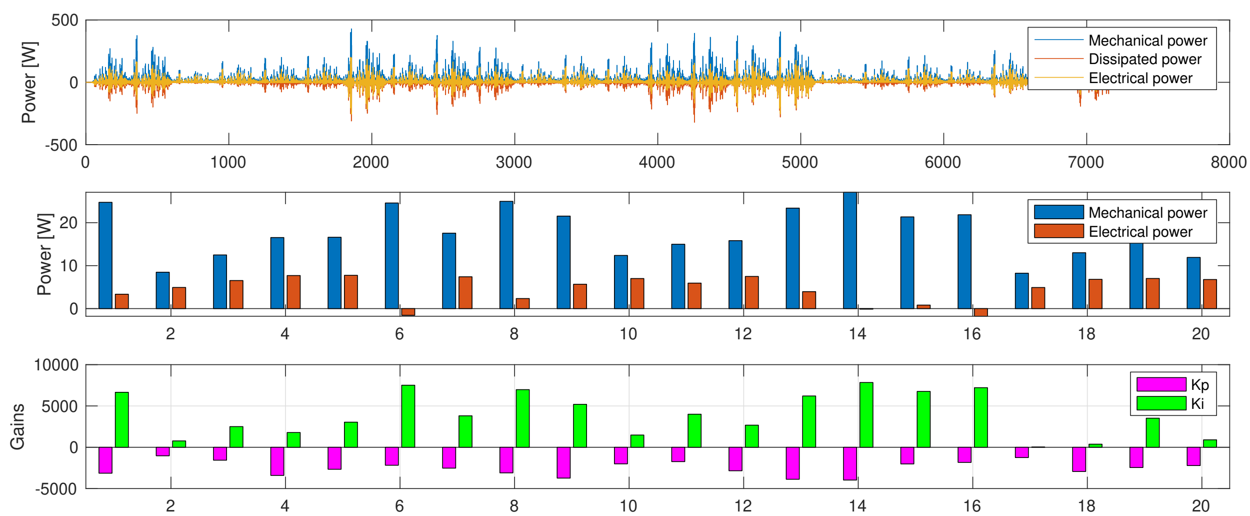

Figure 2-15. Test Case 7 - Power absorption and dissipation profiles for heave PTO.

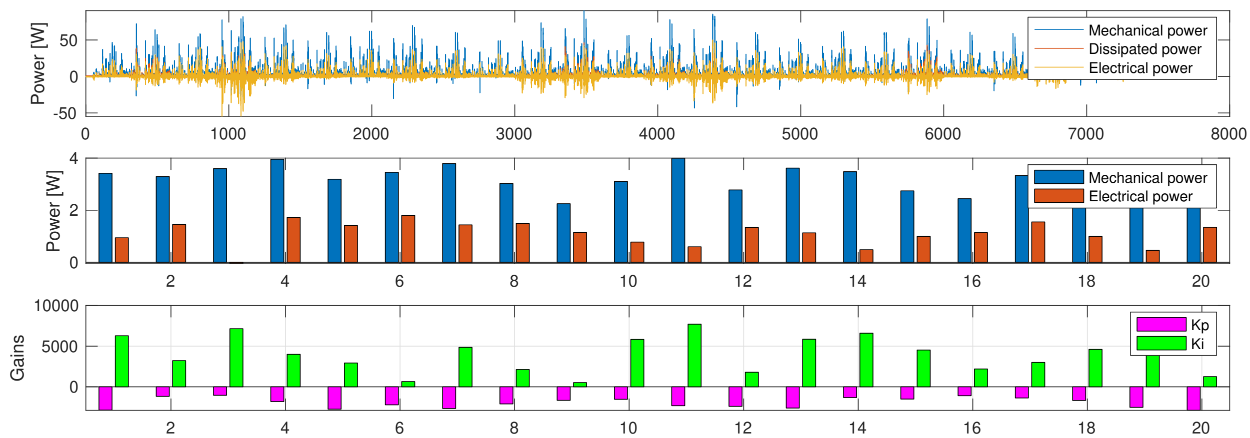

Figure 2-16. Test Case 7 - Power absorption and dissipation profiles for surge PTO.

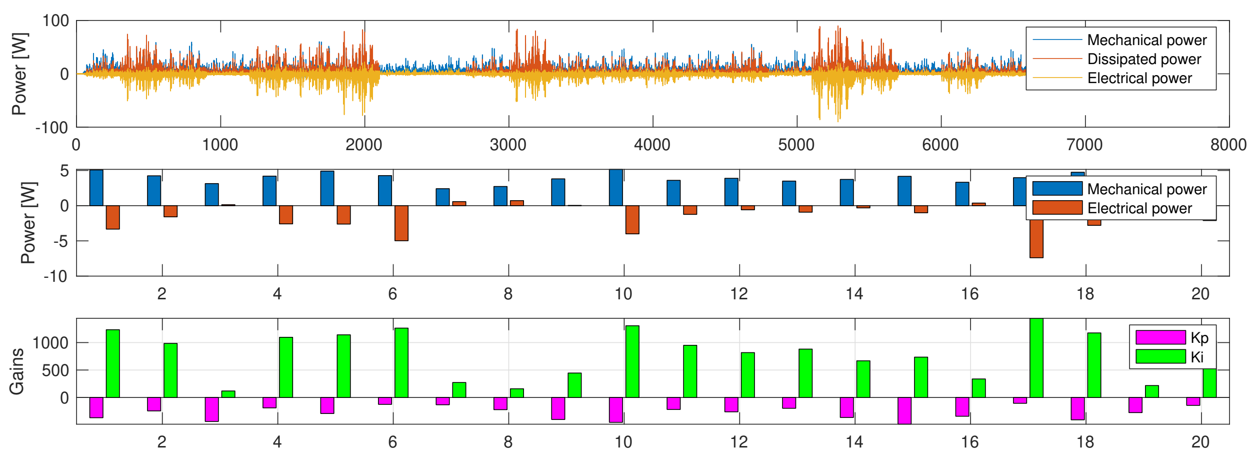

Figure 2-17. Test Case 7 - Power absorption and dissipation profiles for pitch PTO.

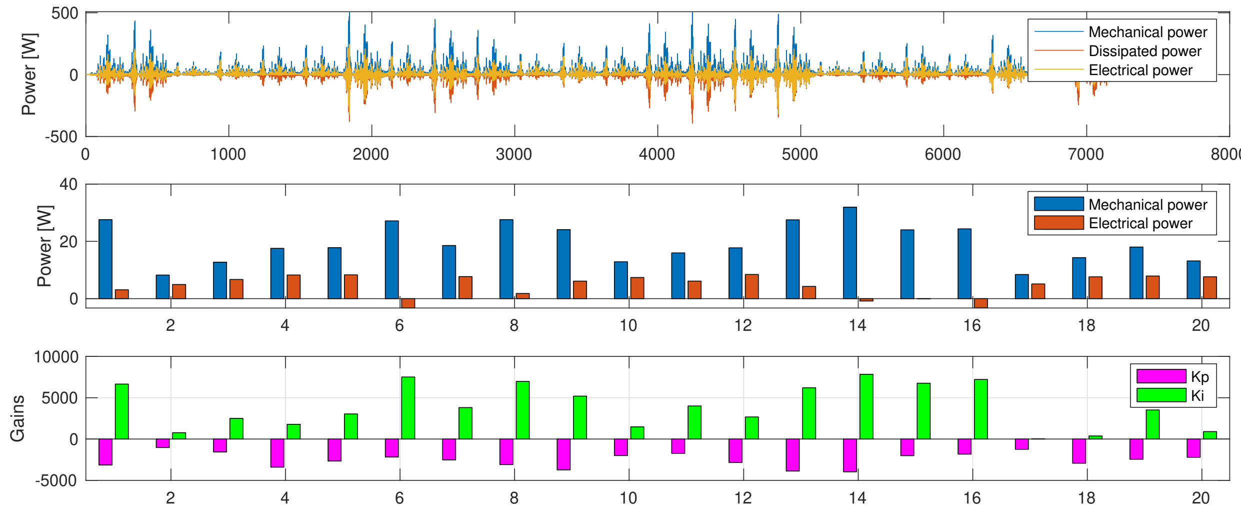

Figure 2-18. Test Case 8 - Power absorption and dissipation profiles for heave PTO.

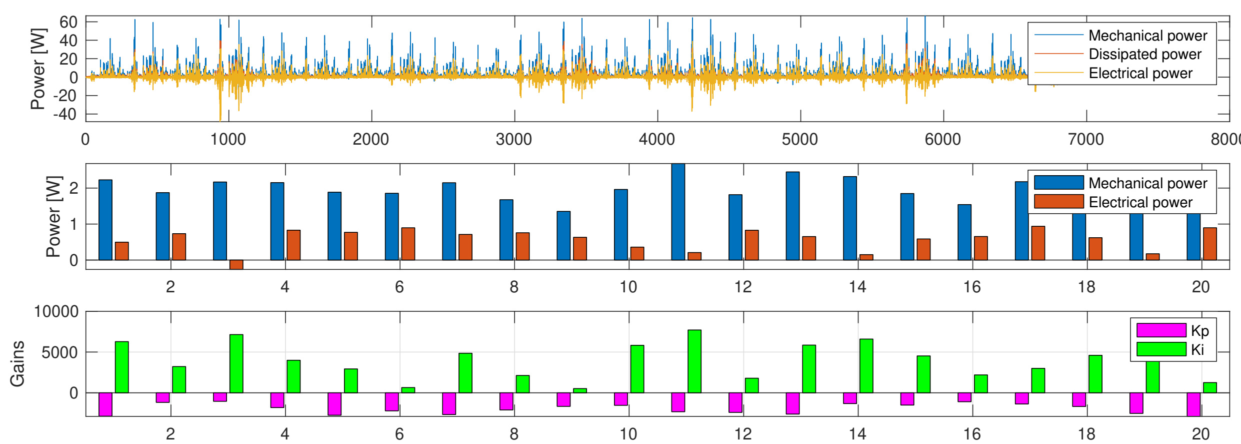

Figure 2-19. Test Case 8 - Power absorption and dissipation profiles for surge PTO.

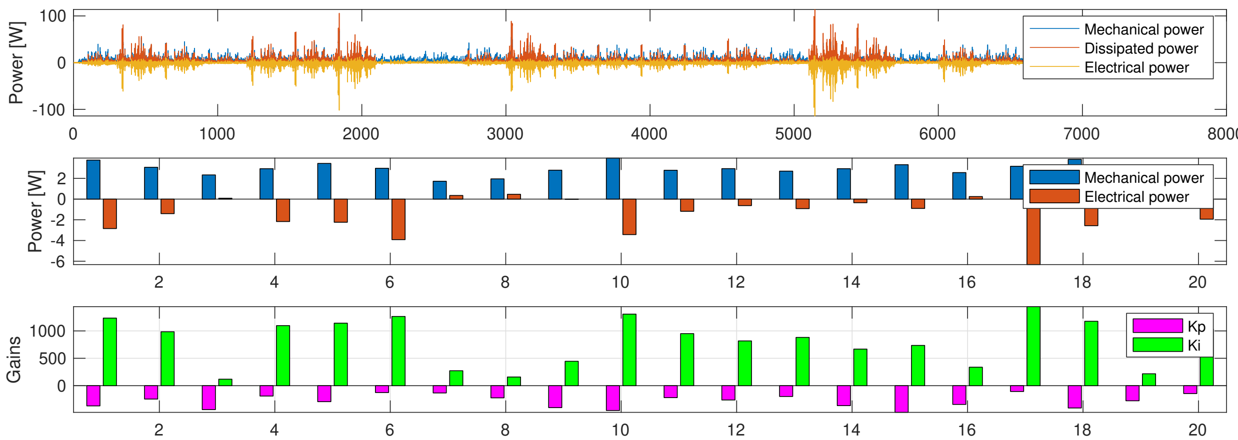

Figure 2-20. Test Case 8 - Power absorption and dissipation profiles for pitch PTO.

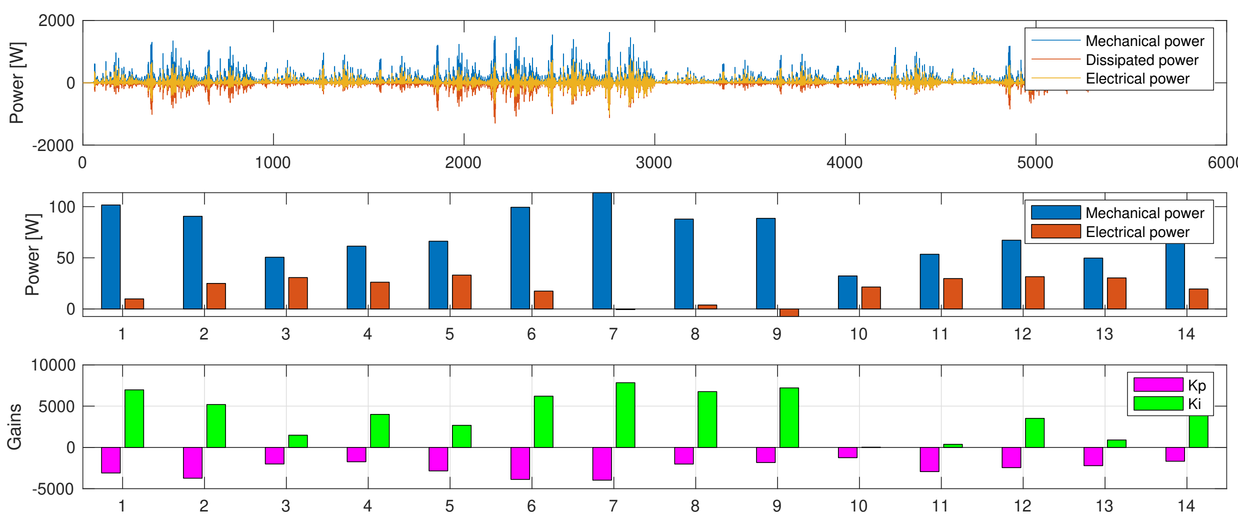

Figure 2-21. Test Case 9 - Power absorption and dissipation profiles for heave PTO.

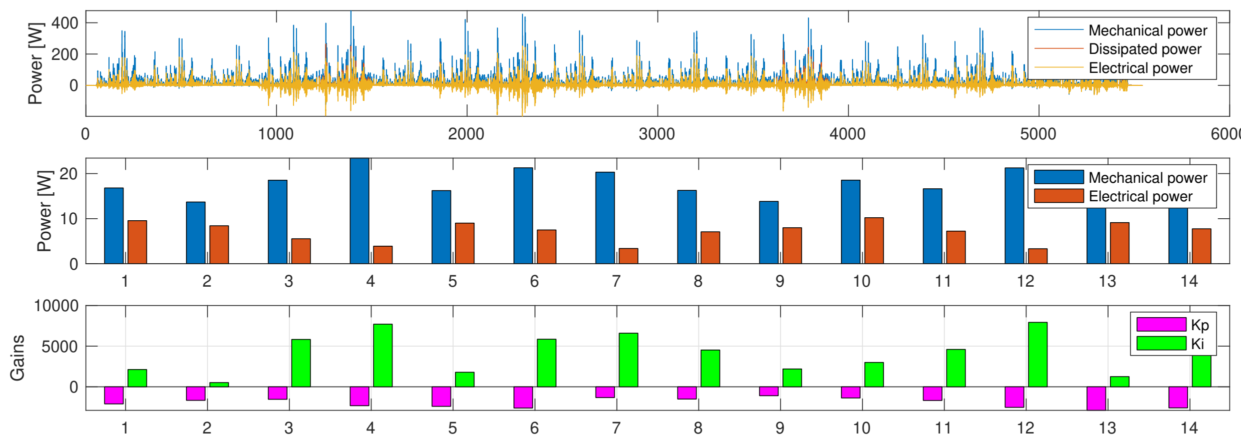

Figure 2-22. Test Case 9 - Power absorption and dissipation profiles for surge PTO.

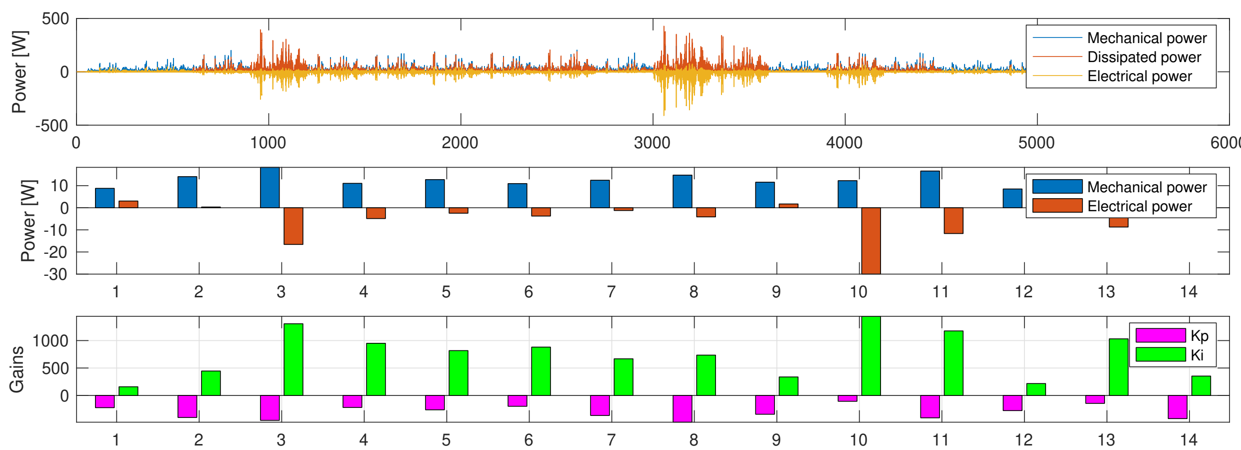

Figure 2-23. Test Case 9 - Power absorption and dissipation profiles for pitch PTO.

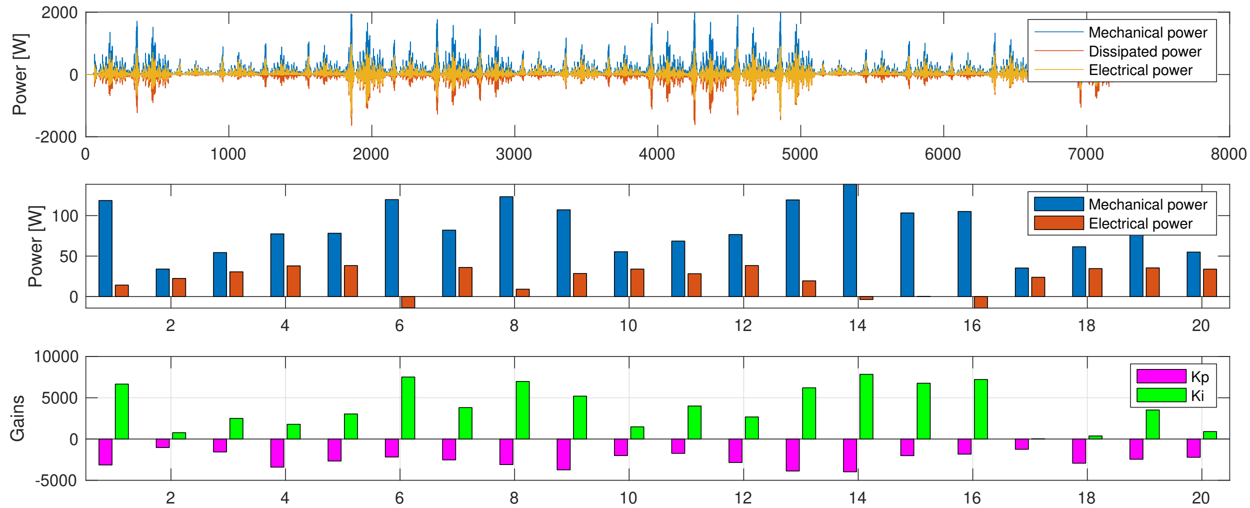

Figure 2-24. Test Case 10 -Power absorption and dissipation profiles for heave PTO.

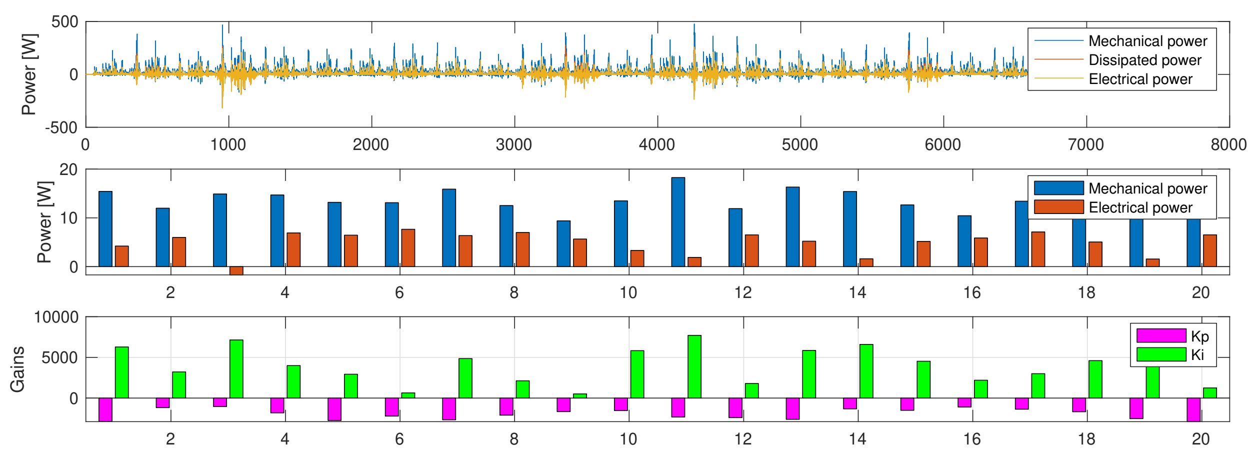

Figure 2-25. Test Case 10 -Power absorption and dissipation profiles for surge PTO.

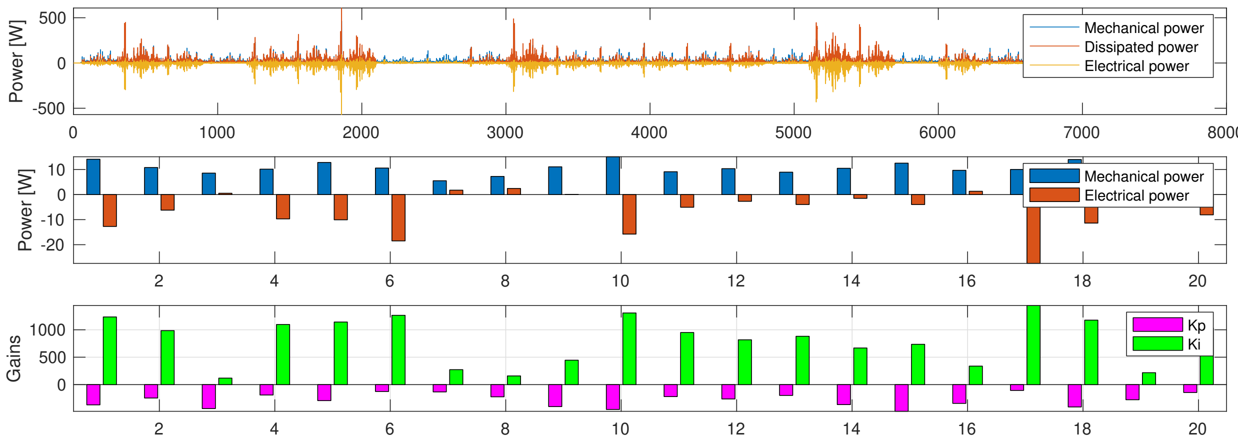

Figure 2-26. Test Case 10 -Power absorption and dissipation profiles for pitch PTO.

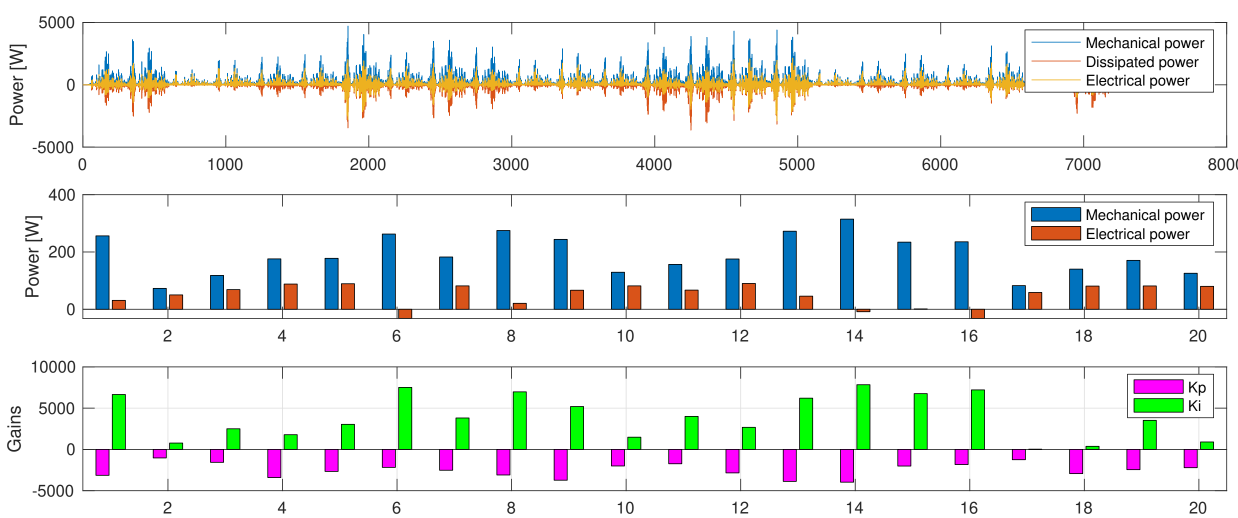

Figure 2-27. Test Case 11 -Power absorption and dissipation profiles for heave PTO.

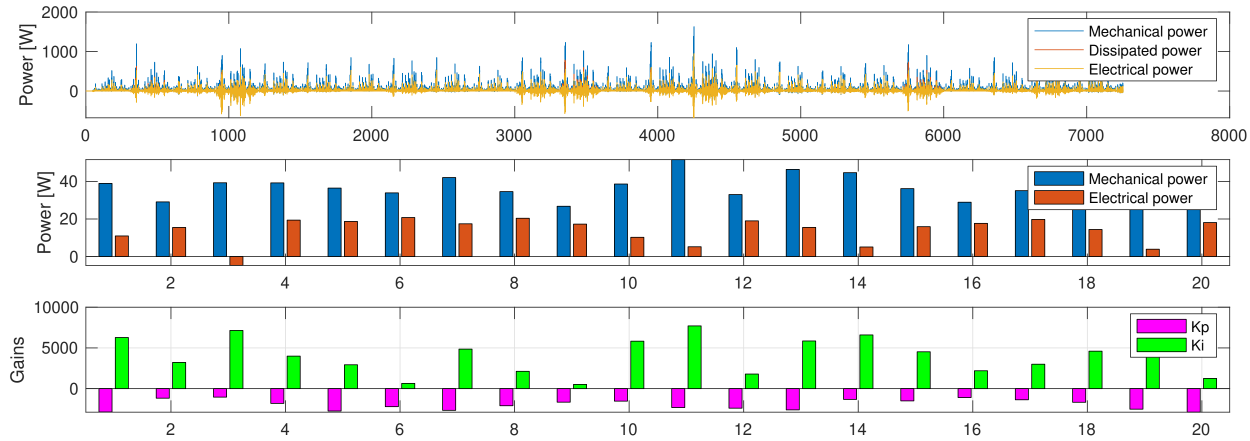

Figure 2-28. Test Case 11 -Power absorption and dissipation profiles for surge PTO.

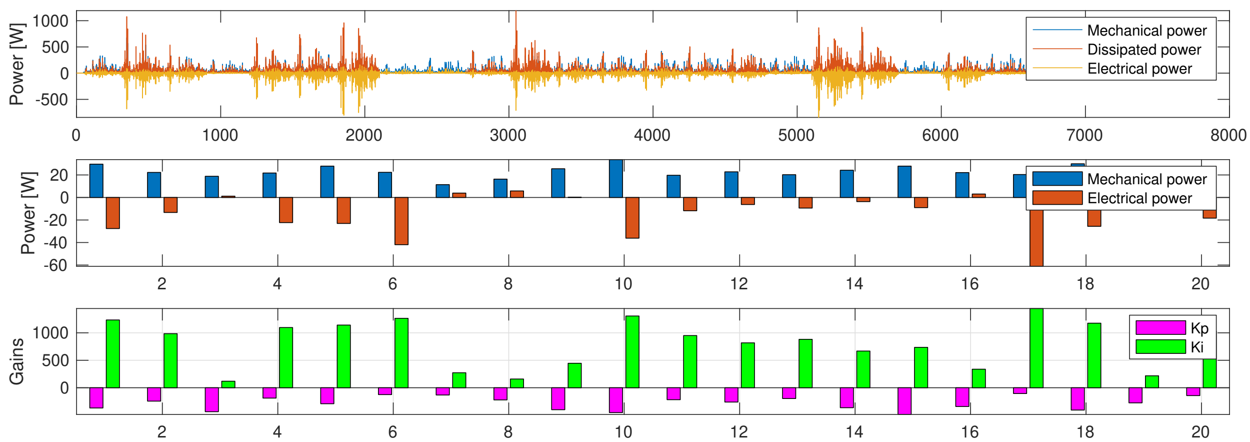

Figure 2-29. Test Case 11 -Power absorption and dissipation profiles for pitch PTO.

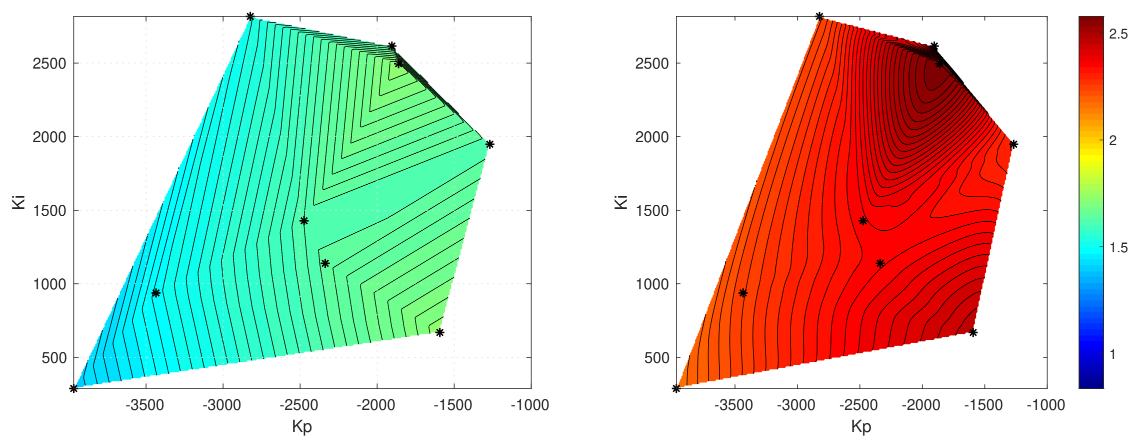

Figure 2-30. Test case 2 - Sensitivity of heave absorption to heave control parameters.

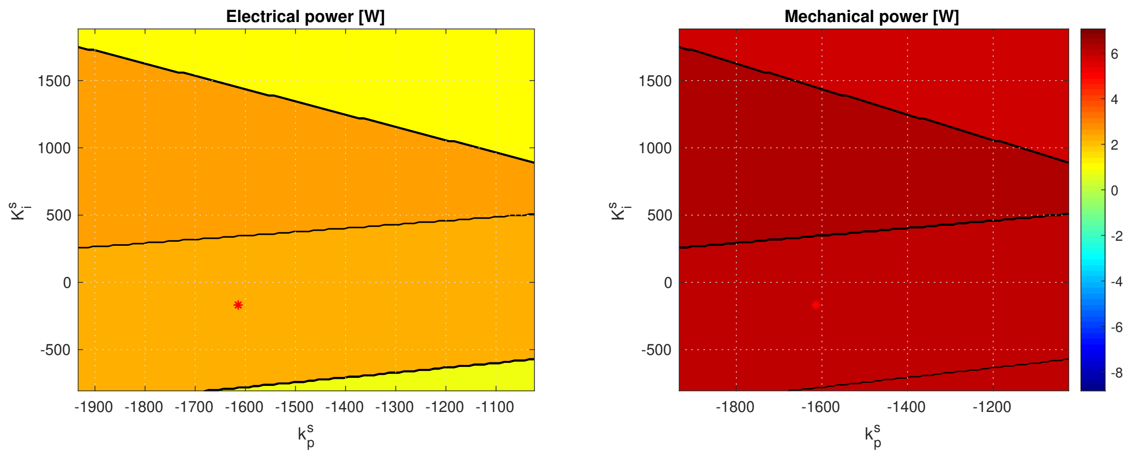

Figure 2-31. Test case 2 - Sensitivity of surge+pitch power absorption to surge control parameters.

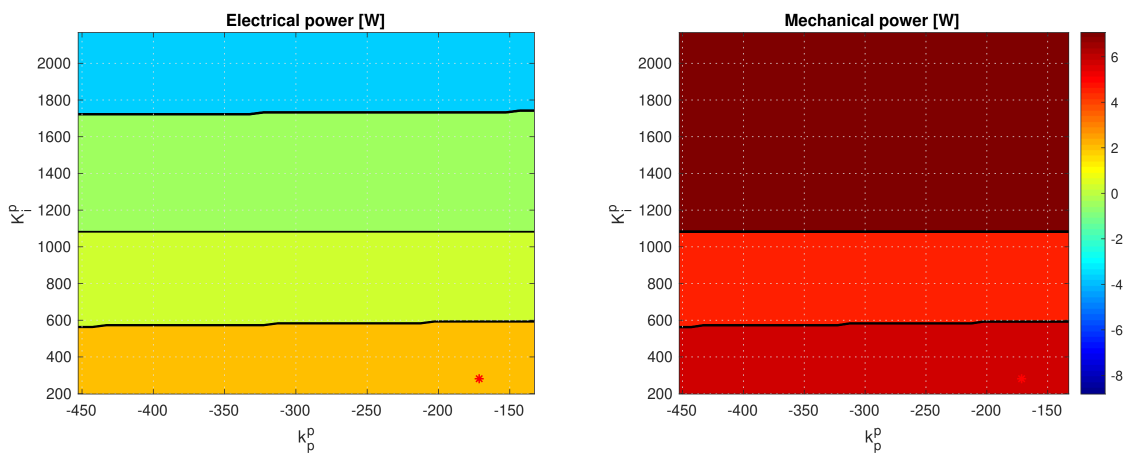

Figure 2-32. Test case 2 - Sensitivity of surge+pitch power absorption to pitch control parameters.

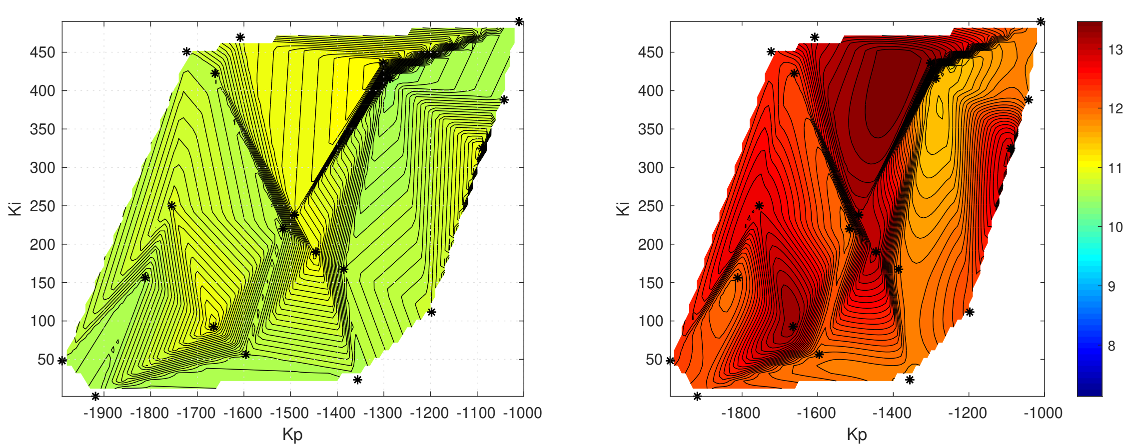

Figure 2-33. Test case 13 - Sensitivity of heave absorption to heave control parameters.

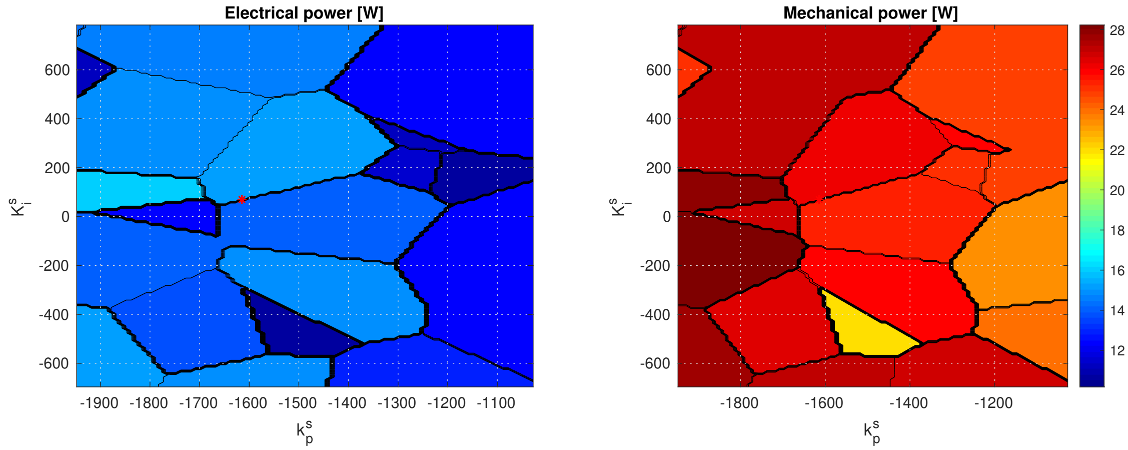

Figure 2-34. Test case 13 - Sensitivity of surge+pitch power absorption to surge control parameters.

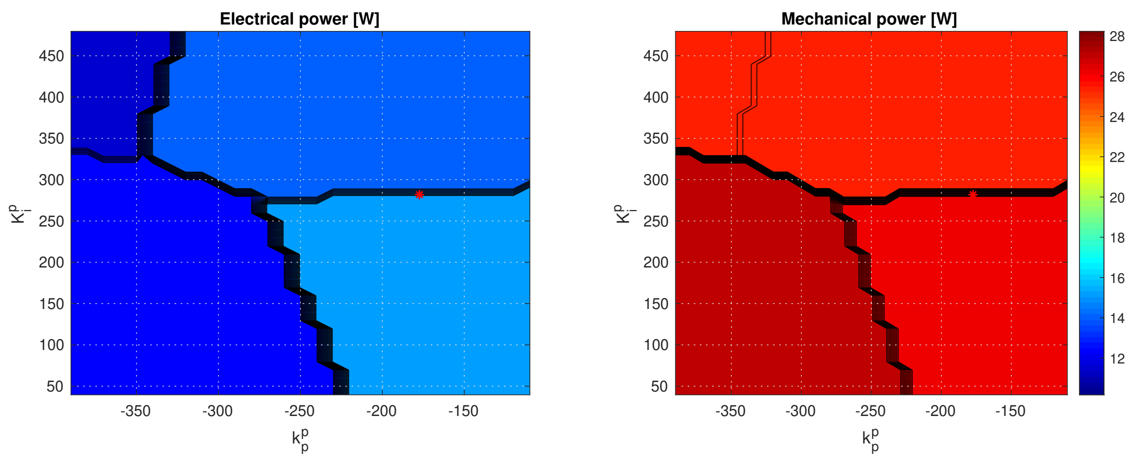

Figure 2-35. Test case 13 - Sensitivity of surge+pitch power absorption to pitch control parameters.

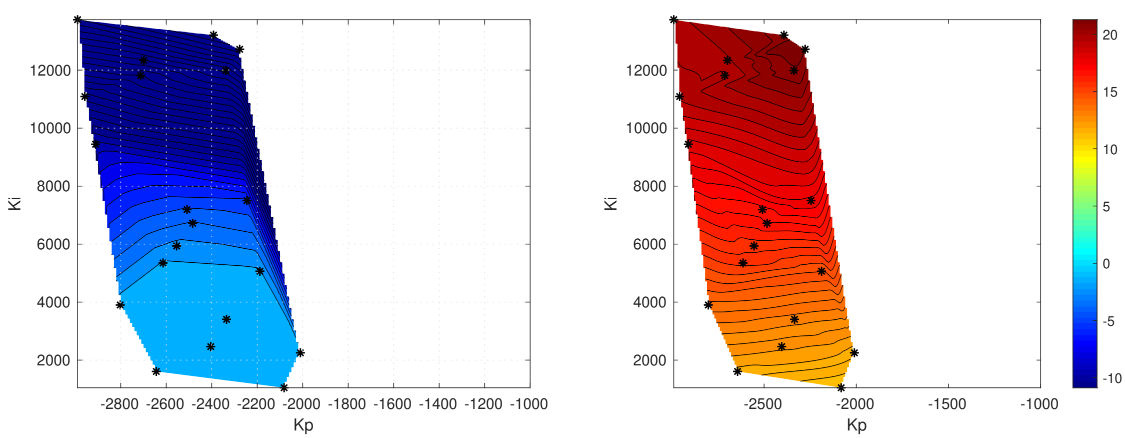

Figure 2-36. Test case 4 - Sensitivity of heave absorption to heave control parameters.

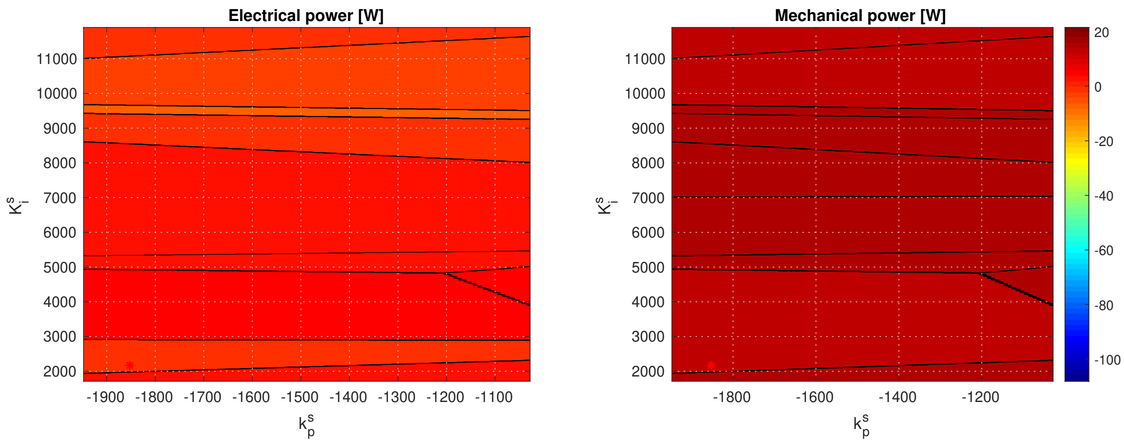

Figure 2-37. Test case 4 - Sensitivity of surge+pitch power absorption to surge control parameters.

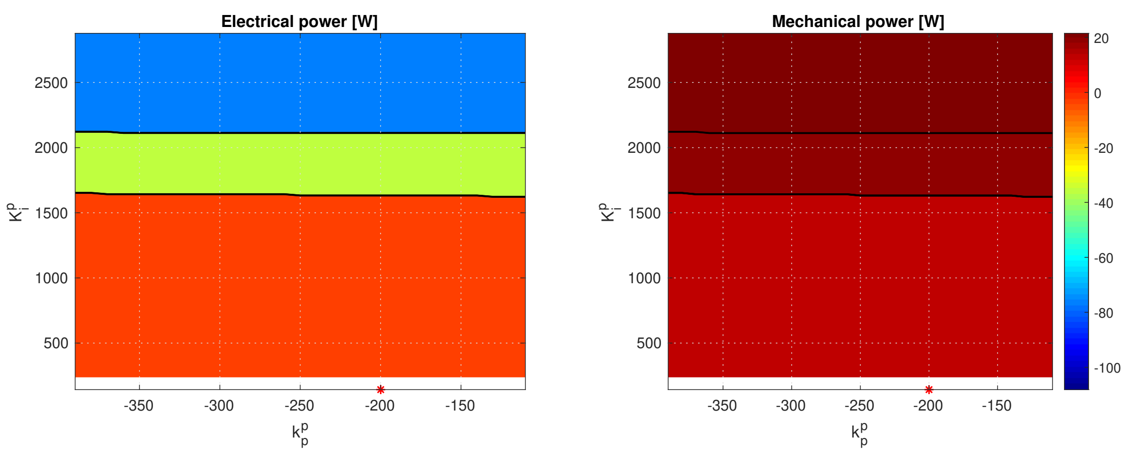

Figure 2-38. Test case 4 - Sensitivity of surge+pitch power absorption to pitch control parameters.

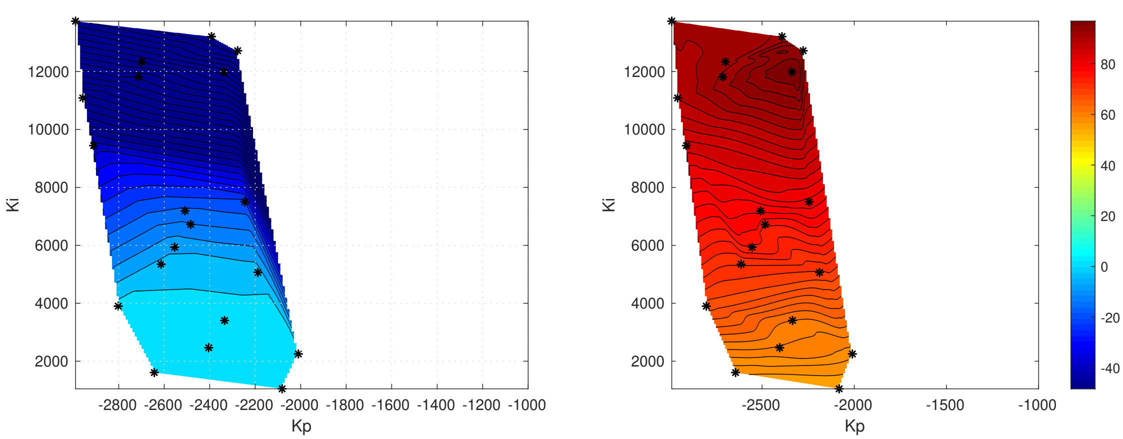

Figure 2-39. Test case 6 - Sensitivity of heave absorption to heave control parameters.

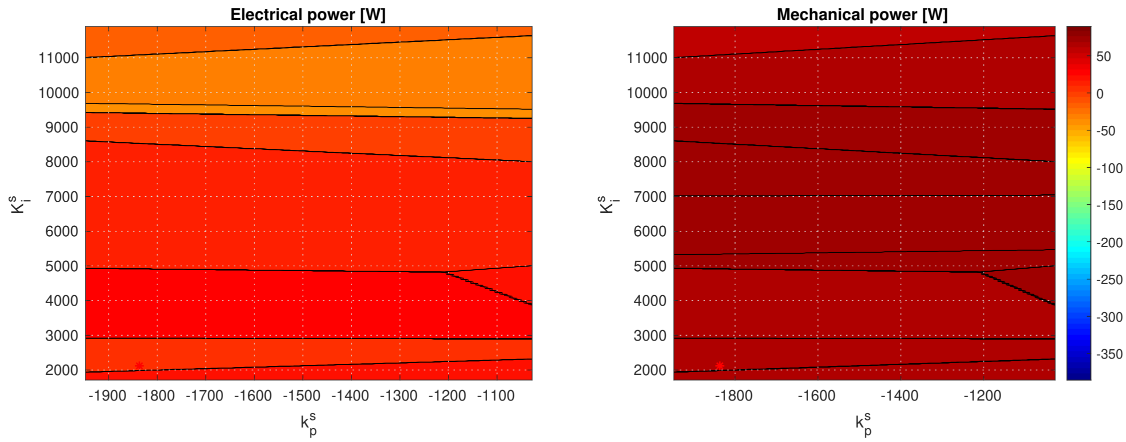

Figure 2-40. Test case 6 - Sensitivity of surge+pitch power absorption to surge control parameters.

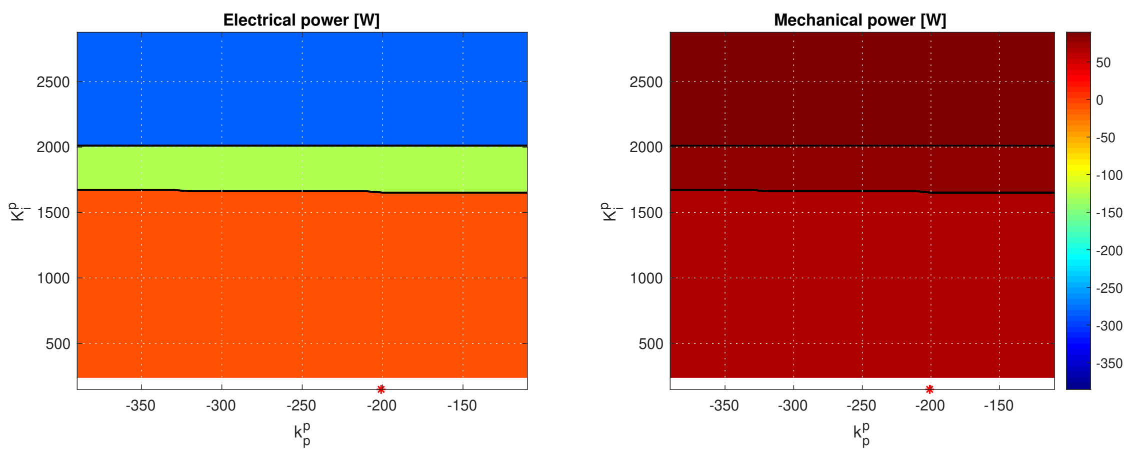

Figure 2-41. Test case 6 - Sensitivity of surge+pitch power absorption to pitch control parameters.

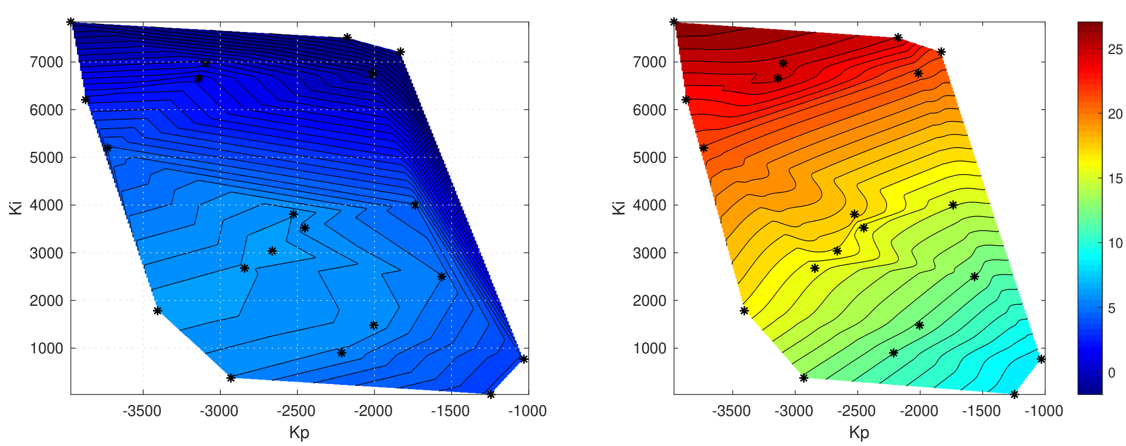

Figure 2-42. Test case 7 - Sensitivity of heave absorption to heave control parameters.

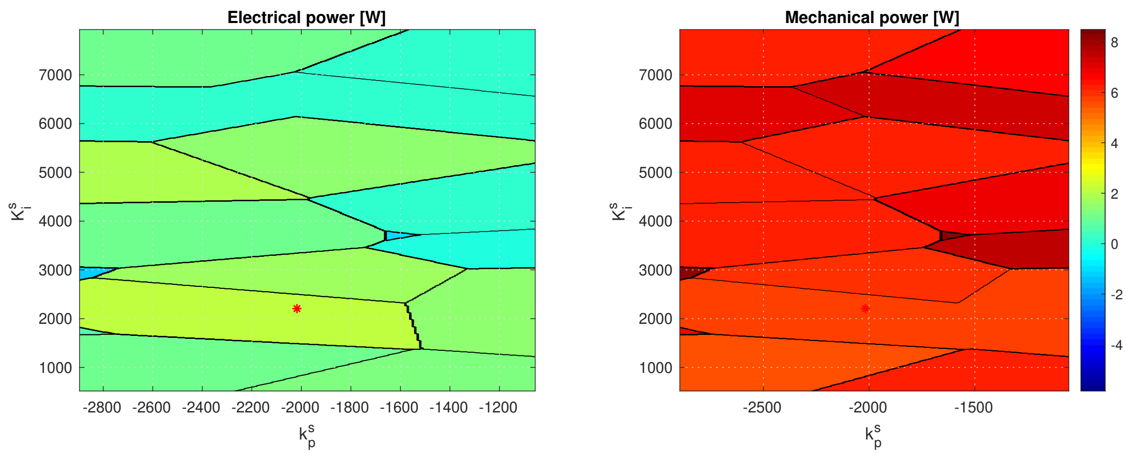

Figure 2-43. Test case 7 - Sensitivity of surge+pitch power absorption to surge control parameters.

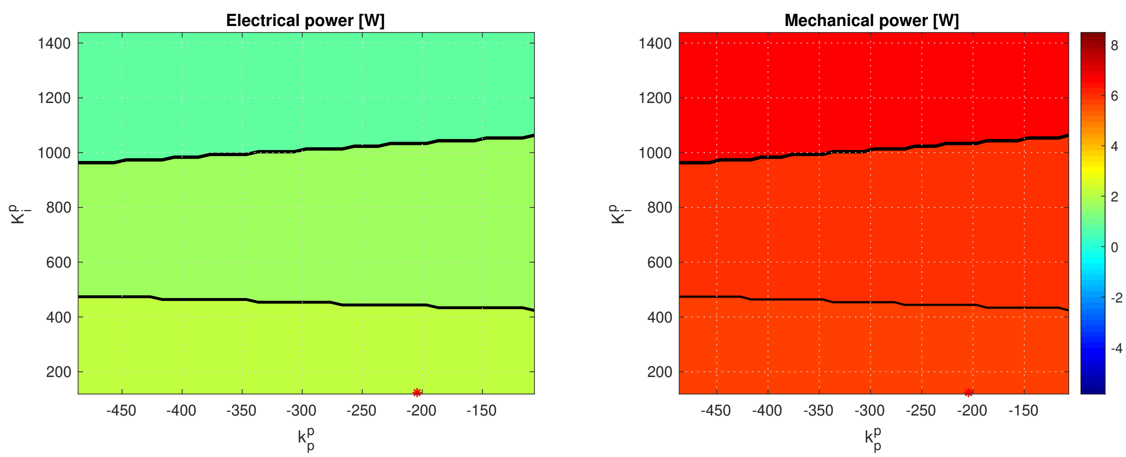

Figure 2-44. Test case 7 - Sensitivity of surge+pitch power absorption to pitch control parameters.

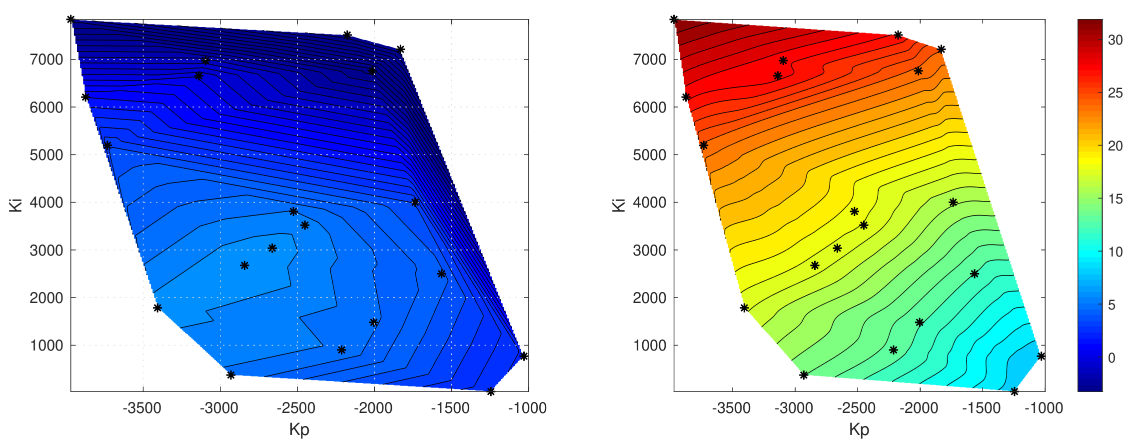

Figure 2-45. Test case 8 - Sensitivity of heave absorption to heave control parameters.

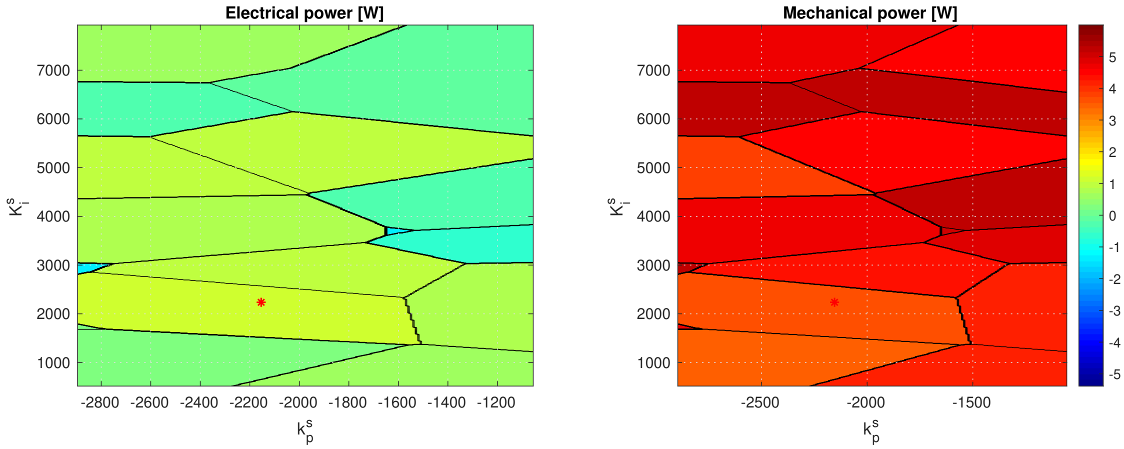

Figure 2-46. Test case 8 - Sensitivity of surge+pitch power absorption to surge control parameters.

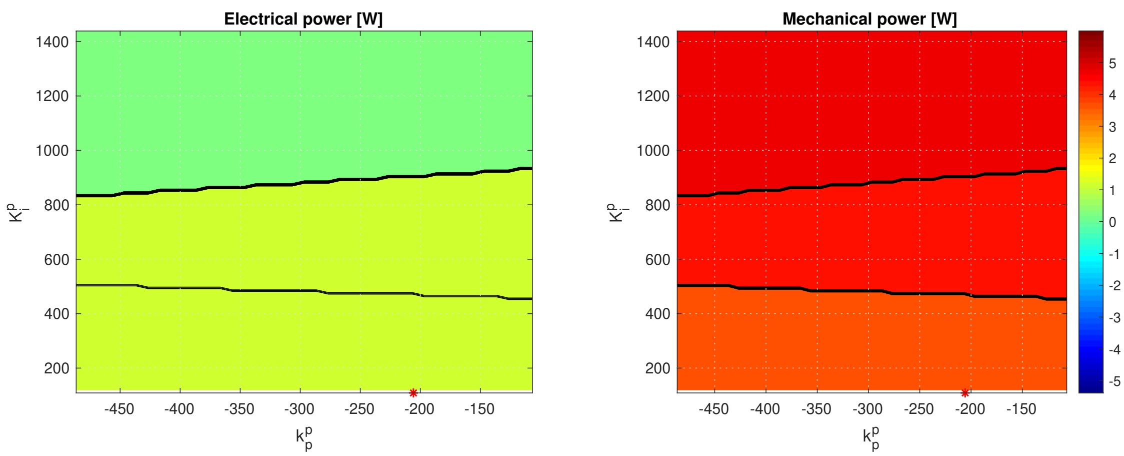

Figure 2-47. Test case 8 - Sensitivity of surge+pitch power absorption to pitch control parameters.

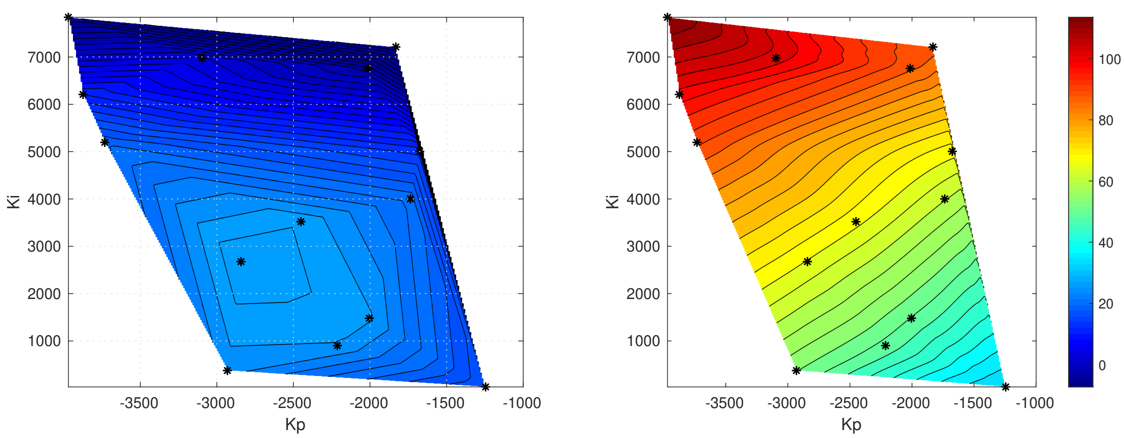

Figure 2-48. Test case 9 - Sensitivity of heave absorption to heave control parameters.

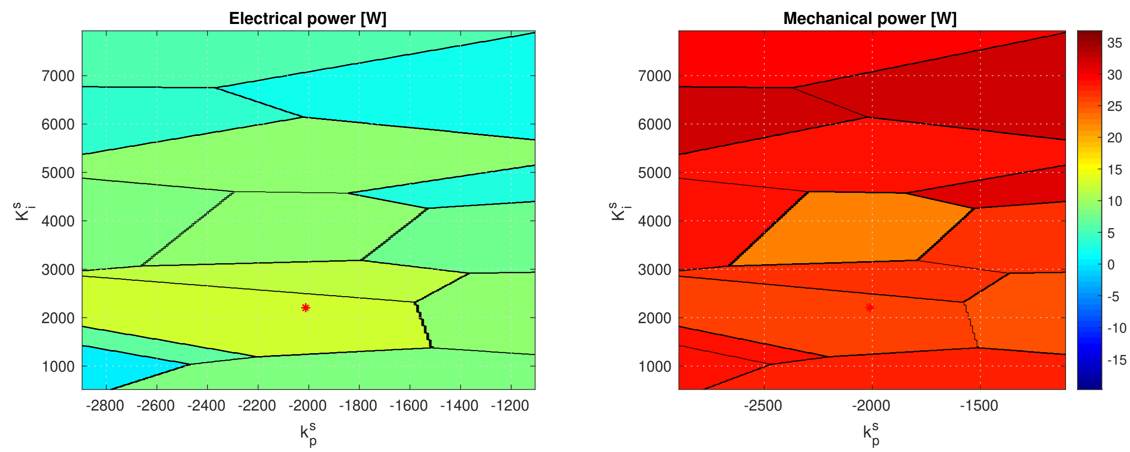

Figure 2-49. Test case 9 - Sensitivity of surge+pitch power absorption to surge control parameters.

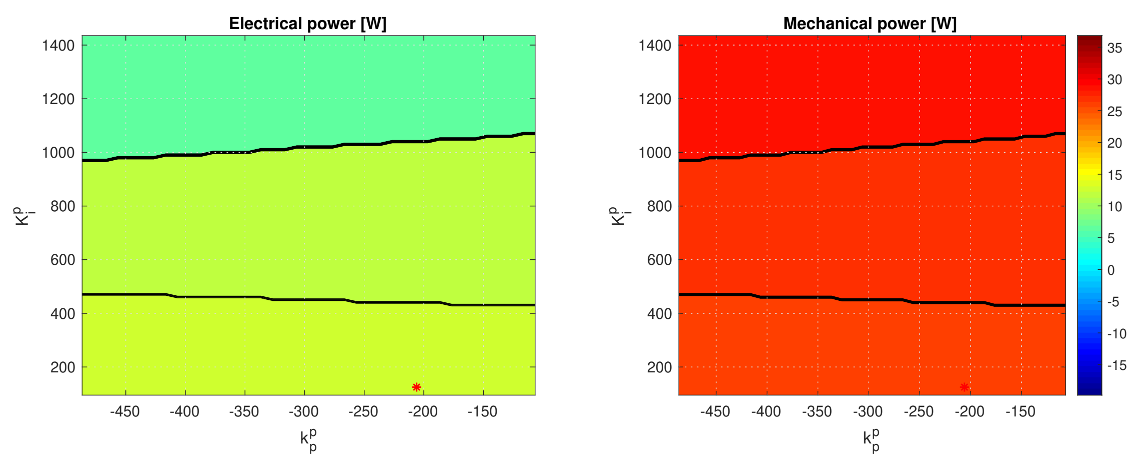

Figure 2-50. Test case 9 - Sensitivity of surge+pitch power absorption to pitch control parameters.

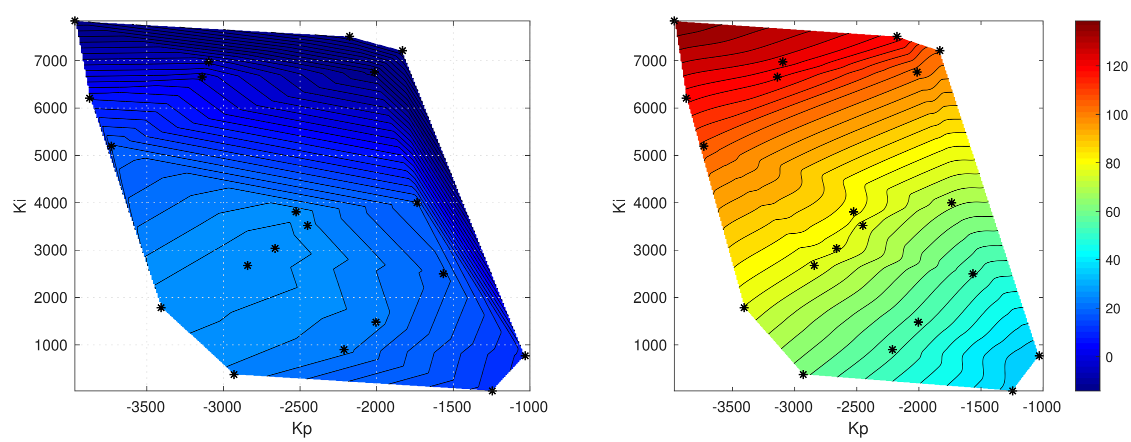

Figure 2-51. Test case 10 - Sensitivity of heave absorption to heave control parameters.

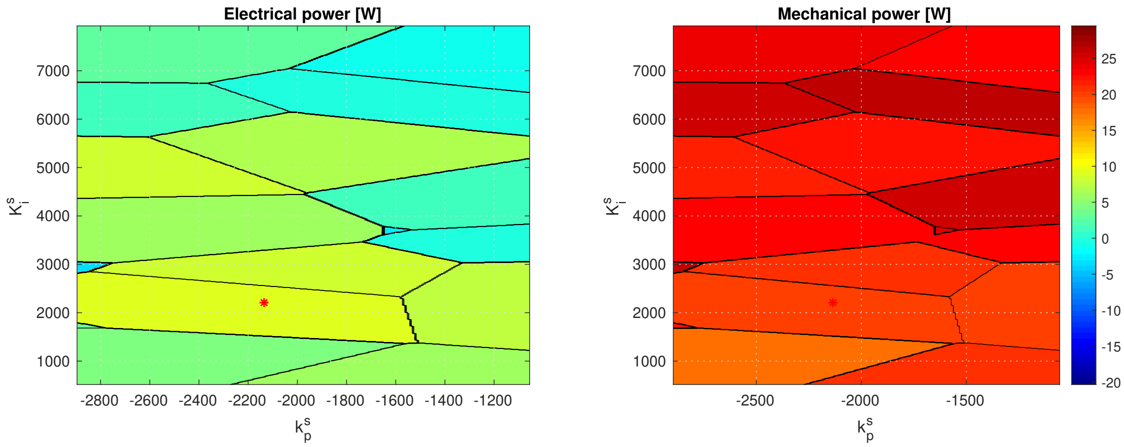

Figure 2-52. Test case 10 - Sensitivity of surge+pitch power absorption to surge control parameters.

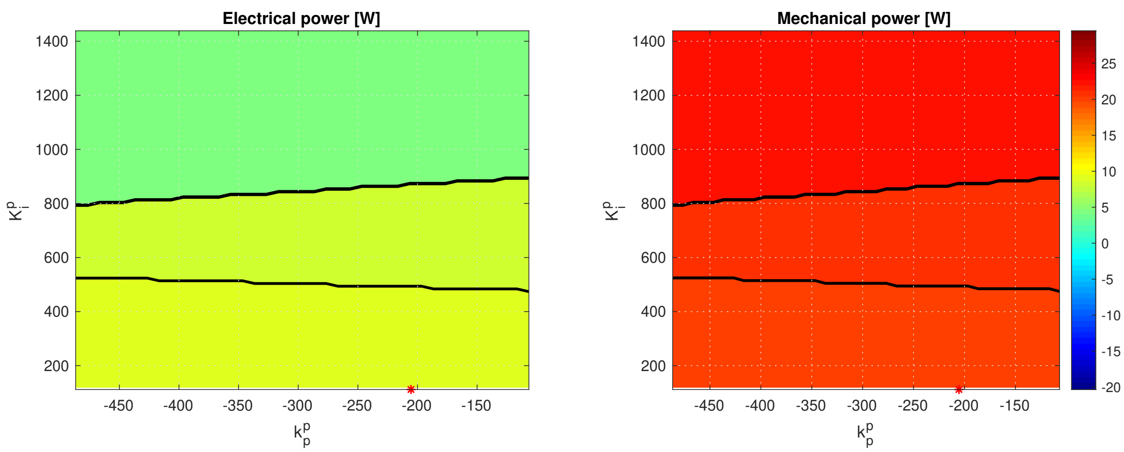

Figure 2-53. Test case 10 - Sensitivity of surge+pitch power absorption to pitch control parameters.

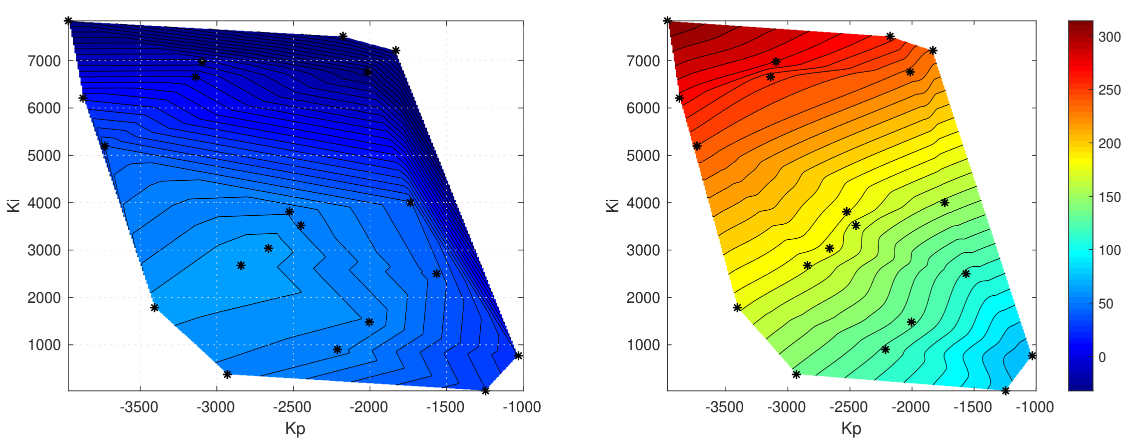

Figure 2-54. Test case 11 - Sensitivity of heave absorption to heave control parameters.

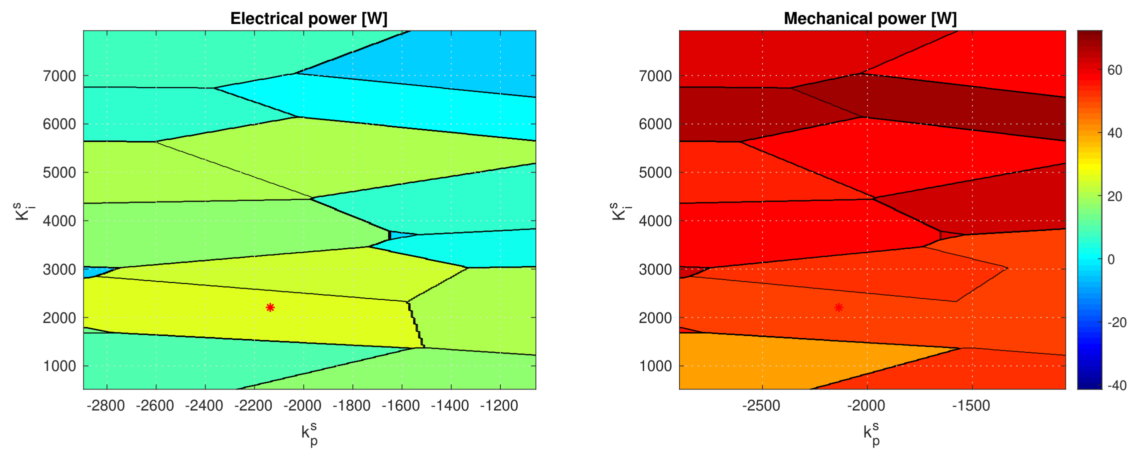

Figure 2-55. Test case 11 - Sensitivity of surge+pitch power absorption to surge control parameters.

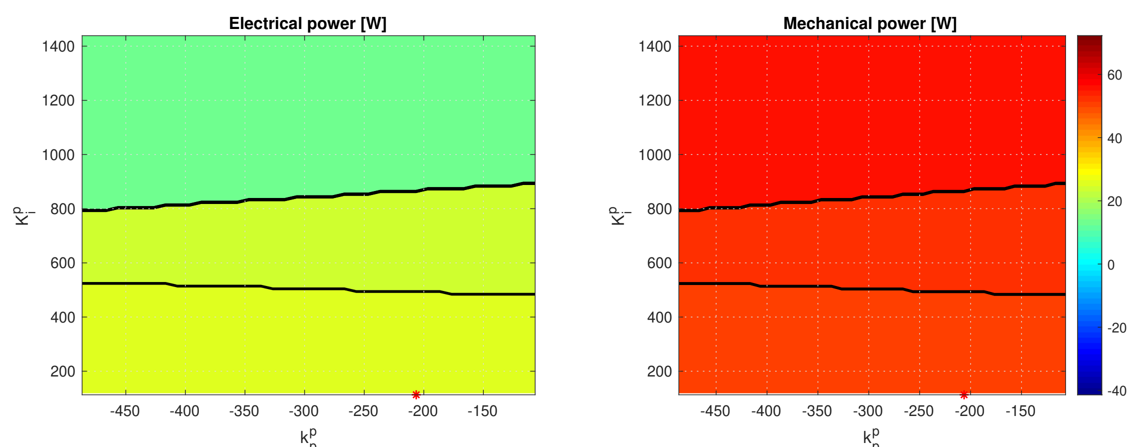

Figure 2-56. Test case 11 - Sensitivity of surge+pitch power absorption to pitch control parameters.

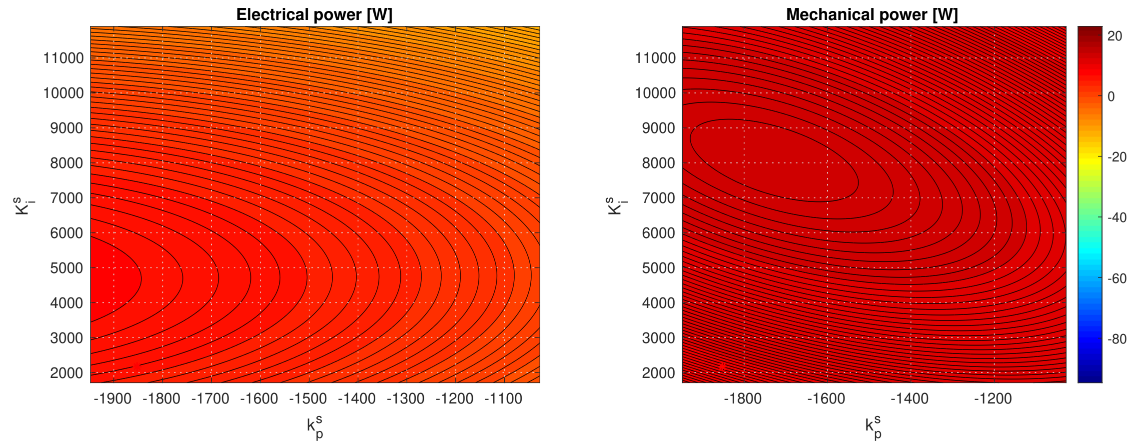

Figure 2-57. Test case 4 - Sensitivity of surge+pitch power absorption to surge control parameters. A second order 4-D polynomial has been used to fit the multidimensional surface relating the absorbed power to the controller parameters. The red mark shows the controller tuning provided by the optimization.

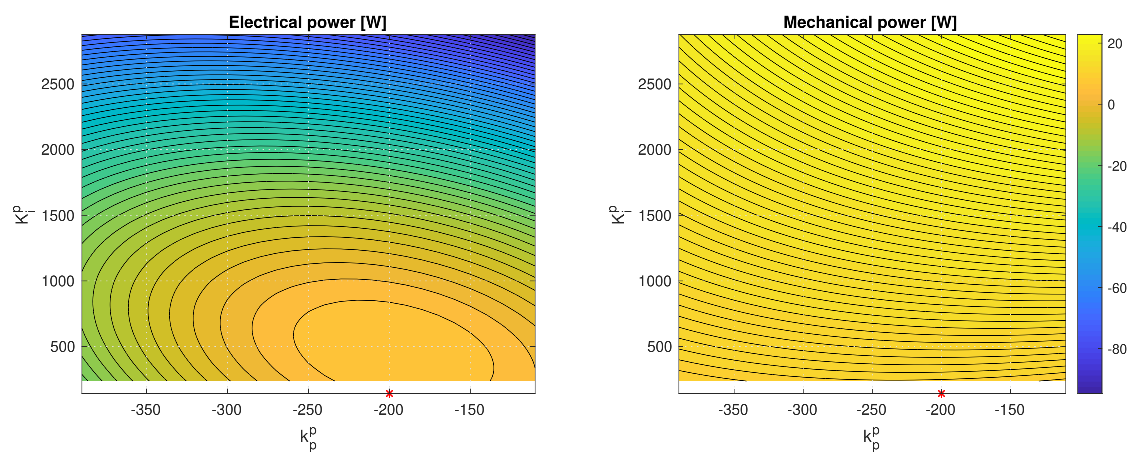

Figure 2-58. Test case 4 - Sensitivity of surge+pitch power absorption to pitch control parameters. A second order 4-D polynomial has been used to fit the multidimensional surface relating the absorbed power to the controller parameters. The red mark shows the controller tuning provided by the optimization.

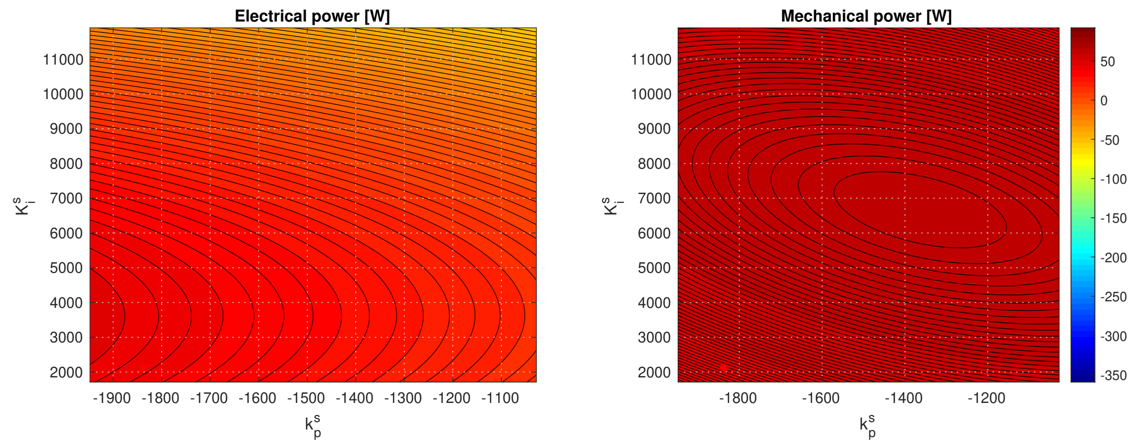

Figure 2-59. Test case 6 - Sensitivity of surge+pitch power absorption to surge control parameters. A second order 4-D polynomial has been used to fit the multidimensional surface relating the absorbed power to the controller parameters. The red mark shows the controller tuning provided by the optimization.

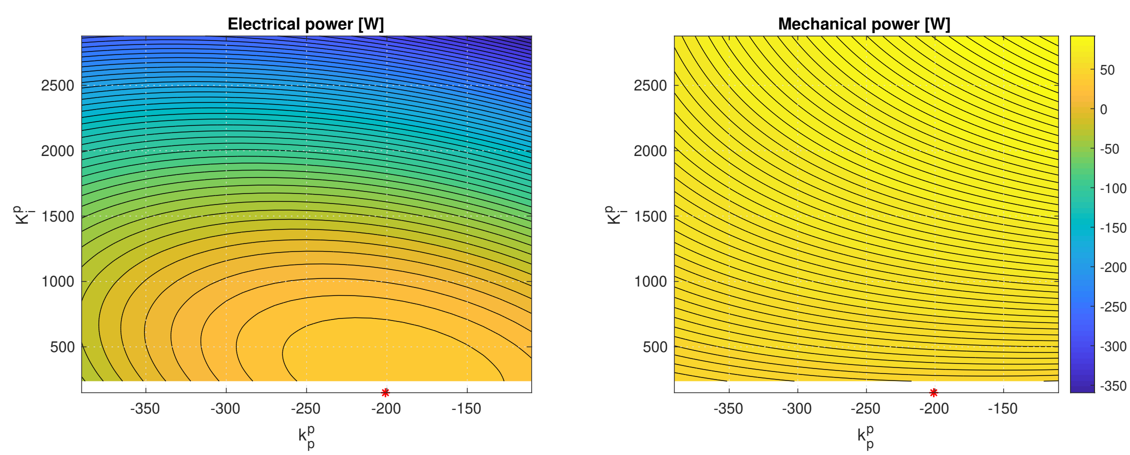

Figure 2-60. Test case 6 - Sensitivity of surge+pitch power absorption to pitch control parameters. A second order 4-D polynomial has been used to fit the multidimensional surface relating the absorbed power to the controller parameters. The red mark shows the controller tuning provided by the optimization.

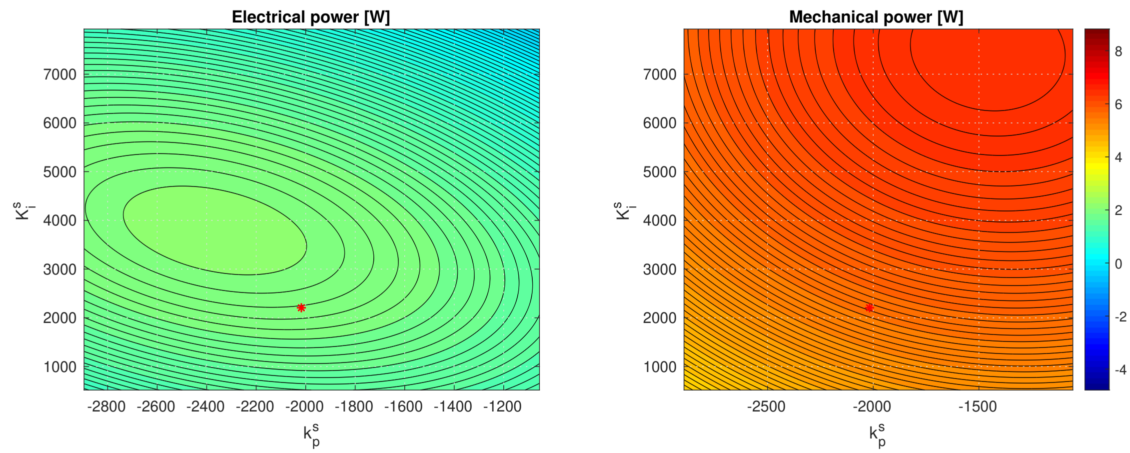

Figure 2-61. Test case 7 - Sensitivity of surge+pitch power absorption to surge control parameters. A second order 4-D polynomial has been used to fit the multidimensional surface relating the absorbed power to the controller parameters. The red mark shows the controller tuning provided by the optimization.

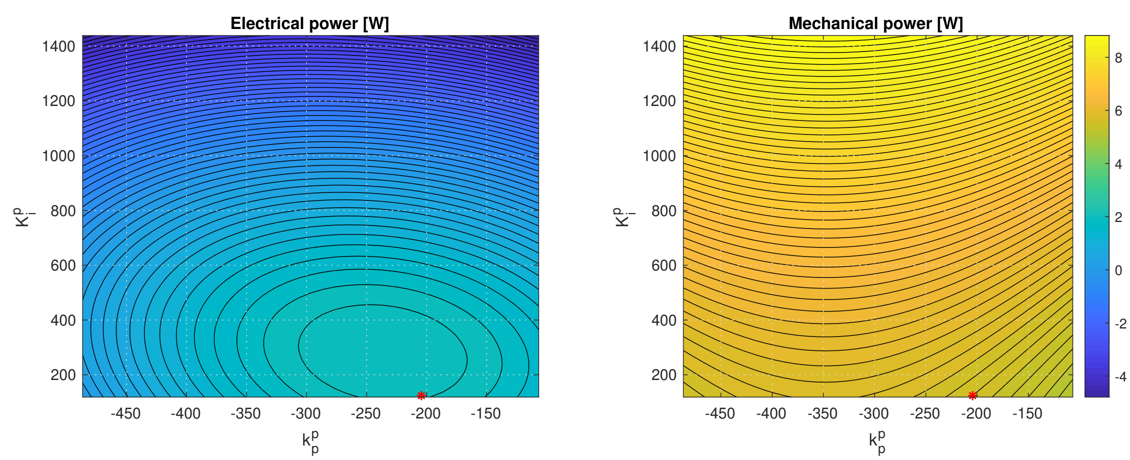

Figure 2-62. Test case 7 - Sensitivity of surge+pitch power absorption to pitch control parameters. A second order 4-D polynomial has been used to fit the multidimensional surface relating the absorbed power to the controller parameters. The red mark shows the controller tuning provided by the optimization.

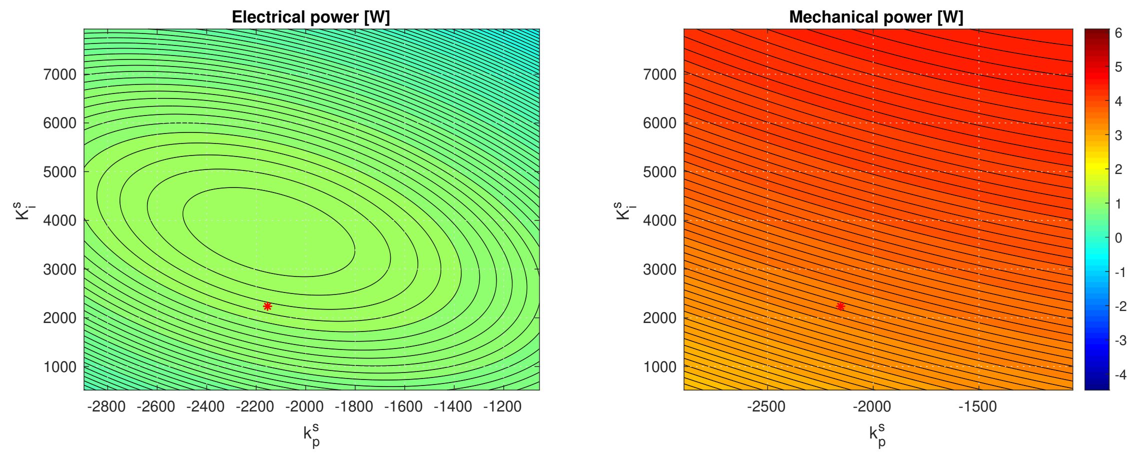

Figure 2-63. Test case 8 - Sensitivity of surge+pitch power absorption to surge control parameters. A second order 4-D polynomial has been used to fit the multidimensional surface relating the absorbed power to the controller parameters. The red mark shows the controller tuning provided by the optimization.

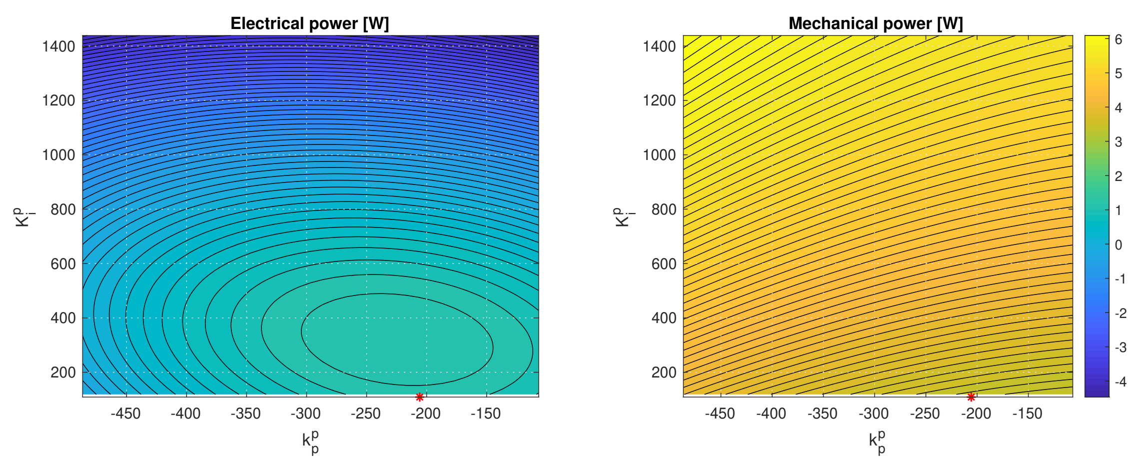

Figure 2-64. Test case 8 - Sensitivity of surge+pitch power absorption to pitch control parameters. A second order 4-D polynomial has been used to fit the multidimensional surface relating the absorbed power to the controller parameters. The red mark shows the controller tuning provided by the optimization.

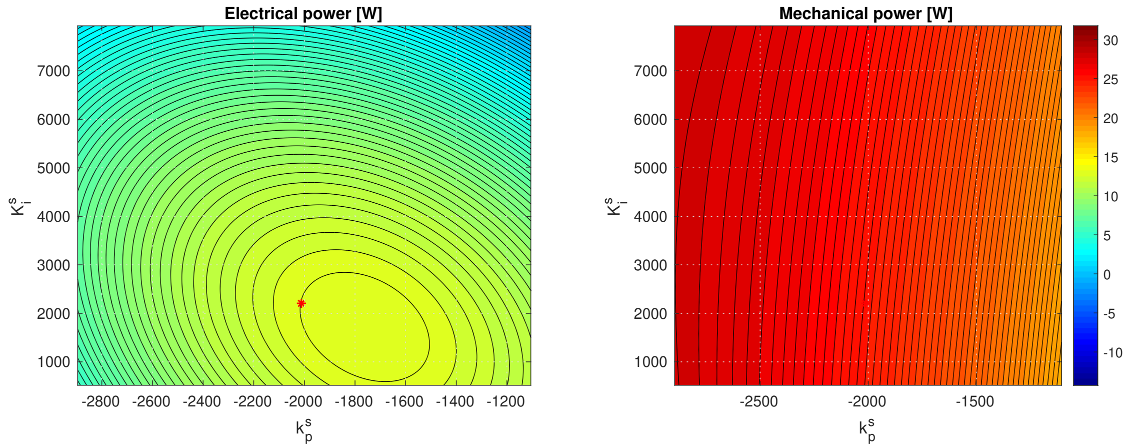

Figure 2-65. Test case 9 - Sensitivity of surge+pitch power absorption to surge control parameters. A second order 4-D polynomial has been used to fit the multidimensional surface relating the absorbed power to the controller parameters. The red mark shows the controller tuning provided by the optimization.

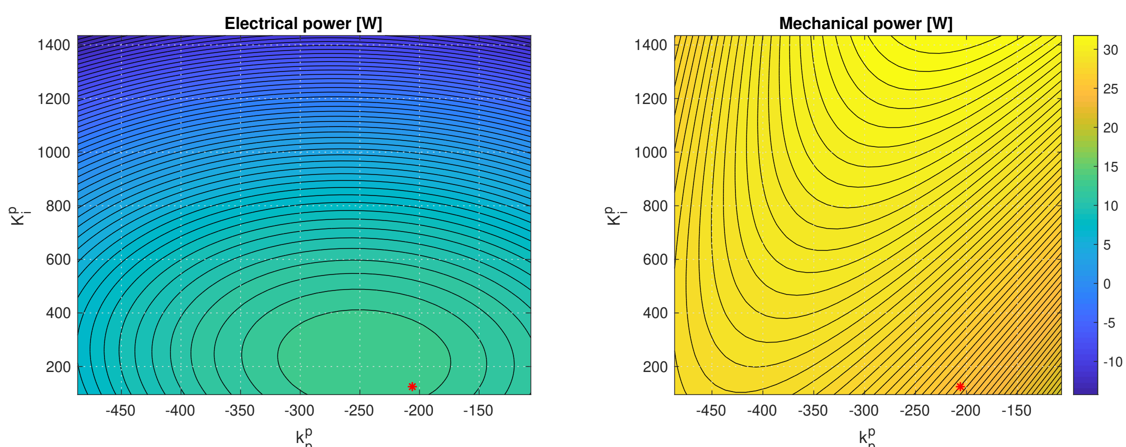

Figure 2-66. Test case 9 - Sensitivity of surge+pitch power absorption to pitch control parameters. A second order 4-D polynomial has been used to fit the multidimensional surface relating the absorbed power to the controller parameters. The red mark shows the controller tuning provided by the optimization.

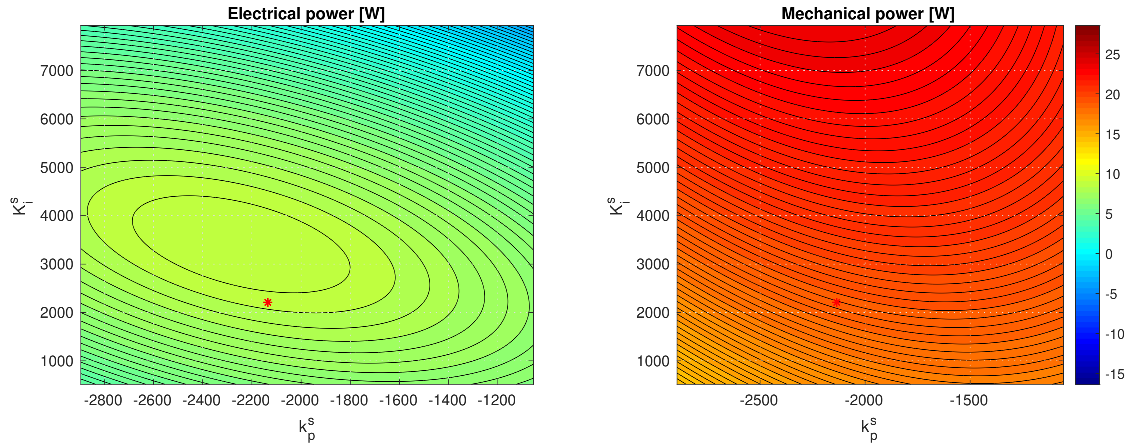

Figure 2-67. Test case 10 - Sensitivity of surge+pitch power absorption to surge control parameters. A second order 4-D polynomial has been used to fit the multidimensional surface relating the absorbed power to the controller parameters. The red mark shows the controller tuning provided by the optimization.

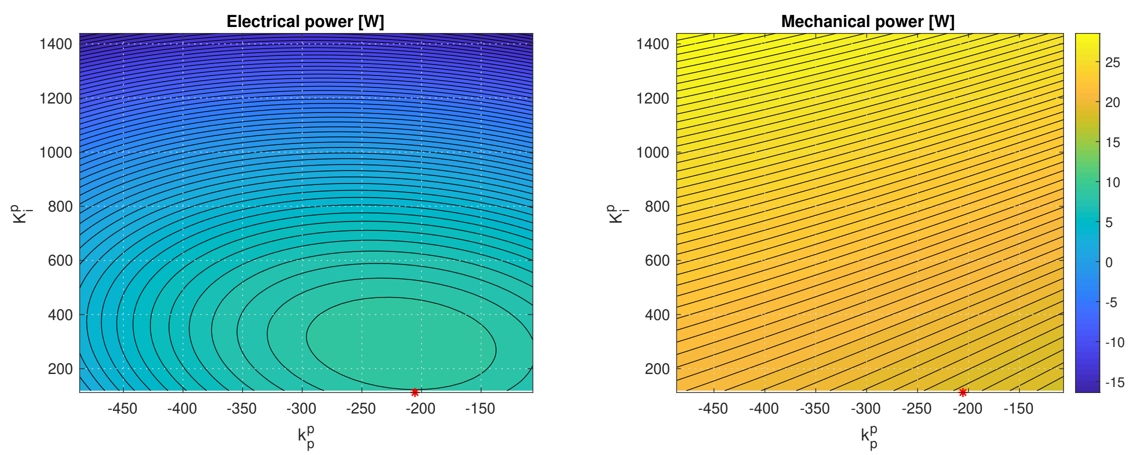

Figure 2-68. Test case 10 - Sensitivity of surge+pitch power absorption to pitch control parameters. A second order 4-D polynomial has been used to fit the multidimensional surface relating the absorbed power to the controller parameters. The red mark shows the controller tuning provided by the optimization.

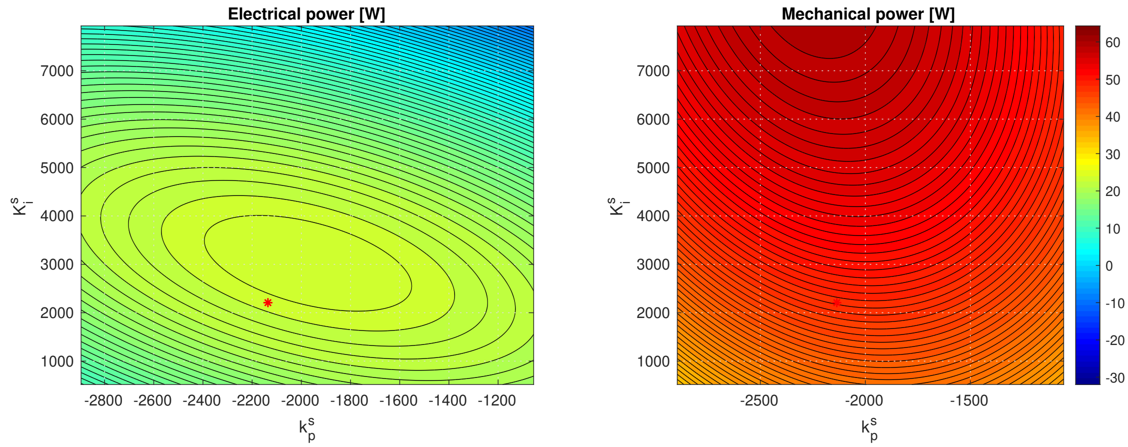

Figure 2-69. Test case 11 - Sensitivity of surge+pitch power absorption to surge control parameters. A second order 4-D polynomial has been used to fit the multidimensional surface relating the absorbed power to the controller parameters. The red mark shows the controller tuning provided by the optimization.

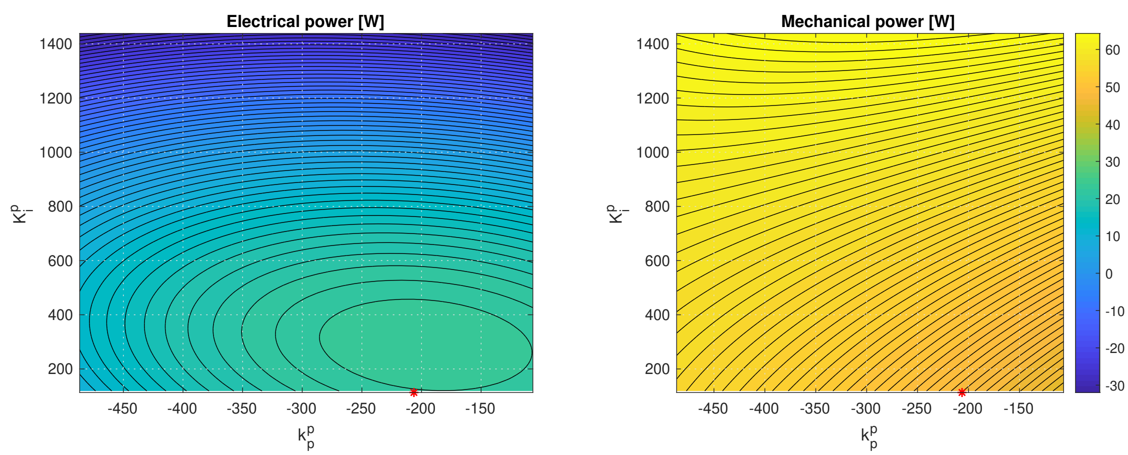

Figure 2-70. Test case 11 - Sensitivity of surge+pitch power absorption to pitch control parameters. A second order 4-D polynomial has been used to fit the multidimensional surface relating the absorbed power to the controller parameters. The red mark shows the controller tuning provided by the optimization.

3. CONTROLLER SELF-TUNING

As discussed in [6], a particular PI gain tuning behaves optimally only at a single frequency. This implies that a WEC operating under PI control in a changing sea state will need to update controller gains to maintain optimal performance. A self-tuning controller was designed in order to update the PI gain tunings of the heave, surge and pitch controllers based on a estimate of the spectral energy density distribution of the incoming wave fields. During these tests, the wave field was intentionally varied to observe controller adaptation.

A linear model of the WEC system was used to estimate the magnitude spectra of the force excitation (Figure 3-1). Here, Z_i is the identified 3×3 impedance model of the WEC (thus $inv(Z_i)$ implies the admittance), H is the 1×3 transfer function relating wave height spectra to excitation force, as $H = \frac{F_{exc}(s)}{\eta(s)}$ where s is the Laplace transform variable, and K_P and K_I are the proportional and integral controller gains (respectively) to be determined. Using WEC velocity spectra $V(\omega)$ and controller force spectra $F_{control}(\omega)$, an estimate of excitation force spectra F_{exc}

$$F_{exc}(\omega) = Z_i^{-1}(\omega)V(\omega) - F_{control}(\omega) \tag{3.1}$$

can be determined for each degree of freedom, heave, pitch and surge. Frequency domain estimates of $V(\omega)$ and $F_{control}(\omega)$ were obtained from real-time experimental time-domain measurements of WEC velocity $v(t)$ and controller force $f_{control}(t)$ by first down-sampling from 1 kHz to 4 Hz and then applying a Hamming window to a buffer of 1024 points (i.e., 256 seconds) and taking the Fourier transform. Subsequent windows overlap by 1020 points, implying that a new window is computed each second. Frequencies between 0.15 and 2 Hz are considered in (3.1), known *a priori* to bound possible wave energy spectra, such that high frequency noise or DC-offsets are not included in $F_{exc}(\omega)$ estimations. Note that H does not need to be known explicitly, and that spectral estimations were found to be largely insensitive to the extent of down-sampling and window length, provided that windows were over sufficient time to estimate the excited frequencies.

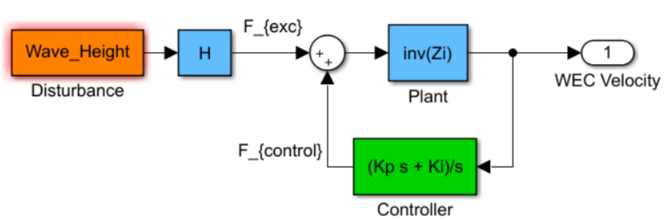

Figure 3-1. Block diagram of the linear system model assumed for controller self-tuning.

By convention, power produced by the WEC has a negative sign. Therefore, using the magnitude $|F_{exc}(\omega)|$, the WEC electrical power P is *minimized* over all frequencies using MATLAB's `fminsearch` algorithm

$$P = \mathrm{Re}\left[\sum_{k=0.15}^{2} (K_e N_g + (R/(N_g K_t))C_k \Omega_k)^{\dagger} \frac{C_k \Omega_k}{N_g K_t}\right] \tag{3.2}$$

by tuning C, the PI controller, of the form

$$C_k = \begin{bmatrix} K_{P,h} - iK_{I,h}/\omega_k & 0 & 0 \\ 0 & K_{P,s} - iK_{I,s}/\omega_k & 0 \\ 0 & 0 & K_{P,p} - iK_{I,p}/\omega_k \end{bmatrix}. \tag{3.3}$$

where, at a single frequency k,

$$\Omega_k = |F_{exc}(\omega_k)|/(Z_{i,k} - C_k) \tag{3.4}$$

For the self-tuning controller, C is diagonal (i.e., no cross-coupling between degrees of freedom) so that there are 6 independent parameters: K_P and K_I for each degree of freedom heave (h), surge (s), and pitch (p) to maximize (3.2). The $'$ implies the vector transpose and is necessary to maintain appropriate dimensions for the subsequent multiplication. Diagonal matrix N_g is the gear ratio between the WEC and the power-take-off (PTO) (see (3.5)).

$$N_g = \begin{bmatrix} N_{g,h} & 0 & 0 \\ 0 & N_{g,s} & 0 \\ 0 & 0 & N_{g,p} \end{bmatrix} = \begin{bmatrix} 12.47 & 0 & 0 \\ 0 & 12.47 & 0 \\ 0 & 0 & 3 \end{bmatrix} \tag{3.5}$$

Similarly, R is electrical resistance in the PTO coils (Ohms), K_t the motor torque constant (Nm/Amp), K_e is the motor back-EMF (V/Nm). All are 3×3 diagonal matrices and the values for each DOF are nominally the same for these parameters as a common type of motor was used for each: $K_t = 6.17$, $K_e = \frac{2}{3}K_t$, and $R = 0.5$. As such, (3.2) is simply the product of voltage (left term) and current (right term).

The self-tuning controller was also attempted with surge and pitch degrees of freedom locked out (and their controllers disabled). Physically, heave response is approximately independent from surge and pitch responses, and in terms of the model, the formulation is functionally unchanged, although the 3×3 system can be reduced to a 1×1 system in heave alone.

Table 3-1. Wave cases considered with self-tuning controller

Wave ID	Test IDs	Degree of Freedom
2R	233, 248	Heave only and all DOF
4R	234, 249	Heave only and all DOF
8R	235, 250	Heave only and all DOF
2R-4R-8R-4R-2R	316	Heave only
2LA	298	All DOF
4LA	293	All DOF
6LA	236, 271	Heave only and all DOF
7LA	262	All DOF
8LA	294	All DOF
9LA	299	All DOF
11LA	240, 252	Heave only and all DOF
2A-6A	238, 253	Heave only and all DOF
2A-10A	239, 251	Heave only and all DOF
CDIP 1/12 scale	247, 266	Heave only and all DOF
CDIP 1/9 scale	265	All DOF
Umpqua	272	All DOF

Table 3-2. CDIP buoys utilized in MASK3 test

ID number	Location	Lat/long.	Notes
CDIP225	Kaneohe Bay, Oahu, Hawaii	21°28'38.5"N, 157°45'20.8"W	Wave Energy Test Site (WETS)
CDIP139	Umpqua, OR	43°46'18.5"N, 124°32'58.2"W	PACWAVE site

3.1. EXPERIMENTAL EVALUATIONS

3.1.1. Changing sea states

Two approaches were used in assessing the performance of self-tuning controllers in changing (non-static) sea states. First, we consider measured data from a deployed ocean buoy (Section 3.1.1.1). These represent scaled versions of realistic sea state variations. Next, we consider synthetic sea states composed by concatenating multiple idealized spectral realizations (Section 3.1.1.2). These represent unrealistically rapid and extreme variations in sea-state intended to test the self-tuning procedure. The test matrix of wave cases run with the self-tuning controller is presented as Table 3-1.

3.1.1.1. CDIP225, May 2019

Methods Two CDIP buoys were considered for this study. These buoys are listed in Table 3-2. The CDIP buoys perform spectral analysis on 24 minute and 40 second windows. Every hour, two PSDs are reported, this allows for 3 minutes and 20 seconds of data upload time.

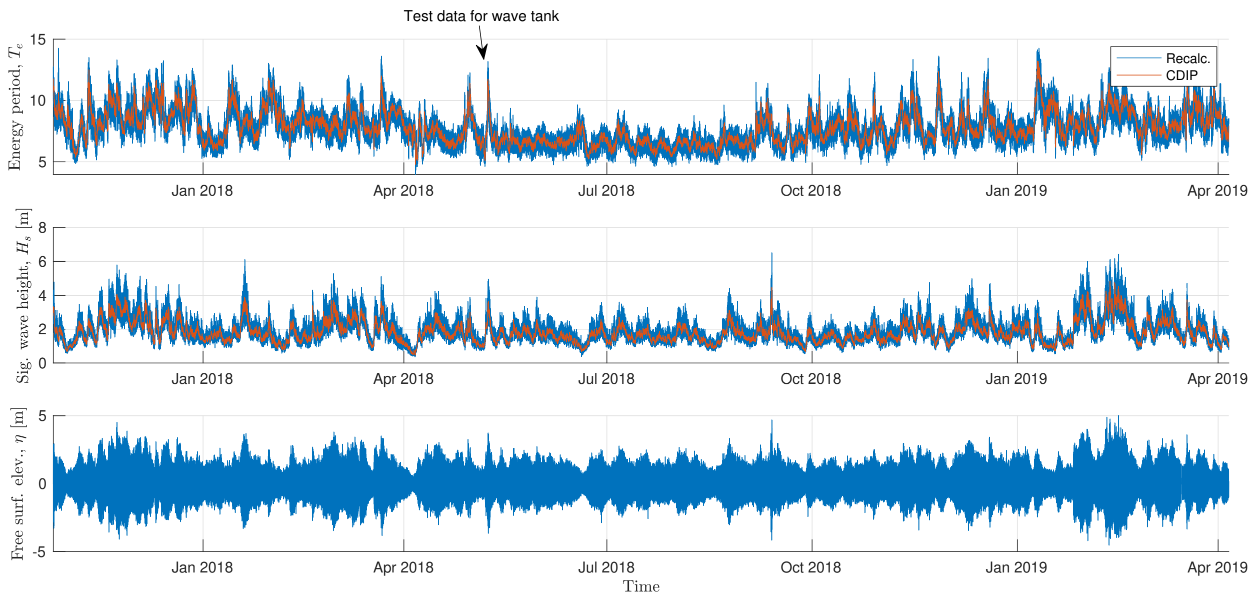

Figure 3-2. CDIP buoy data (deployment 3).

Table 3-3. CDIP225 May 8th, 2018 model scale experiments.

λ	1	1/9	1/12
Test length [hr]	24	8.0	6.9
Mean sig. wave height [m]	2.793	0.310	0.233
Mean energy period [s]	9.17	3.06	2.65
Max wave height [m]	7.41	0.82	0.62
WEC diameter [m]	1.76	15.84	21.12
WEC mass [t]	0.858	1876	5136

In one case, CDIP buoy data was assessed to find a historical record in which the sea state (in particular the spectral energy location) changed rapidly.

Considering roughly 2.5 years of displacement data available from the CDIP225 buoy located at the Wave Energy Test Site (WETS) in Kanehoeh Bay, data from for the 24 hours starting at midnight on May 8th, 2018 were selected. This point in the dataset is shown with an arrow in Figure 3-2. This data was selected for a the rapid change in energy period.

The time series and spectral characteristics (energy period and significant wave height) for the 24 hours of full scale data used in the experiment are shown in Figure 3-3. This data was used to conduct two experiments at 1/12 and 1/9 scale. The average spectral parameters, maximum wave height, and test length for these two experiments are shown in Table 3-3. Table 3-3 also shows the WEC device diameter and mass.

A time history comparing a section of the tests with the measured CDIP data is shown in Figure 3-4. Table 3-4 shows a comparison of the spectral parameters for the CDIP225 $\lambda = 1/12$ wave calibration test (Exp 093). The spectral energy densities are compared in Figure 3-5.

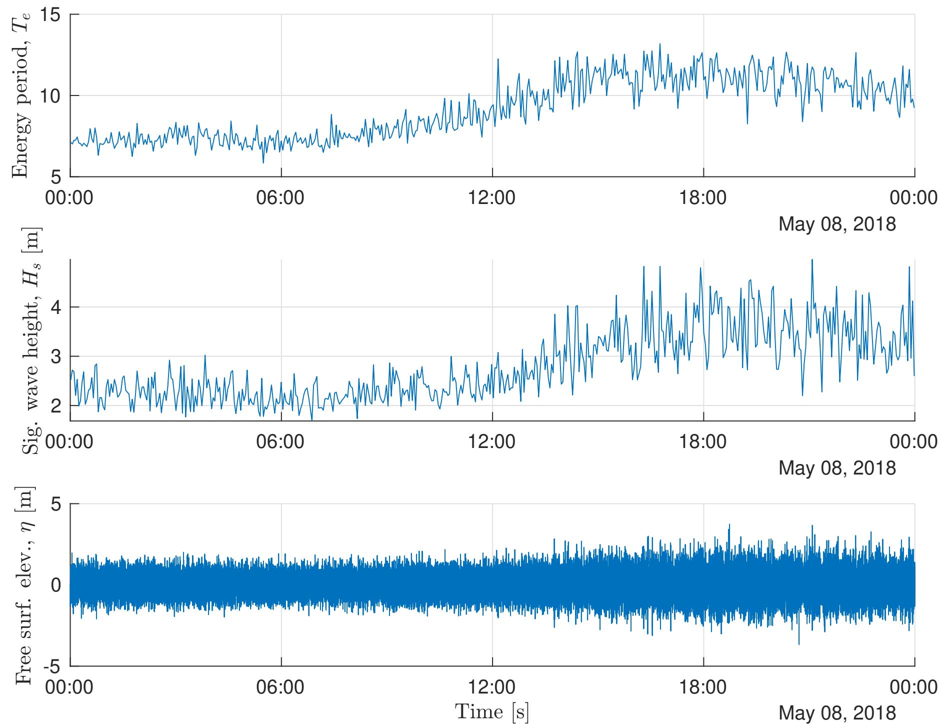

Figure 3-3. Wave time series selected for experiment (full scale).

	H_{m0} [m]	T_e [s]
Target (CDIP)	0.126	4.059
Wave tank mean	0.118	4.363
BUOY02	0.117	4.346
BUOY04	0.119	4.320
BUOY05	0.118	4.324

Table 3-4. CDIP225 case spectral parameter comparison (Exp 093).

Results The spectrogram of wave spectra is shown with time series of controller gains in heave, surge, and pitch to show the adaptation over time. Contrasting wave states at times 7000 s (wave state 1) and 24600 s (wave state 2) are then examined in detail.

As the energy in the waves increases, the controller applied damping (K_P) increases. The dominant period of the increasingly excited waves lengthens towards WEC resonance in heave, and the expected reduction in K_I gain demonstrates the correct adaptation.

A comparison between estimated excitation force spectra using (3.1) and excitation force spectra calculated from measured wave height spectra at WEC location during the calibration study as

$$F_{exc,actual}(\omega) = H(\omega)\eta(\omega) \tag{3.6}$$

where H is the identified transfer function between input wave height to output excitation force. This

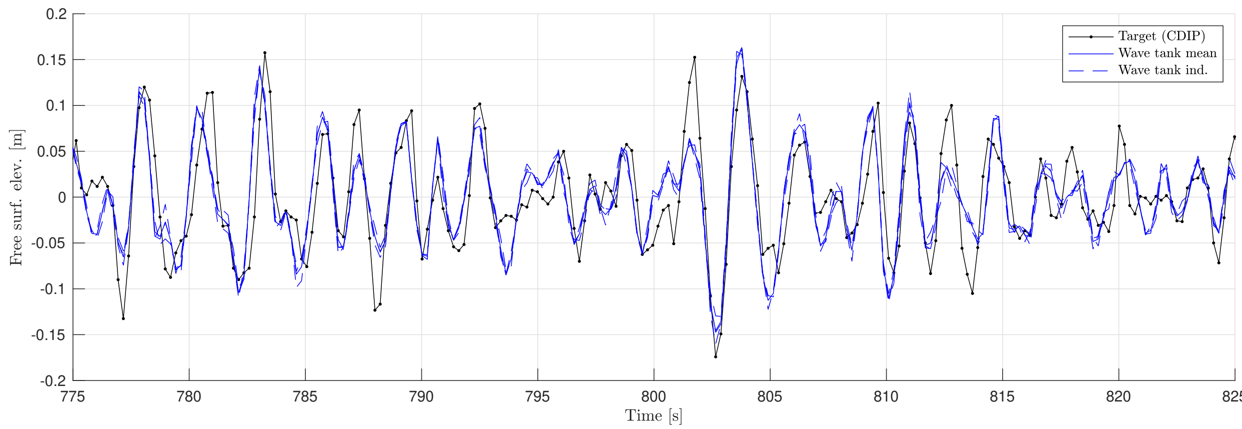

Figure 3-4. Segment of time history for CDIP225 $\lambda = 1/12$ wave calibration (Exp 093).

estimate from measured wave height is compared to the estimate used by the self-tuning controller from (3.1) (which does not use a measurement of wave height). The comparison is given as Figure 3-7. Both estimates agree closely: the elevation in spectral energy at the decreased frequency for the second wave state is clearly seen in both estimations, although (3.1) tends to slightly over-predict excitation force at higher frequencies (0.8 to 1 Hz).

The resulting gain tuning for each of these wave states can be compared to a post-calculated grid over which the estimated device power (see (3.2)) was calculated for a grid of gains. The result describes a surface of power absorbed by the WEC as a function of gain selection, where the optimal WEC power production will be indicated by a minimum. The location of the self-tuning controller gain is shown as the black dot, and is near the minimum of the power surface (indicating a maximized WEC power production) for all degrees of freedom for both wave states (Figure 3-8). Note that the surface has small gradients near the minimum: this implies both that an optimizer may not reliably converge precisely to the minimum, and that, given the flatness of the surface near the minimum, system power is not sensitive to gain selection within this region.

3.1.1.2. Concatenation

Methods In a second set of tests, idealized spectra were used. For these tests, 5 min realization of the two sea states were constructed and then concatenated back to back. This approach effectively produces a step change in terms of the sea state. While totally unrealistic for a real ocean deployment, this approach is attractive as a test of self-tuning capability, allowing generalization results.

Practically speaking, only a very small subset of ocean measurement buoys record time domain displacement measurements - by far the majority of buoys record only spectral measurements, usually at a rate on the order of 3 hr. Given the rarity of time-domain measurements, it is likely that the targeted deployment site of a WEC will be at a location where time domain displacement measurements are not available. This concatenation approach allows for changing sea state experiments to be synthetically generated. The rate change produced by this approach is entirely arbitrary. At one extreme, we can look at a strong step change

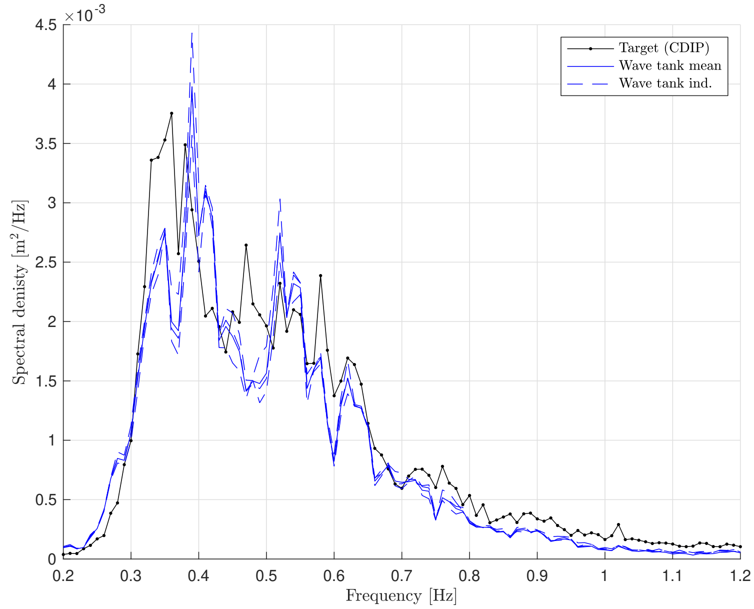

Figure 3-5. Spectral energy density comparison for CDIP225 $\lambda = 1/12$ **wave calibration (Exp 093).**

that is physically unrealistic. At another, if for example spectral data is available at 30 min intervals, we can approximate this change closely by discretizing the changing wave state into several transitions.

The timescales relevant for changes in sea states ($\mathcal{O}$(hours)) are sufficiently large compared to the timescales relevant for measurement, estimation, and retuning of a WEC controller ($\mathcal{O}$(seconds)) so as to make the problem trivial in most cases,[1] There remains some potential value in understanding how well devices can adaptively tune.

Figure 3-9 shows the results from a wave calibration test (Exp 088) in which the sea state is varied between 2A and 6A every 5 min. From Figure 3-9, we can clearly see the distinct difference between sea state 2A and 6A in both the time history and power spectrogram.

Results As an example of concatenated wave series, the spectrogram of wave spectra is shown for Test ID 251 in Figure 3-10, alternating wave state 2A to 10A over 5 minute intervals, with time series of controller gains in heave, surge, and pitch to show the adaptation over time. Contrasting wave states at time 250 s and 1200 s are then examined in detail.

Note that in this case, the peak wave period of state 2A is 1.58 s (0.63 Hz), which is near the WEC resonant frequency in heave. As expected, the K_I gain in heave is near zero during this wave state. The explicitly known transition time of a concatenated wave series allows consideration of the gain adaptation time. The wave state transition is implemented at multiples of 300 s, and the gain adjustment begins approximately 200 s after this. The delay is due to two factors. Firstly, inspection of the spectrogram indicates that the commanded wave transition takes approximately 60 s to manifest in the basin. Second and more

[1] This may not be so trivial if, for example, retuning of the WEC device is accomplished by some physical reconfiguration with a longer adaptation time (e.g., ballasting).

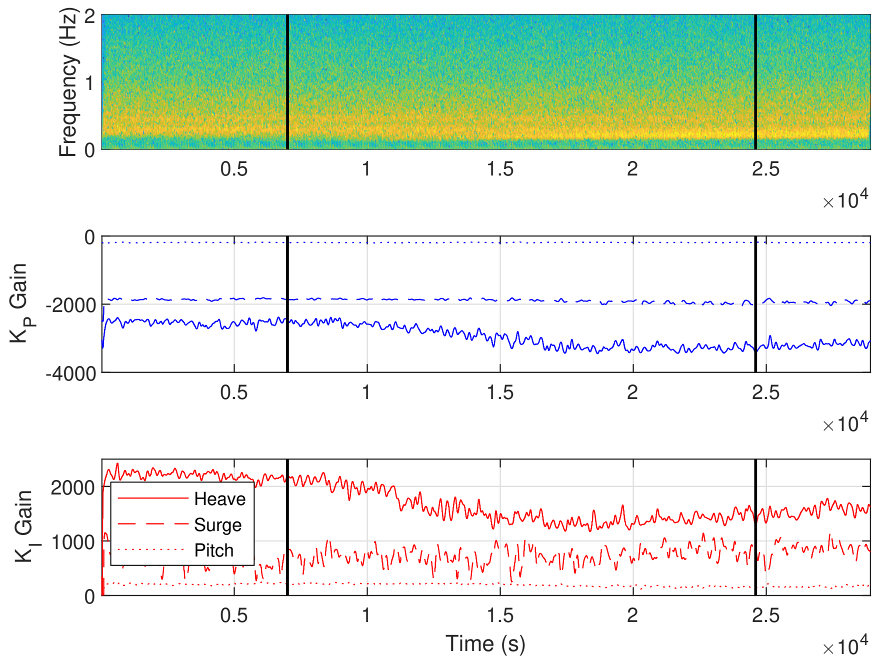

Figure 3-6. Self-tuning controller gains for the CDIP225 wave state.

significantly, the window length of 256 s will only fully reflect the next sea state after this length of time, and the interim gain will be calculated based upon an average of the two wave states.

The estimated spectra predict excited frequencies well, but tend to slightly under-predict the amplitude of excitation for the most excited frequencies (0.2 to 0.4 Hz; Figure 3-11). In contrast, estimated amplitudes are slightly over-predicted for less excited frequencies (i.e., 0.5 to 0.6 Hz).

The gain surface for this wave series is given as Figure 3-12. Note that the indicated self-tuning controller gains lie near the minimum of the post-calculated surface, which is again flat in the surrounding region, for each wave state and degree of freedom. Also, note that the minima location changes more significantly for heave than for surge and pitch, indicating the latter modes to be less sensitive to this changing sea state.

3.1.2. Bimodal seas

Methods In many locations, bimodal seas, composed of distinct wind and swell components with substantial spectral separation, are the norm. This is of particular interest in the U.S., since such sea states are extremely common in the Pacific Northwest along the coasts of Oregon and Washington, which is considered an attractive wave energy resource for development.

Thus, wave data from the Umpqua, OR CDIP buoy (CDIP139) was to investigate performance in bi-modal seas. Four hours of data at full-scale from 10-Apr-2009 (06:40:45 to 10:40:45) was selected for scaled replication in the wave tank. Figure 3-13 shows the spectral energy density of the sea state at full scale.

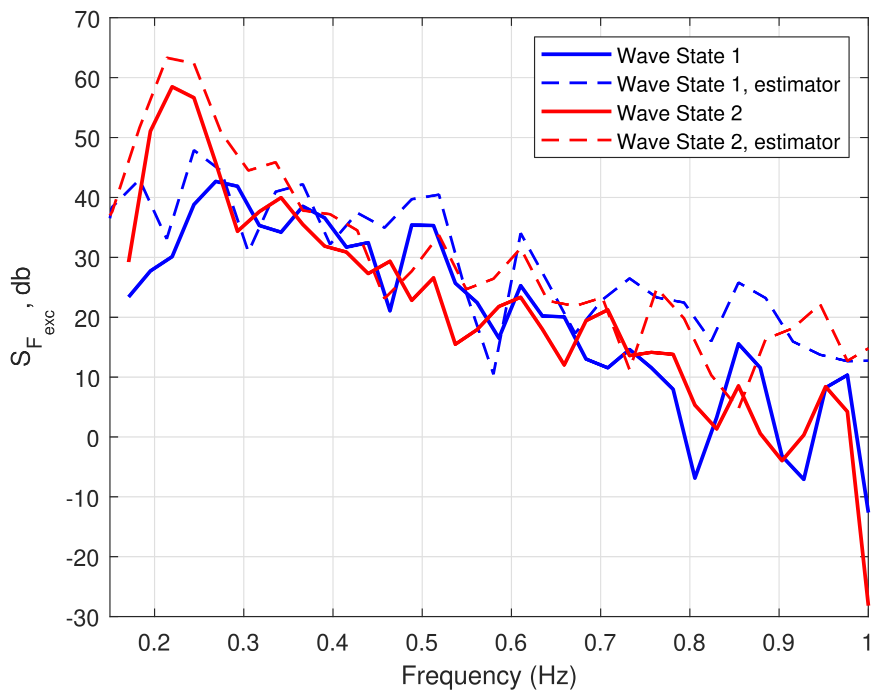

Figure 3-7. Estimates of excitation force spectra from wave height measurements (solid lines) and as estimated by the self-tuning controller (dotted lines) for two contrasting wave states in the CDIP225 wave series.

The spectrogram of CDIP139 as recreated in the wave basin, a bimodal sea-state, is given as Figure 3-14. Unlike the concatenated or gradually changing sea-state, the bimodal sea-state does not significantly change in time. As such, the gain adjustment is not expected to vary significantly in time, and only one time instance at 2250 s is selected for analysis.

Results The excitation force spectra as estimated and calculated (using the same method as Figure 3-11) at time 2250 s show that the estimated spectra consistently slightly over-estimate the 0.24 Hz peak while under-estimating the second mode at 0.39 Hz, though both the spectral calculation methods capture the bi-modal features of the wave state.

Similar to the other presented wave cases, the gain surface is flat near the minima, and the self-tuning gains approximate these minima. This is illustrated in Figure 3-16. It does not appear that the the bimodal sea state had a large effect on the shape of the power surface or the effectiveness of the self-tuning controller.

3.2. DISCUSSION

The six-parameter self-tuning controller was implemented successfully in real-time with 1 kHz sampling. The solutions for optimal gains converged quickly once the buffer used for spectral estimate calculation was filled. It is evident, particularly for concatenated wave states, that the 256 s buffer window appears to

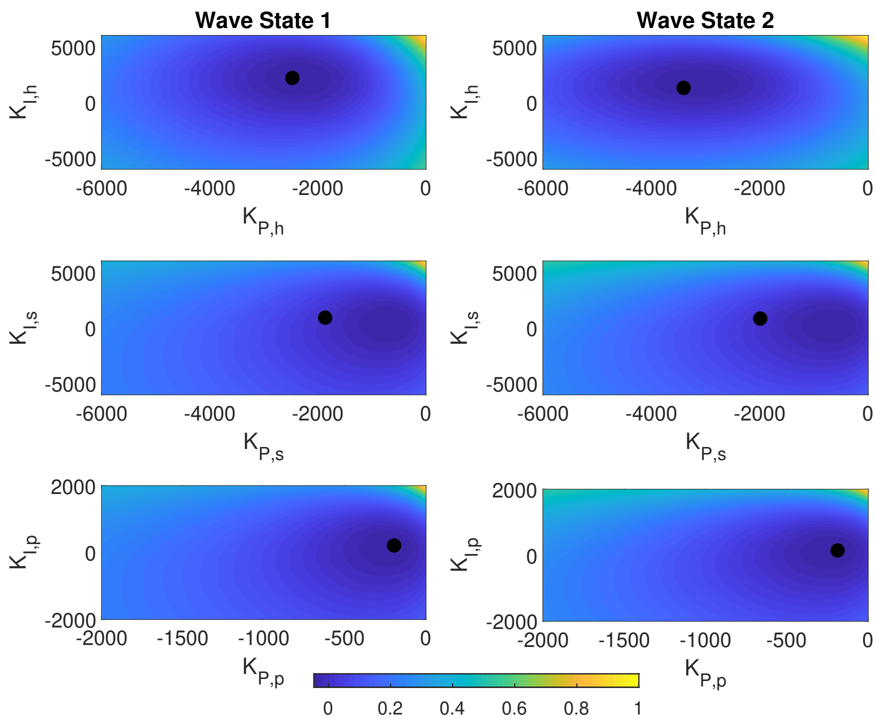

Figure 3-8. The WEC power surface as a function of gain tuning for each degree of freedom and wave state for the CDIP225 wave. The color bars are normalized by the maximum absorbed power such that they are common between degrees of freedom.

significantly delay gain tuning. While it is likely possible to reduce this window time, the spectral estimate is robust and accurate, tuning times are effective for wave states that changed over longer, more realistic, time scales, and convergence to optimal gains. Since the convergence with this configuration is on the order of minutes, this is considered more than adequate for sea states changing over realistic time scales (hours to days), as evidenced particularly by the CDIP225 sea-state.

Converged self-tuning gains consistently approximate the optimal gains for each degree of freedom and wave state. However, there are some consistent trends in approximation errors. Generally, K_I gains for each degree of freedom are nearly optimal. As the surface in the K_I direction appears to have steeper gradients, it is not unexpected that more precise convergence occurs for this parameter. Surge, K_P gains are consistently a larger negative value than optimal. By similar reasoning, the relatively shallow gradient in the negative K_P direction from the minima may explain this inconsistent convergence. The flatness of the surface implies that these errors have minimal effect on actual power production, but nonetheless suggests a shortcoming of the optimization approach that can be improved. In particular, `fminsearch` is a gradient-free optimizer. While this adds robustness in the presence of signal noise or non-smooth optimization surfaces, the convex K_P, K_I power surface suggests that a gradient-based optimizer may yield performance improvements. The flatness of the electrical power surface as a function of gain tuning in all examined wave cases suggests that this may be a robust feature of this device that is not expected to vary significantly with wave state.

With regard to software implementation, in order to run in real-time, the optimization must converge

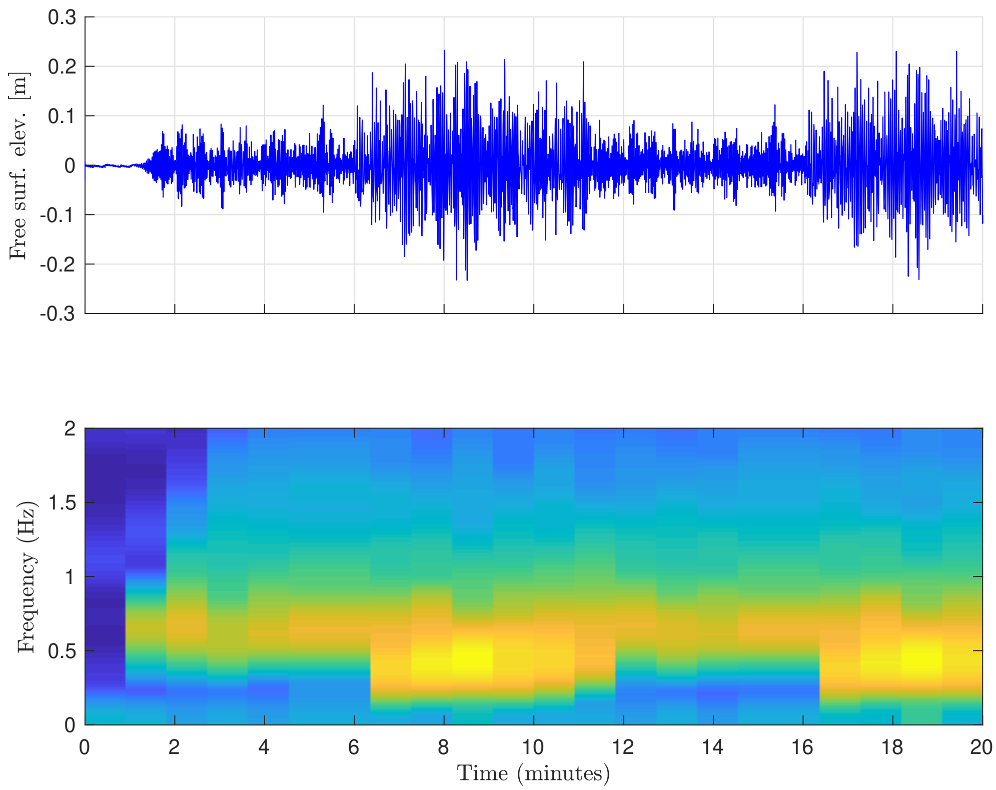

Figure 3-9. Free surface time history (top) and power spectrogram (bottom) for concatenated changing sea state (Exp 088). Sea state alternates between 2A and 6A.

before the spectra are updated. This somewhat limits the potential gain adjustment time. Further, is the optimization problem is not convex, convergence over any reasonable interval may not be possible in real-time. In this instance, a look-up table correlating pre-calculated gains to the estimated sea-state could instead be employed. While the PI controller relies on feedback, the `fminsearch` gain-tuning procedures (and the suggested table look-up or gradient-based optimizers) are open-loop, using the model of system intrinsic impedance. Any inaccuracy in this model, or a change in the system over a long deployment will reduce the efficacy of this method. Assuming the gain optimization problem remains sufficiently convex, this limitation could be addressed by incorporating an extremum-seeking controller using power feedback to adjust model-informed gains to account for modeling error or a change in system impedance over time.

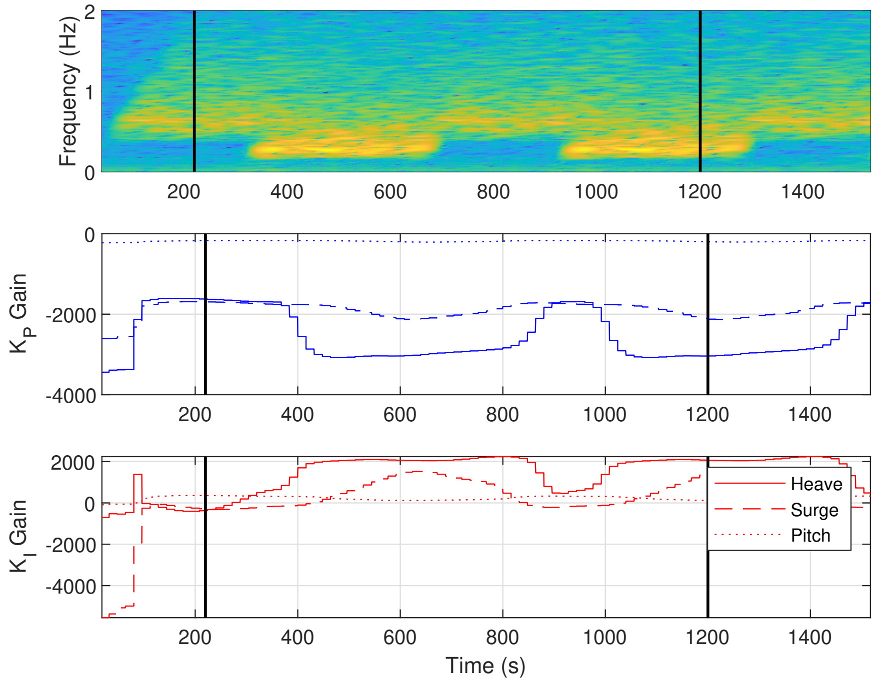

Figure 3-10. Self-tuning controller gains for changing 2A-10A wave state.

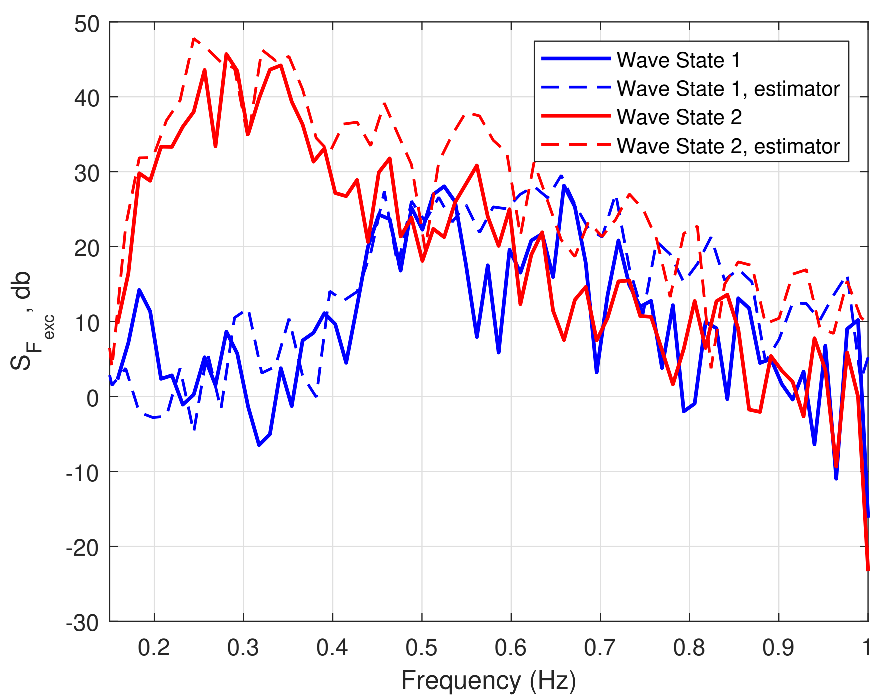

Figure 3-11. Comparison of excitation force spectra as estimated by the self-tuning controller to spectra calculated from wave height measurements for concatenated wave states 2A - 10A.

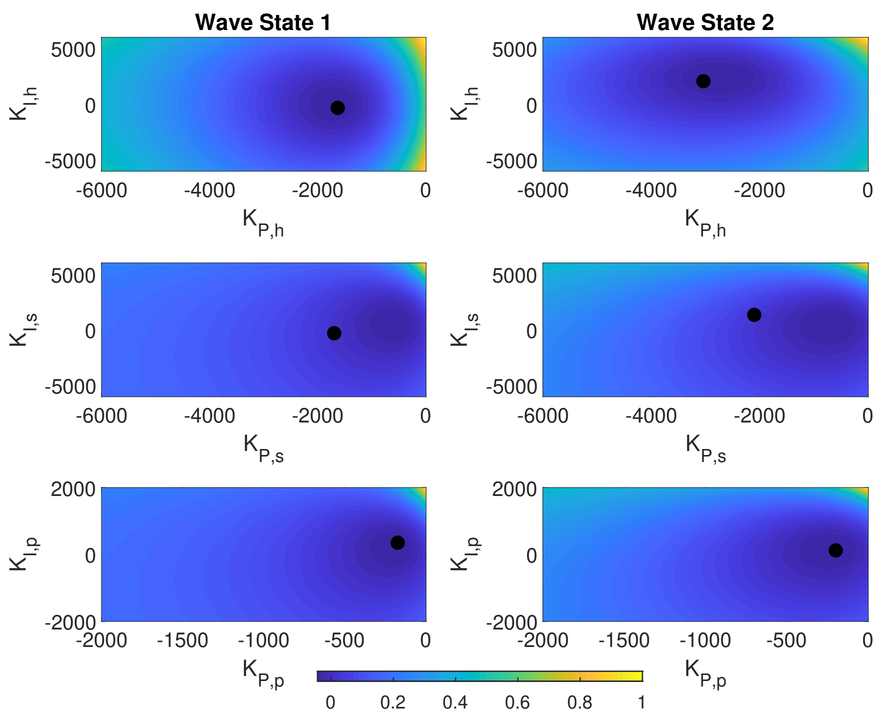

Figure 3-12. The WEC power surface as a function of gain tuning for each degree of freedom and wave state for the 2A-10A concatenated wave. The color bars are normalized by the maximum absorbed power such that they are common between degrees of freedom.

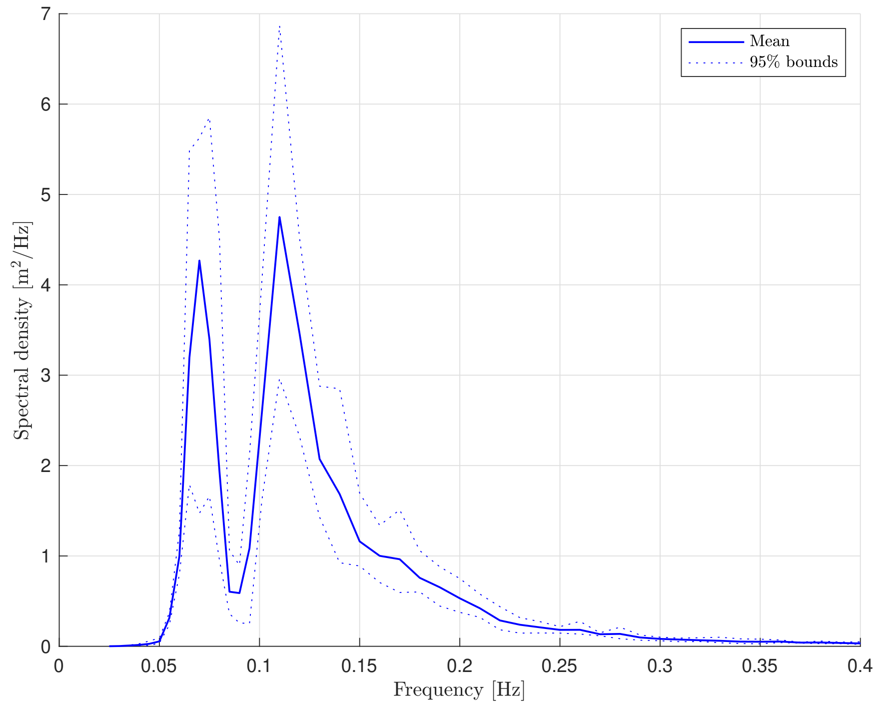

Figure 3-13. Bimodal spectrum from CDIP139 on 10-Apr-2009 (06:40:45 to 10:40:45).

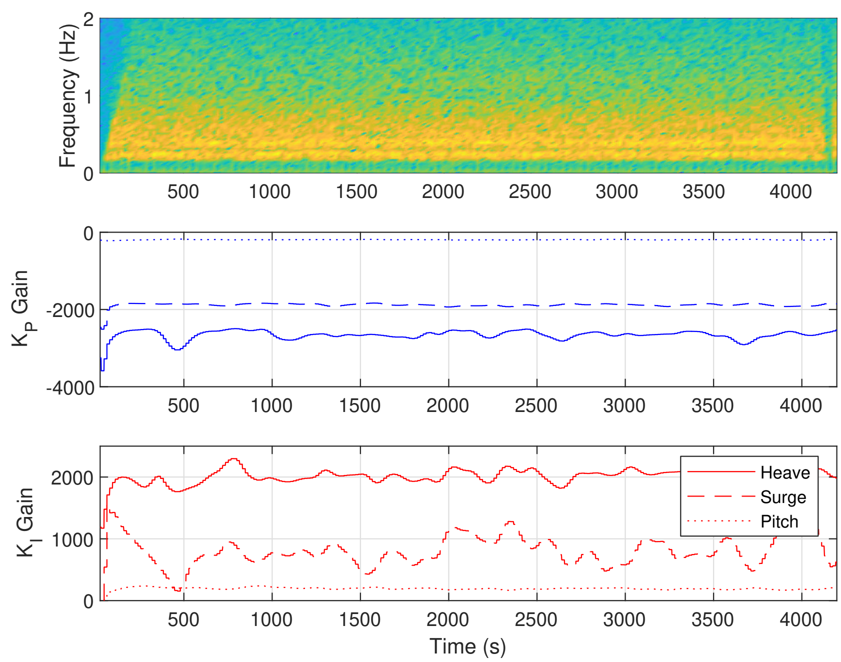

Figure 3-14. Self-tuning controller gains for bimodal CDIP139 sea state.

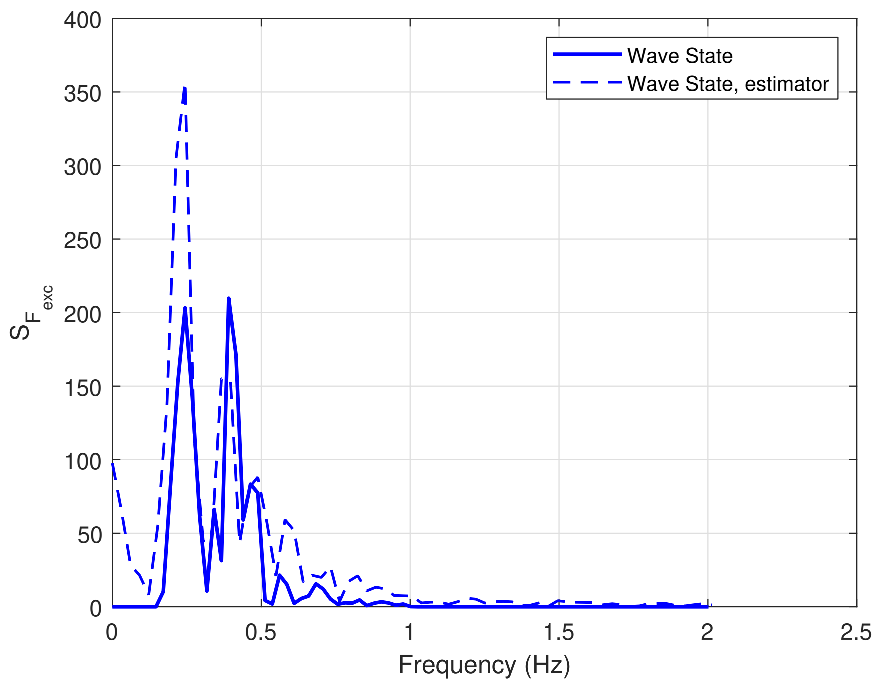

Figure 3-15. Comparison of excitation force spectra as estimated by the self-tuning controller to spectra calculated from wave height measurements for wave state CDIP139.

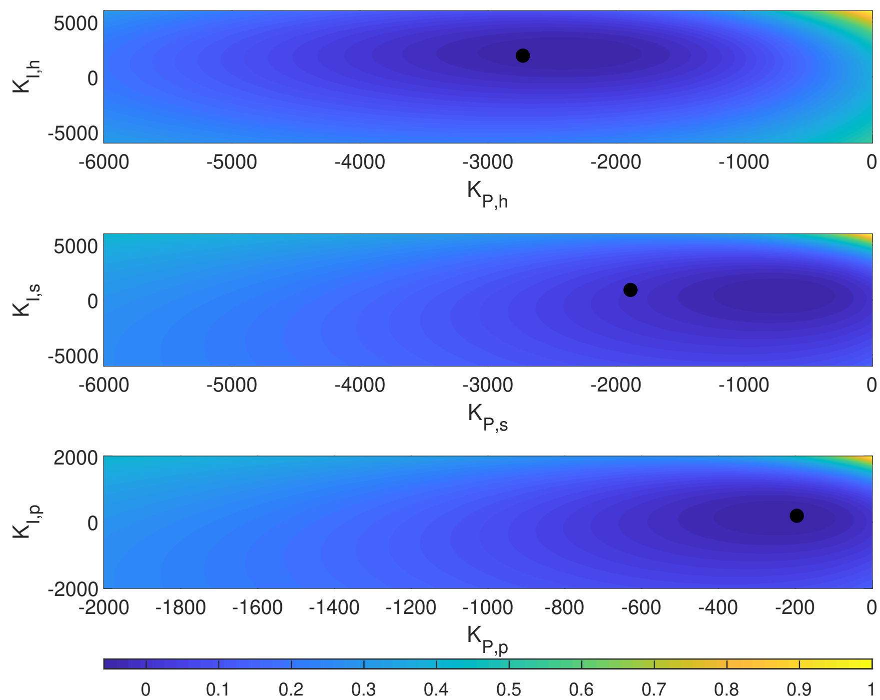

Figure 3-16. The WEC power surface as a function of gain tuning for each degree of freedom for the bi-modal wave. The color bars are normalized by the maximum absorbed power such that they are common between degrees of freedom.

4. SYSTEM IDENTIFICATION WITH WAVELETS

Based on work with a private WEC developer, a new procedure for executing system identification (SID) testing has been designed and tested with the WaveBot. For the deployment of their WEC device, the private developer will need to conduct SID tests. These will be performed initially in the Columbia River. At this location, the private developer will have only a limited size generator, not capable of providing large amounts of power and energy to perform extended SID tests that are more easily conducted in the wave basin. To alleviate this issue, Sandia has suggested using wavelet signals for the SID tests. This process has now been tested on the WaveBot, for which an accurate model for system dynamics is already know and can be compared to as a "ground truth." This component of testing will thus directly support the private developer in their upcoming deployment and will be disseminated through publication for wider usage among industry. The use of wavelets is particularly appealing because they can be tuned to excite a specific frequency range, corresponding for example to a given seas state. Therefore, they are a tool for efficiently deriving a model for controller tuning for full-scale devices.

In tests 151, 152, and 153, wavelets were conducted on the heave actuator with the pitch and surge modes locked out. Each of these experiments contains a 3×3 test matrix by varying the wavelet center frequency as $f_0 \in [0.2857, 0.4000, 0.6329]$ Hz and the bandwidth scaling factor as $s \in [5, 10, 20]$. Thus, each experiment contains nine wavelets[1]. Using this matrix of center frequencies and bandwidth scaling factors, the three experiments with run with different amplitudes (controller gains of 1e3, 2e4, and 4e3 for test 151, 152, and 153, respectively).

Figure 4-1 shows the experiments 151, 152, and 153 (top, middle, and bottom plots, respectively). Using each of these individual 26 wavelets, a 2nd-order transfer function was estimated. Each of these local linear models are shown in Figure 4-2. These can be thought of each as local linear models, each with a regime (in terms of bandwidth, center frequency, and amplitude) that it is designed to cover. There is some visible variation amongst the models, but they are generally quite close. The line colors in Figure 4-2 distinguish the controller gains (blue: 1e3, green: 2e3, magenta: 4e3). It is clear that the center frequency and bandwidth scaling factors play as large of a role in determining the model as the amplitude of the input.

Taking the natural frequencies of the models shown in Figure 4-2, we can produce the histogram shown in Figure 4-3. Here, we can see that the variation amongst these models creates a set of natural frequencies with the range $0.51 \leq f_n \leq 0.64$ Hz. The distribution is slightly biased toward the high frequencies and a mean value of 0.59 Hz.

[1]Test 153 was stopped early due to dangerous overtopping during the final wavelet ($f_0 = 0.6329$ Hz, $s = 20$)

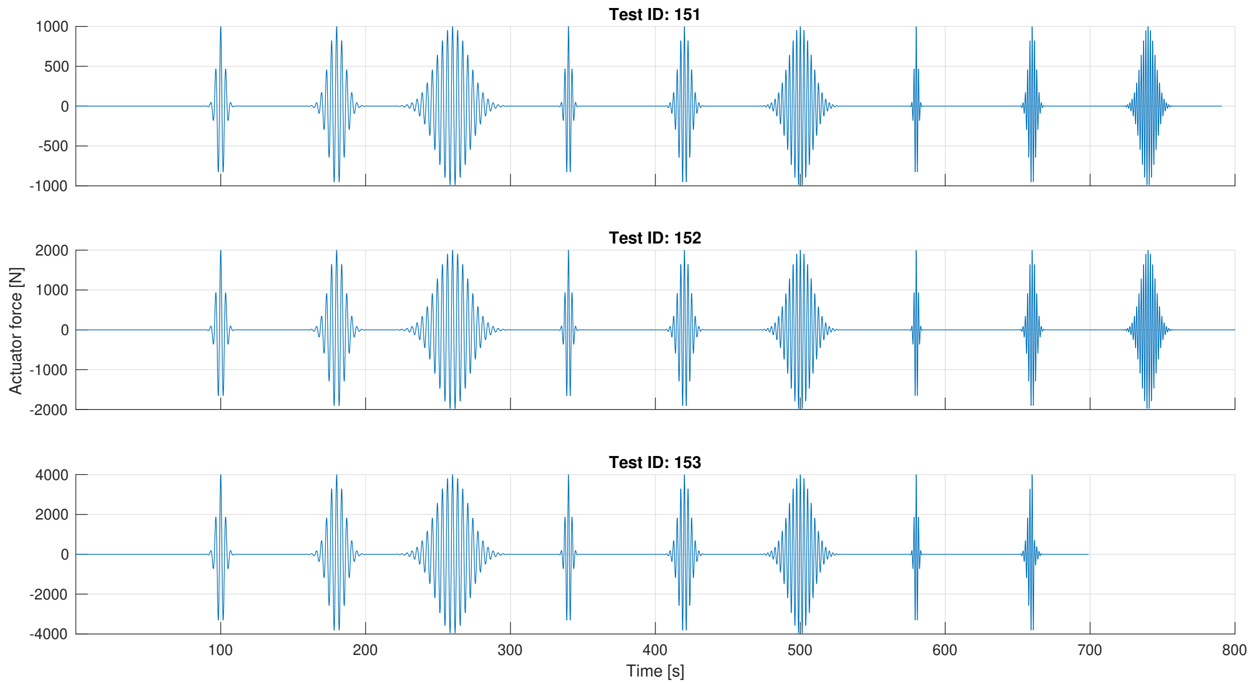

Figure 4-1. Heave only wavelet applied force.

Figure 4-4 shows a subset of the models from Figure 4-2. Here, models with $f_0 = 0.286$ Hz and $s = 5$ are shown for the three controller gains of 1e3, 2e3, and 4e3. We can see that response increase as the amplitude of input increases, which is consistent with a Coulomb friction dominated system.

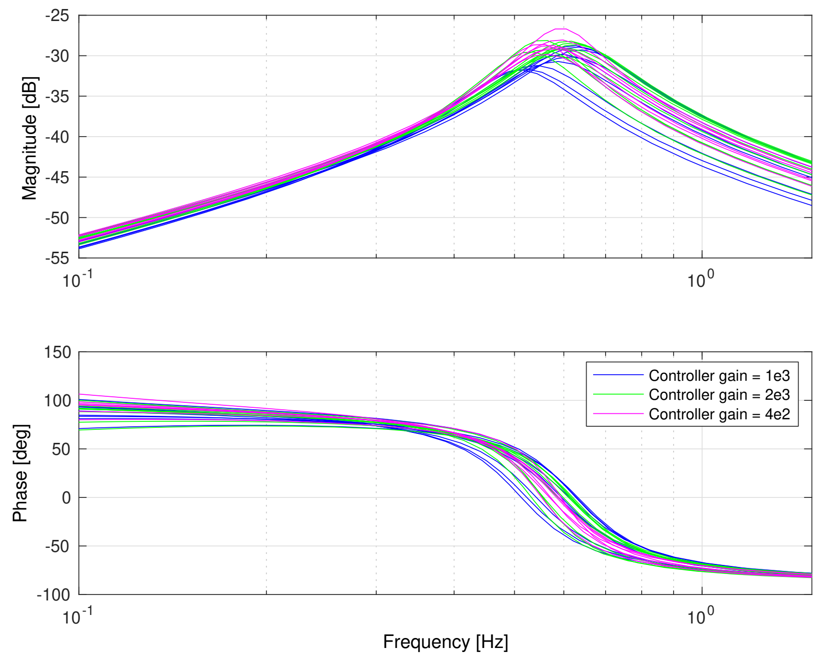

Figure 4-2. Transfer function models obtained from 26 wavelets. Controller gains are shown by blue: 1e3, green: 2e3, magenta: 4e3.

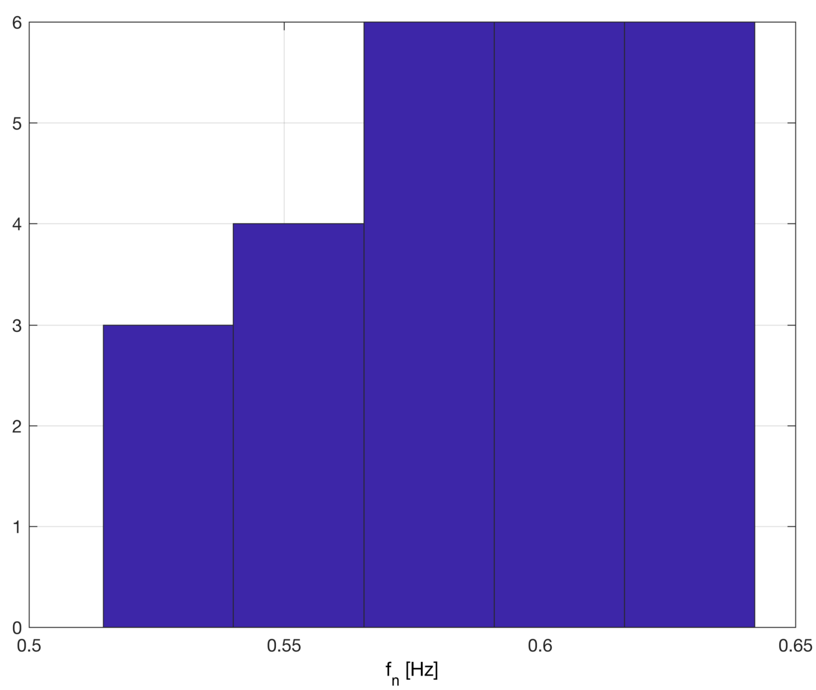

Figure 4-3. Distribution of natural frequencies from transfer function models obtained from 26 wavelets.

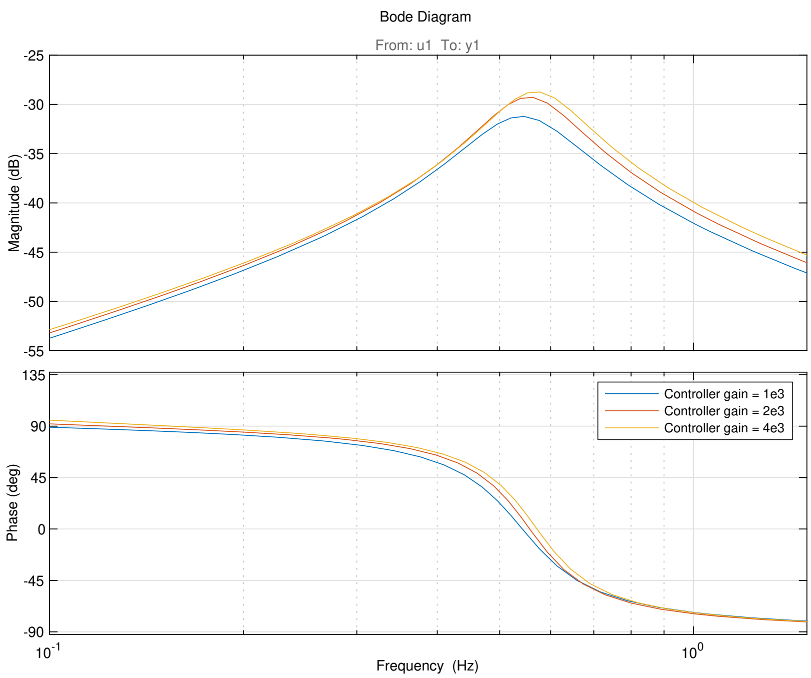

Figure 4-4. Transfer function models obtained from three wavelets of different amplitude (all with $f_0 = 0.286$ Hz, $s = 5$).

5. FOCUSED WAVES

These waves have multiple frequency components with phasings aligned so as to focus at the WEC location. These waves are considered to be a potentially useful tool for studying extreme response in WECs, especially in cases where limitations in the capabilities of the wave maker and/or time constraints prohibit executing longer irregular wave tests.

Large focused wave tests were run to support extreme response modeling. These tests have been carried out using different tuning for the controller: normal operation and large damping to prevent excessively large motion. These waves are summarized in Table 5-1.

Time series of the wave probe data from the wave calibration test, for which no WEC was present, are shown in the top row of plots in Figure 5-1. The results from three wave probes, all of which have the same position relative to wave propagation as the device, are shown. The layout of these wave probes is shown in Figure 1-3. It is clear to see from (shown in blue in Figure 5-1) that the steepness of these waves is often beyond the limit under which sonic wave probes are viable. However, the target wave is also shown in (shown in blue in Figure 5-1) and we can see that when the probe is able to measure, the agreement is fairly good.

Rows two through four of plots in Figure 5-1 show the surge, heave, and pitch responses, respectively, of the WEC in these waves. Two experiments with the WEC were run for each focused wave: one in which the optimal PI tuning for this sea state is used (shown in blue in Figure 5-1) and a second in which some suboptimal tuning is used (shown in red in Figure 5-1).

Similarly, Figure 5-2 shows the forces and moments applied by the WEC PTO during these focused waves. Similar forces are shown in heave and surge. The largest reactions are seen in the 5F wave.

Table 5-1. Focused wave cases

ID	Tp [s]	Hs [m]	γ	Cal. experiment	WEC experiments
3F	2.5	0.127	1	008	305, 312
5F	2.5	0.254	1	004	306, 313
7F	3.5	0.127	1	011	307, 311

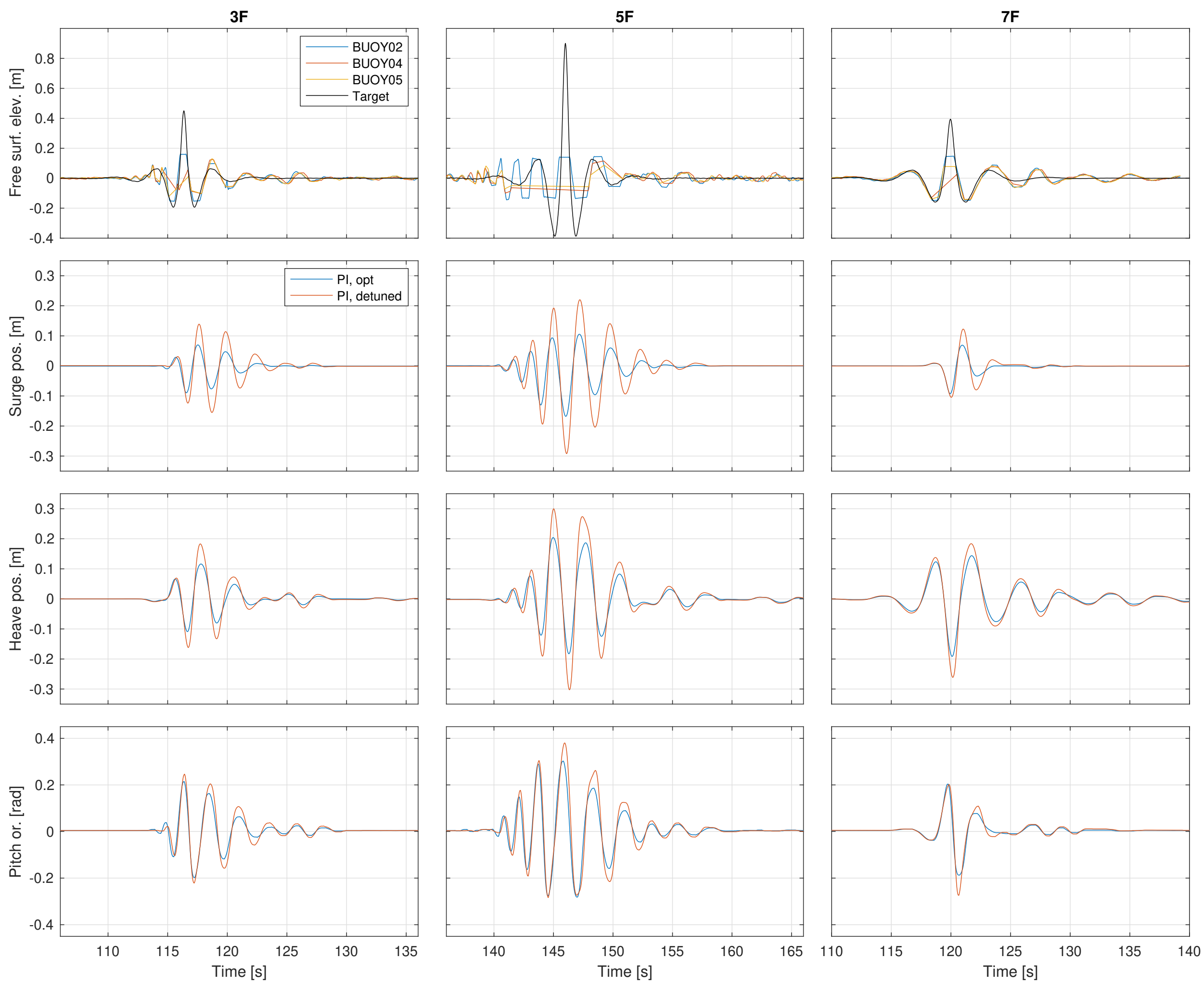

Figure 5-1. Focused wave measured calibration results and WEC responses.

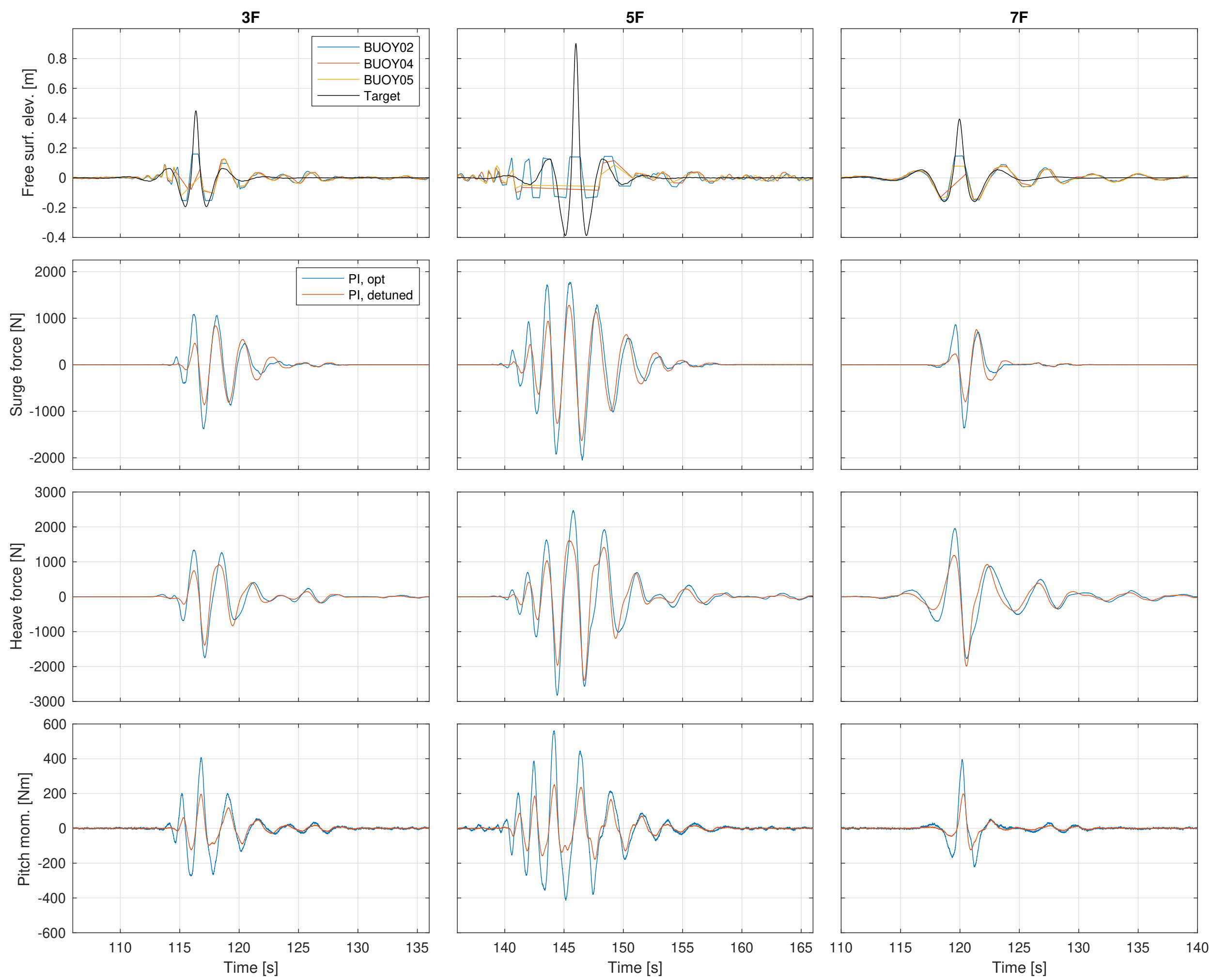

Figure 5-2. Focused wave measured calibration results and WEC PTO reactions.

APPENDICES

A. EXPERIMENTAL DETAILS

A. TESTING PROCEDURES

The following steps were used in conducting wave tank tests:

1. Confirm wave case
2. Sandia begins collection
3. Sandia signals ready for waves to begin
4. Sandia begins operation of WEC
5. Waves end
6. Sandia ends WEC operation and collection
7. Confirm file number (sequential from beginning)

Each day, Sandia will run a check-out case before beginning other testing.

B. WAVE DEFINITIONS

B.1. Regular waves

Regular wave cases were run at a number of frequencies and amplitudes. These cases provide a useful means of confirming the optimal tunings for a feedback controller.

B.2. Stationary JONSWAP

These spectra were realized with multiple phasings (up to three in some cases). The realizations used two different spectral discretizations, resulting in repeat periods of either 5 min or 60 min. The 5 min repeat period cases are considered useful for SID/model validation as well as control performance assessment. The 60 min repeat period cases are intended for use in cases where statistical measures will be needed (e.g., extreme response and fatigue).

B.3. Multi-directional seas

While not tested with the WaveBot, which is not designed for off-axis loading, multi-directional cases were run without the WEC installed. These tests are intended to support ongoing work on wave prediction/forecasting.

B.4. Pink

As discussed in [2], pink spectrum waves are useful for SID.

$$a \propto \frac{1}{f} \tag{A.1}$$

Two magnitudes of pink waves, which have been defined in previous tests, were used.

B.5. Chirp

To investigate the nonlinear effects, three chirp waves, with frequencies of

$$f(t) = f_0 + \beta t, \tag{A.2}$$

where β is the rate change of the frequency and f_0 is the starting frequency. Here, waves with $\beta = -2E - 4$ Hz/s and $f_0 = 0.667$ Hz. In more intuitive units, considering the rate change of the of the period of the wave every minute, $\beta = -0.0875$ s/min. These waves were run for 30 min. Thus the frequency changes linearly from the starting point of 0.667 Hz to 0.286 Hz. Chirp waves with amplitude of 0.127, 0.254, and 0.381 m (5, 10, and 15 in) were run.

B. TEST LOG

Table B-1. MASK3 experimental test log.

Test ID	Wave ID	Type	Tp [s]	Hs [m]	γ	Heave	Surge	Pitch
1	5A	JONSWAP	2.5	0.254	1	WEC absent	WEC absent	WEC absent
2	6A	JONSWAP	2.5	0.254	3.3	WEC absent	WEC absent	WEC absent
3	5F	Focused	2.5	0.254	1	WEC absent	WEC absent	WEC absent
4	5F	Focused	2.5	0.254	1	WEC absent	WEC absent	WEC absent
6	2A-10A	Changing	1.58->3.5	0.127->0.254	3.3	WEC absent	WEC absent	WEC absent
8	3F	Focused	2.5	0.127	1	WEC absent	WEC absent	WEC absent
10	7F	Focused	3.5	0.127	1	WEC absent	WEC absent	WEC absent
11	7F	Focused	3.5	0.127	1	WEC absent	WEC absent	WEC absent
12	2A	JONSWAP	1.58	0.127	3.3	WEC absent	WEC absent	WEC absent
13	2A-6A	Changing	1.58->2.5	0.127->0.254	3.3	WEC absent	WEC absent	WEC absent
14	7A	JONSWAP	3.5	0.127	1	WEC absent	WEC absent	WEC absent
15	11LA	JONSWAP	3.5	0.381	3.3	WEC absent	WEC absent	WEC absent
16	7LA	JONSWAP	3.5	0.127	1	WEC absent	WEC absent	WEC absent
18	CDIP225d03-20180508-2hr-12	CDIP	Te=2s	0.181		WEC absent	WEC absent	WEC absent
19	8A	JONSWAP	3.5	0.127	3.3	WEC absent	WEC absent	WEC absent
20	9A	JONSWAP	3.5	0.254	1	WEC absent	WEC absent	WEC absent
21	10A	JONSWAP	3.5	0.254	3.3	WEC absent	WEC absent	WEC absent
22	11A	JONSWAP	3.5	0.381	3.3	WEC absent	WEC absent	WEC absent
23	Small Chirp	chirp	1.5->3.5	0.127		WEC absent	WEC absent	WEC absent
24	Med. Chirp	chirp	1.5->3.5	0.254		WEC absent	WEC absent	WEC absent
25	Large Chirp	chirp	1.5->3.5	0.381		WEC absent	WEC absent	WEC absent
26	2R	Reg.	1.58	0.127		WEC absent	WEC absent	WEC absent
27	4R	Reg.	2.5	0.127		WEC absent	WEC absent	WEC absent
28	8R	Reg.	3.5	0.127		WEC absent	WEC absent	WEC absent
29	6R	Reg.	2.5	0.254		WEC absent	WEC absent	WEC absent
30	10R	Reg.	3.5	0.254		WEC absent	WEC absent	WEC absent
31	11R	Reg.	3.5	0.381		WEC absent	WEC absent	WEC absent
32	12A	JONSWAP	2.5	0.381	3.3	WEC absent	WEC absent	WEC absent
33	CDIP225d03-20180508-24hr-12	CDIP				WEC absent	WEC absent	WEC absent
34	2A+6A	Multidir. (20deg and 90 deg)	1.58, 2.5	0.127, 0.254	3.3	WEC absent	WEC absent	WEC absent
35	2A+10A	Multidir. (20deg and 90 deg)	1.58, 3.5	0.127, 0.254	3.3	WEC absent	WEC absent	WEC absent
36	Small Pink	Pink				WEC absent	WEC absent	WEC absent
37	Med Pink	Pink				WEC absent	WEC absent	WEC absent
38	10LA	JONSWAP	3.5	0.254	3.3	WEC absent	WEC absent	WEC absent
39	CDIP225d03-20180508-24hr-09	CDIP				WEC absent	WEC absent	WEC absent
40	6LA	JONSWAP	2.5	0.254	3.3	WEC absent	WEC absent	WEC absent
41	8LA	JONSWAP	3.5	0.127	3.3	WEC absent	WEC absent	WEC absent
42	9LA	JONSWAP	3.5	0.254	1	WEC absent	WEC absent	WEC absent
49	None					Ramps	Ramps	Ramps
50	None					Ramps	Ramps	Ramps
51	None					Waveform A Amp=2000	Waveform B Amp=2000	Waveform C Amp=250
52	None					Waveform A Amp=4000	Waveform B Amp=4000	Waveform C Amp=500
53	None					Waveform B Amp=2000	Waveform C Amp=2000	Waveform A Amp=250
54	None					Waveform C Amp=2000	Waveform A Amp=2000	Waveform B Amp=250
55	None					Waveform C Amp=2000	Waveform B Amp=2000	Waveform A Amp=250

Test ID	Wave ID	Type	Tp [s]	Hs [m]	γ	Heave	Surge	Pitch
56	None					Waveform A Amp=2000	Waveform C Amp=2000	Waveform B Amp=250
58	4R	Reg.	2.5	0.127		Kp=-2400 Ki=10000	Kp=-1500 Ki=1e4 CCKp=150 CCKi=2000	Kp=-200 Ki=4000
59	4R	Reg.	2.5	0.127		(various) Kp=-2400 Ki=10000	(Various)Kp=-1500 Ki=1e4 CCKp=150->0 CCKi=2000->0	(Various) Kp=-200 Ki=3600
62	None					Ramps	Ramps	Ramps
63	12R	Reg.	2	0.127		PI Matrix	PI Matrix	PI Matrix
64	12R	Reg.	2	0.127		PI Matrix	PI Matrix	PI Matrix
76	JONSWAP	7A	3.5	0.127	1	WaveFormA, Amp=1000	WaveFormB, Amp=1000	WaveFormC, Amp=100
82	None					Shakedown	Shakedown	Shakedown
83	None					Shakedown	Shakedown	Shakedown
88	6R	Reg.	2.5	0.254		PI Matrix	PI Matrix	PI Matrix
89	None					Shakedown	Shakedown	Shakedown
91	6R	Reg.	2.5	0.254		PI Matrix	PI Matrix	PI Matrix
92	None					Shakedown	Shakedown	Shakedown
93	6R	Reg.	2.5	0.254		PI Matrix	PI Matrix	PI Matrix
94	Med Pink	Pink	N/A	N/A	N/A	Waveform A Amp=2000	Waveform B Amp=2000	Waveform C Amp=200
96	Med Pink	Pink	N/A	N/A	N/A	Waveform C Amp=2000	Waveform A Amp=2000	Waveform B Amp=200
97	Med Pink	Pink	N/A	N/A	N/A	Waveform A Amp=2000	Waveform C Amp=2000	Waveform B Amp=200
105	None					Waveform B Amp=3000	Waveform C Amp=3000	Waveform A Amp=300
117	None					Shakedown	Shakedown	Locked out
118	Small chirp	chirp	1.5->3.5	0.127		PI = -3270,2425	Locked out	Locked out
119	Med chrip	chirp	1.5->3.5	0.254		PI = -3270,2425	Locked out	Locked out
120	Med chrip	chirp	1.5->3.5	0.254		PI	Locked out	Locked out
121	Med chrip	chirp	1.5->3.5	0.254		PI = -1900,2984	Locked out	Locked out
122	Med chrip	chirp	1.5->3.5	0.254		PI = -3084,3552	Locked out	Locked out
123	Med chrip	chirp	1.5->3.5	0.254		P = -3084	Locked out	Locked out
124	Med chrip	chirp	1.5->3.5	0.254		P = -3084	Locked out	Locked out
125	Med chrip	chirp	1.5->3.5	0.254		PI = -4545.3 3352.8	Locked out	Locked out
126	Med chrip	chirp	1.5->3.5	0.254		PI = -3354.8 2024.7	Locked out	Locked out
127	Med chrip	chirp	1.5->3.5	0.254		PI = -2395.9 4229	Locked out	Locked out
128	Med chrip	chirp	1.5->3.5	0.254		PI = -4040 2499.6	Locked out	Locked out
129	None					Shakedown	Locked out	Locked out
130	None					Sine waves	Locked out	Locked out
131	None					Sine waves	Locked out	Locked out
132	None					Shakedown	locked out	locked out
133	None					Shakedown	locked out	locked out
134	None					Shakedown w/ P = -3084	locked out	locked out
135	Med chrip	chirp	1.5->3.5	0.254		P = -3084	Locked out	Locked out
136	Small pink					P = -3084	Locked out	Locked out
137	Med pink					P = -3084	Locked out	Locked out
138	Med chrip	chirp	1.5->3.5	0.254		PI = -3084,3552	Locked out	Locked out
139	Small pink					PI = -3084,3552	Locked out	Locked out
140	Med pink					PI = -3084,3552	Locked out	Locked out
141	Small pink					PI = -3270,2425	Locked out	Locked out
142	Med pink					PI = -3270,2425	Locked out	Locked out
143	Small pink					PI = -4040 2499.6	Locked out	Locked out
144	Med pink					PI = -4040 2499.6	Locked out	Locked out
145	Small pink					PI = -1900,2984	Locked out	Locked out
146	Med pink					PI = -1900,2984	Locked out	Locked out
147	Small pink					PI = -2395.9 4229	Locked out	Locked out
148	Med pink					PI = -2395.9 4229	Locked out	Locked out
149	2R	Reg.	1.58	0.127		PI LHS matrix	Locked out	Locked out
150	11R	Reg.	3.5	0.381		PI LHS matrix	Locked out	Locked out
151	None					Wavelets 1000	Locked out	Locked out
152	None					Wavelets 2000	Locked out	Locked out
153	None					Wavelets 4000	Locked out	Locked out
155	None					Shakedown	Shakedown	Shakedown
156	4R	Reg.	2.5	0.127		PI LHS matrix	PI LHS matrix	PI LHS matrix
157	10A	JONSWAP	3.5	0.254	3.3	PI LHS matrix	PI LHS matrix	PI LHS matrix
158	10A	JONSWAP	3.5	0.254	3.3	PI LHS matrix	PI LHS matrix	PI LHS matrix
159	10A	JONSWAP	3.5	0.254	3.3	PI LHS matrix	PI LHS matrix	PI LHS matrix
160	6R	Reg.	2.5	0.254		PI LHS matrix	PI LHS matrix	PI LHS matrix
161	None					Shakedown	Shakedown	Shakedown
162	None					Shakedown	Shakedown	Shakedown
163	2A+6A	Bimodal				PI = -2450 2950	PI = -2100 3150, CCPI = -340 825	PI = -630 2400, CCPI = -340 825

Test ID	Wave ID	Type	Tp [s]	Hs [m]	γ	Heave	Surge	Pitch
164	2A+10A	Bimodal				PI = -3000 2550	PI = -2900 2700, CCPI = -250 40	PI = -900 2400, CCPI = -250 40
165	None					Sine	Locked out (power on)	Sine
166	11R	Reg.	3.5	0.381		PI = -3761 2231	Locked out	PI LHS matrix
167	None					Const.	Unlocked, but no command	Sine and Const.
168	2A-10A	Changing	1.58->3.5	0.127->0.254	3.3	PI = -2450 2950	PI = -2100 3150, CCPI = -340 825	PI = -630 2400, CCPI = -340 825
169	CDIP225d03-20180508-24hr-9	CDIP	Te = 2.4	0.24		PI = -2450 2950	PI = -2100 3150, CCPI = -340 825	PI = -630 2400, CCPI = -340 825
170	CDIP225d03-20180508-24hr-9	CDIP	Te = 2.4	0.22		PI = -2450 2950	PI = -2100 3150, CCPI = -340 825	PI = -630 2400, CCPI = -340 825
171	CDIP225d03-20180508-24hr-9	CDIP	Te = 2.2	0.277		PI = -3000 2550	PI = -2900 2700, CCPI = -250 40	PI = -900 2400, CCPI = -250 40
172	CDIP225d03-20180508-24hr-9	CDIP	Te = 3.8	0.392		PI = -3000 2550	PI = -2900 2700, CCPI = -250 40	PI = -900 2400, CCPI = -250 40
173	None					Shakedown	Shakedown	Shakedown
200	None					Shakedown	Shakedown	Shakedown
201	2R	Reg.	1.58	0.127		PI LHS	PI LHS	PI LHS
202	4R	Reg.	2.5	0.127		PI LHS	PI LHS	PI LHS
203	6R	Reg.	2.5	0.254		PI LHS	PI LHS	PI LHS
204	4R	Reg.	2.5	0.127		PI LHS	PI LHS	PI LHS
205	4R	Reg.	2.5	0.127		PI LHS	PI LHS	PI LHS
206	8R	Reg.	3.5	0.127		PI LHS	PI LHS	PI LHS
207	10R	Reg.	3.5	0.254		PI LHS	PI LHS	PI LHS
208	None					Shakedown	Shakedown	Shakedown
209	None					Shakedown	Shakedown	Shakedown
210	11R	Reg.	3.5	0.381		PI LHS	PI LHS	PI LHS
211	11R	Reg.	3.5	0.381		PI LHS	PI LHS	PI LHS
212	11R	Reg.	3.5	0.381		PI LHS	PI LHS	PI LHS
213	4R	Reg.	2.5	0.127		PI LHS	Locked out	PI LHS
214	6R	Reg.	2.5	0.254		PI LHS	Locked out	PI LHS
215	8R	Reg.	3.5	0.127		PI LHS	Locked out	PI LHS
216	10R	Reg.	3.5	0.254		PI LHS	Locked out	PI LHS
217	2A	JONSWAP	1.58	0.127	3.3	PI LHS matrix	PI LHS matrix	PI LHS matrix
218	2A	JONSWAP	1.58	0.127	3.3	PI LHS matrix	PI LHS matrix	PI LHS matrix
219	5A	JONSWAP	2.5	0.254	1	PI LHS matrix	PI LHS matrix	PI LHS matrix
220	5A	JONSWAP	2.5	0.254	1	PI LHS matrix	PI LHS matrix	PI LHS matrix
221	5A	JONSWAP	2.5	0.254	1	PI LHS matrix	PI LHS matrix	PI LHS matrix
222	5A	JONSWAP	2.5	0.254	1	PI LHS matrix	PI LHS matrix	PI LHS matrix
223	11R	Reg.	3.5	0.381		PI LHS	PI LHS	PI LHS
224	None					Shakedown	Shakedown	Shakedown
226	6A	JONSWAP	2.5	0.254	3.3	PI LHS matrix	PI LHS matrix	PI LHS matrix
227	6A	JONSWAP	2.5	0.254	3.3	PI LHS matrix	PI LHS matrix	PI LHS matrix
228	None					Shakedown	Shakedown	Shakedown
229	None					Shakedown	Shakedown	Shakedown
230	9A	JONSWAP	3.5	0.254	1	PI LHS matrix	PI LHS matrix	PI LHS matrix
231	9A	JONSWAP	3.5	0.254	1	PI LHS matrix	PI LHS matrix	PI LHS matrix
232	10A	JONSWAP	3.5	0.254	3.3	PI LHS matrix	PI LHS matrix	PI LHS matrix
233	2R	Reg	1.58	5		Autotune	Locked out	Locked out
234	4R	Reg	2.5	5		Autotune	Locked out	Locked out
235	8R	Reg	3.5	5		Autotune	Locked out	Locked out
236	6LA	JONSWAP	2.5	0.254	3.3	Autotune	Locked out	Locked out
237	2A-6A	Changing	1.58->2.5	0.127->0.254	3.3	Autotune	Locked out	Locked out
238	2A-6A	Changing	1.58->2.5	0.127->0.254	3.3	Autotune	Locked out	Locked out
239	2A-10A	Changing	1.58->3.5	0.127->0.254	3.3	Autotune	Locked out	Locked out
240	11LA	JONSWAP	3.5	0.381	3.3	Autotune	Locked out	Locked out
241	8R	Reg.	3.5	0.127		PI LHS matrix	PI LHS matrix	Locked out
242	None					Shakedown	0	Locked out
243	None					Shakedown	unlocked but not active	Locked out
244	6R	Reg.	2.5	0.254		PI LHS	Locked out	PI LHS
245	6R	Reg.	2.5	0.254		PI LHS	Locked out	PI LHS
246	CDIP225d03-20180508-24hr-12	CDIP				autotune	Locked out or stiff	Locked out or stiff
247	CDIP225d03-20180508-24hr-12	CDIP				autotune	Locked out or stiff	Locked out or stiff
248	2R	Reg	1.58	0.127		Autotune	Autotune	Autotune
249	4R	Reg	2.5	0.127		Autotune	Autotune	Autotune
250	8R	Reg	3.5	0.127		Autotune	Autotune	Autotune
251	2A-10A	Changing	1.58->3.5	0.127->0.254	3.3	Autotune	Autotune	Autotune
252	11LA	JONSWAP	3.5	0.381	3.3	Autotune	Autotune	Autotune
253	2A-6A	Changing	1.58->2.5	0.127->0.254	3.3	Autotune	Autotune	Autotune
254	None					Shakedown	Shakedown	Shakedown

Test ID	Wave ID	Type	Tp [s]	Hs [m]	γ	Heave	Surge	Pitch
256	None					Shakedown	Shakedown	Shakedown
257	None					Shakedown	Shakedown	Shakedown
258	CDIP225d03-20180508-24hr-12	CDIP				autotune	autotune	autotune
259	CDIP225d03-20180508-24hr-13	CDIP				autotune	autotune	autotune
260	CDIP225d03-20180508-24hr-12	CDIP				autotune	autotune	autotune
262	7LA	JONSWAP	3.5	0.127	1	Autotune	Autotune	Autotune
263	None					Shakedown	Shakedown	Shakedown
264	None					Shakedown	Shakedown	Shakedown
265	CDIP225d03-20180508-24hr-09	CDIP				autotune	autotune	autotune
266	CDIP225d03-20180508-24hr-12	CDIP				autotune	autotune	autotune
267	None					Shakedown	Shakedown	Shakedown
268	None					Shakedown	Shakedown	Shakedown
269	None					Shakedown	Shakedown	Shakedown
270	6LA	JONSWAP	2.5	0.254	3.3	Autotune	Autotune	Autotune
271	6LA	JONSWAP	2.5	0.254	3.3	Autotune	Autotune	Autotune
272	Umpqua	CDIP				autotune	autotune	autotune
273	12A	JONSWAP	2.5	0.381	3.3	PI LHS matrix	PI LHS matrix	PI LHS matrix
274	11A	JONSWAP	3.5	0.381	3.3	PI LHS matrix	PI LHS matrix	PI LHS matrix
275	8A	JONSWAP	3.5	0.127	3.3	PI LHS matrix	PI LHS matrix	PI LHS matrix
276	4A	JONSWAP	2.5	0.127	3.3	PI LHS matrix	PI LHS matrix	PI LHS matrix
277	None					Shakedown	Shakedown	Shakedown
278	None					Shakedown	Shakedown	Shakedown
279	None					0	Wavelets	Wavelets
280	None					0	Wavelets	Wavelets
281	None					0	Wavelets	Wavelets
282	None					0	Wavelets	Wavelets
283	None					0	Wavelets	Wavelets
284	None					0	Wavelets	Wavelets
285	None					0	Wavelets	Wavelets
286	None					0	Wavelets	Wavelets
287	6LA	JONSWAP	2.5	0.254	3.3	fixed gains	fixed gains	fixed gains
288	12A	JONSWAP	2.5	0.381	3.3	fixed gains	fixed gains	fixed gains
289	11A	JONSWAP	3.5	0.381	3.3	fixed gains	fixed gains	fixed gains
290	7A	JONSWAP	3.5	0.127	1	PI LHS matrix	PI LHS matrix	PI LHS matrix
291	4LA	JONSWAP	2.5	0.127	3.3	fixed gains	fixed gains	fixed gains
292	4A	JONSWAP	2.5	0.127	3.3	fixed gains	fixed gains	fixed gains
293	4LA	JONSWAP	2.5	0.127	3.3	Autotune	Autotune	Autotune
294	8LA	JONSWAP	3.5	0.127	3.3	Autotune	Autotune	Autotune
295	8LA	JONSWAP	3.5	0.127	3.3	fixed gains	fixed gains	fixed gains
296	8A	JONSWAP	3.5	0.127	3.3	fixed gains	fixed gains	fixed gains
297	None					Shakedown	Shakedown	Shakedown
298	2LA	JONSWAP	1.58	0.127	3.3	Autotune	Autotune	Autotune
299	9LA	JONSWAP	3.5	0.254	1	Autotune	Autotune	Autotune
300	9LA	JONSWAP	3.5	0.254	1	fixed gains	fixed gains	fixed gains
301	9A	JONSWAP	3.5	0.254	1	fixed gains	fixed gains	fixed gains
302	11LA	JONSWAP	3.5	0.381	3.3	fixed gain	fixed gain	fixed gain
303	7LA	JONSWAP	3.5	0.127	1	fixed gains	fixed gains	fixed gains
304	13A	JONSWAP	1.58	0.254	3.3	PI LHS matrix	PI LHS matrix	PI LHS matrix
305	3F	Focused	2.5	0.127		High Kp=-5e3	High Kp=-5e3	High Kp=-5e2
306	5F	Focused	2.5	0.254		High Kp=-5e3	High Kp=-5e3	High Kp=-5e2
307	7F	Focused	3.5	0.127		High Kp=-5e3	High Kp=-5e3	High Kp=-5e2
308	12A	JONSWAP	2.5	0.381	3.3	fixed gains	fixed gains	fixed gains
309	11A	JONSWAP	3.5	0.381	3.3	fixed gains	fixed gains	fixed gains
310	7F	Focused	3.5	0.127		PI optimal	PI optimal	PI optimal
311	7F	Focused	3.5	0.127		PI optimal	PI optimal	PI optimal
312	3F	Focused	2.5	0.127		PI optimal	PI optimal	PI optimal
313	5F	Focused	2.5	0.254		PI optimal	PI optimal	PI optimal
314	7A	JONSWAP	3.5	0.127	1	fixed gains	fixed gains	fixed gains
315	13R	Reg.	1.58	0.254		PI LHS matrix	PI LHS matrix	PI LHS matrix
316	2R-4R-8R-4R-2R	Changing				force based autotuner	locked out	locked out
320	None					0	wavelets	wavelets
321	None					0	wavelets	wavelets
322	None					0	wavelets	wavelets
324	None					Shakedown	Shakedown	Shakedown

Test ID	Wave ID	Type	Tp [s]	Hs [m]	γ	Heave	Surge	Pitch
326	12R	Reg.				WEC absent	WEC absent	WEC absent
327	13R	Reg.				WEC absent	WEC absent	WEC absent
328	4A	JONSWAP	2.5	0.127	3.3	WEC absent	WEC absent	WEC absent
329	7A	JONSWAP	3.5	0.127	1	WEC absent	WEC absent	WEC absent
330	13A	JONSWAP	1.58	0.254	3.3	WEC absent	WEC absent	WEC absent
331	2R-4R-8R-4R-2R	Changing				WEC absent	WEC absent	WEC absent
332	2LA	JONSWAP	1.58	0.127	3.3	WEC absent	WEC absent	WEC absent
333	4LA	JONSWAP	2.5	0.127	3.3	WEC absent	WEC absent	WEC absent
335	8LA	JONSWAP	3.5	0.127	3.3	WEC absent	WEC absent	WEC absent
336	CDIP139d04-20190410-12-TD	CDIP				WEC absent	WEC absent	WEC absent
337	2A+6A Uni	Bimodal				WEC absent	WEC absent	WEC absent

C. SAFETY

All test participants must adhere to the safety procedures outlined QMS procedure 5000-15 Health and Safety Policy. In general, when on the carriage or around the basin, all test participants must be aware that the basin and the presence of water create potentially dangerous conditions. All test participants working in or near the basin must wear United States Coast Guard approved Personal Floatation Devices (PFD) as supplied by Building 18 facilities personnel (Code 896 of the MASK, Water & Wind Tunnels Operations (Mechanical) Branch, 227-2885). This requirement also applies to any work on the shore or carriage or bridge that involves leaning over or being outside of guard rails in close proximity to the water. Further explanation of the PFD requirement is provided in the Code 1503 Memorandum dated 30 June 1989 posted at the MASK entrance.

The Test Director or designee shall be the only personnel to provide instructions to the carriage and wavemaker operator during the tests and will discuss the emergency stop procedures with the operators prior to commencing testing. Both carriage and wavemaker will sound an alarm prior to movement. The carriage also will flash a red light when moving and the wavemaker will transition its light stakes from green to red to flashing yellow depending on the machine's operational state. Green indicates the machine is safe to access, red indicates the paddles are armed and ready, and flashing yellow occurs when the machine is operating.

Red mushroom e-stops are located on each of the 27 electronic cabinets along the wavemaker's upper catwalk along with one downstairs and one upstairs in the wavemaker/model control room. These are intended for test team and facility operator usage to stop operations due to imminent danger to the wavemaker or model. Access to the wavemaker's upper catwalk while the wavemaker is operational is permissible provided all flooring panels are in place. Access to the shelf level of the wavemaker, the area behind the paddles, is strictly forbidden by all other than authorized personnel and then only while the wavemaker is not operational. Operational lockouts are provided at each access door to the shelf level to keep the wavemaker from starting when they are opened. Safe operating procedures require these doors to remain open while personnel are on the shelf level and are to be closed only by those exiting the shelf.

A red mushroom e-stop is located on the carriage at the east ceiling area of the center bay to provide user emergency stop access control of carriage operations. Safety restrictions require all carriage riders to stay within the confines of the carriage structure when moving. Entry and exit to and from the carriage is only to be attempted after the carriage warning light has stopped flashing and eye contact with the operator is made and he/she motions you to proceed.

When moving the carriage beyond the arresting gear hook the carriage driver and mechanical technician must override the system which adds pressure to the system. This is a safety concern and when in these locations no one must enter or exit the carriage through the bridge, all movements will need to be down via the water, on a punt. Prior to the start of the test, all personnel involved in the test will be briefed on what to do if the system fails when the carriage is past the arresting gear.

D. DEMO CODE

As a way to disseminate some of a methods developed for this test, a set of MATLAB and Simulink files have been release along with the data on `https://mhkdr.openei.org`. This demonstration code shows the process for designing both PI gains and feedback-tuned model predictive controller (MPC) for the WaveBot. These controllers are then demonstrated in a Simulink model. Requirements for this demonstration code are listed in Table D-1 along with the tested versions of each module.

Table D-1. Demonstration code requirements.

Code	Version tested	Website
MATLAB	R2018a	`https://www.mathworks.com/products/matlab.html`
Simulink	R2018a	`https://www.mathworks.com/products/simulink.html`
MATLAB MPC Toolbox	R2018a	`https://www.mathworks.com/products/mpc.html`
YALMIP	25-April-2019	`https://yalmip.github.io/`
SeDuMi	1.3	`http://sedumi.ie.lehigh.edu`
WAFO	2017	`http://www.maths.lth.se/matstat/wafo/`

A. CODE STRUCTURE

The work-flow for this example code is illustrated in Figure D-1. The inputs to the process, highlighted in yellow, are the intrinsic impedance, Z_i, the excitation transfer function, H, and the sea state spectrum. As illustrated in Figure D-1, the impedance and excitation transfer functions have been obtained from experimental data [2]. In the example code, the sea state spectrum is generated using WAFO.

The three inputs are passed to a function to find the optimal PI gains (K_p and K_i). Additionally, a set of motor properties are used to find the composite impedance so that the electrical power may be considered (see Section 2). While the gains can be determined explicitly for a single frequency wave, an optimization algorithm is used to find the solution for an arbitrary sea state. As described in (2.15), the optimal gains for a given system described by the composite impedance are dependent on the sea state and, more specifically, the excitation force created by that sea state.

Similarly for the MPC, we desire to create an MPC which can approximate the feedback controller, but do so while incorporating constraints, such as limits on stroke and PTO force; this concept is discussed in detail in [5, 6]. Thus, we must pass the desired feedback gains, along with the plant model, to the MPC tuning function. In order to reduce the order of the plant model, we also use the sea state spectrum and excitation transfer function to weight the frequency range of interest.

To run the code, simply run `fbCntrlDes_demo.m`. This will begin a process of prompting the user for the sea state and MPC parameters. The code will first perform the PI tuning and plotting and next the MPC tuning. Finally, both the PI and MPC controllers will be simulated in Simulink.

Figure D-2 shows a contour of the PI gain tuning results. From Figure D-2, we can see both the mechanical and electrical optimal tunings. The contour in Figure D-2 shows the normalized electrical power. It is clear to see that the optimal mechanical tunings result in *negative* electrical power.

Figure D-3 shows a normalized spectral plot of the controller efficiency. The normalized spectral energy from the waves is shown in black. The colored curves show the results for power absorption normalized by the optimal complex conjugate control power ($P_{CC}^{mech,max}$).

- The $P_{CC}^{mech}/P_{CC}^{mech,max}$ shows the normalized optimal capture.
- The $P_{PI}^{mech}/P_{CC}^{mech,max}$ shows the normalized PI controller capture for a perfect (lossless) PTO.
- The $P_{PI}^{elec}/P_{CC}^{mech,max}$ shows the normalized PI controller capture for a real (finite efficiency) PTO.
- The $P_{PI}^{elec}/P_{CC}^{mech,max}$ shows the normalized P controller ("resistive damping") capture for a real (finite efficiency) PTO.

Figure D-4 shows sample simulation results from Simulink. In this example, the MPC has a hard constraint of $F_{PTO} \leq 5 \times 10^3$ N and a soft constraint of $z \leq 0.5$ m. We can see that the MPC tracks the PI when the constraints are not being enforced.

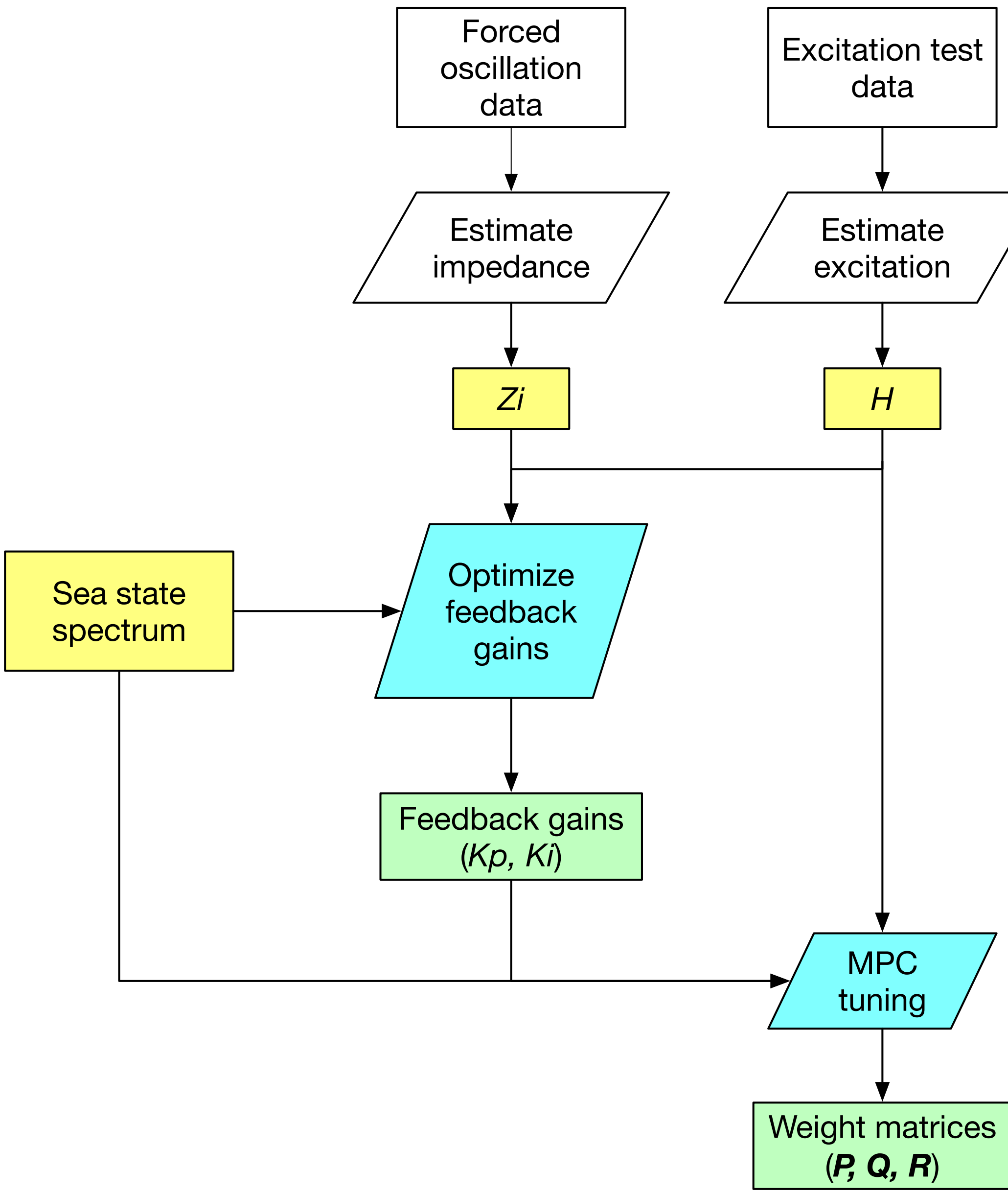

Figure D-1. Control design work-flow for demonstration code.

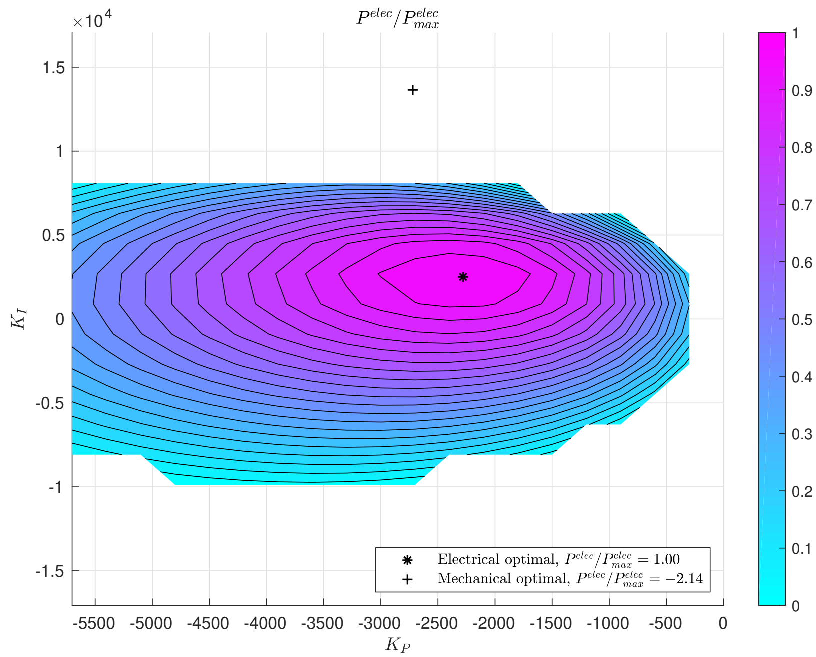

Figure D-2. Sample PI tuning results from demonstration code.

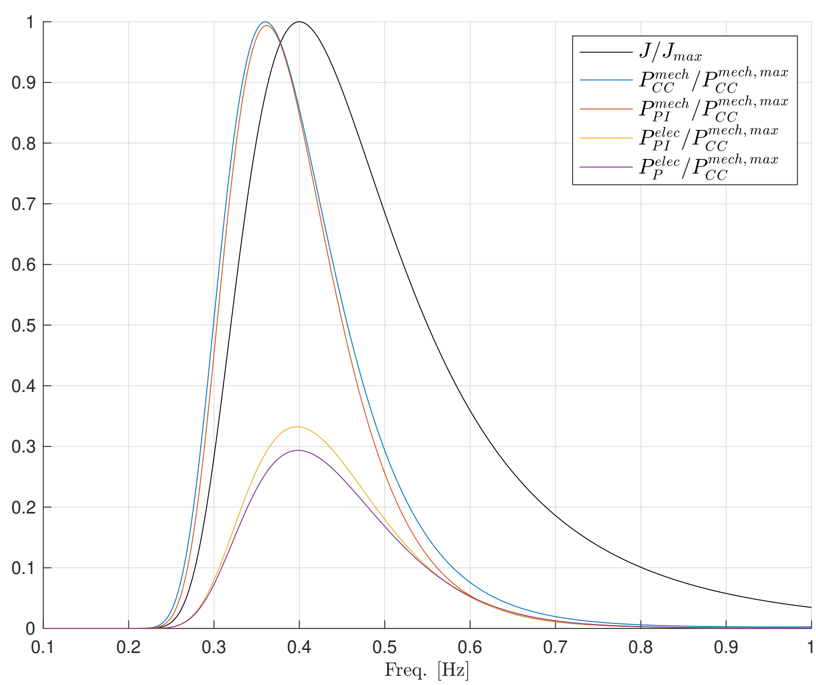

Figure D-3. Sample spectral efficiency results from demonstration code.

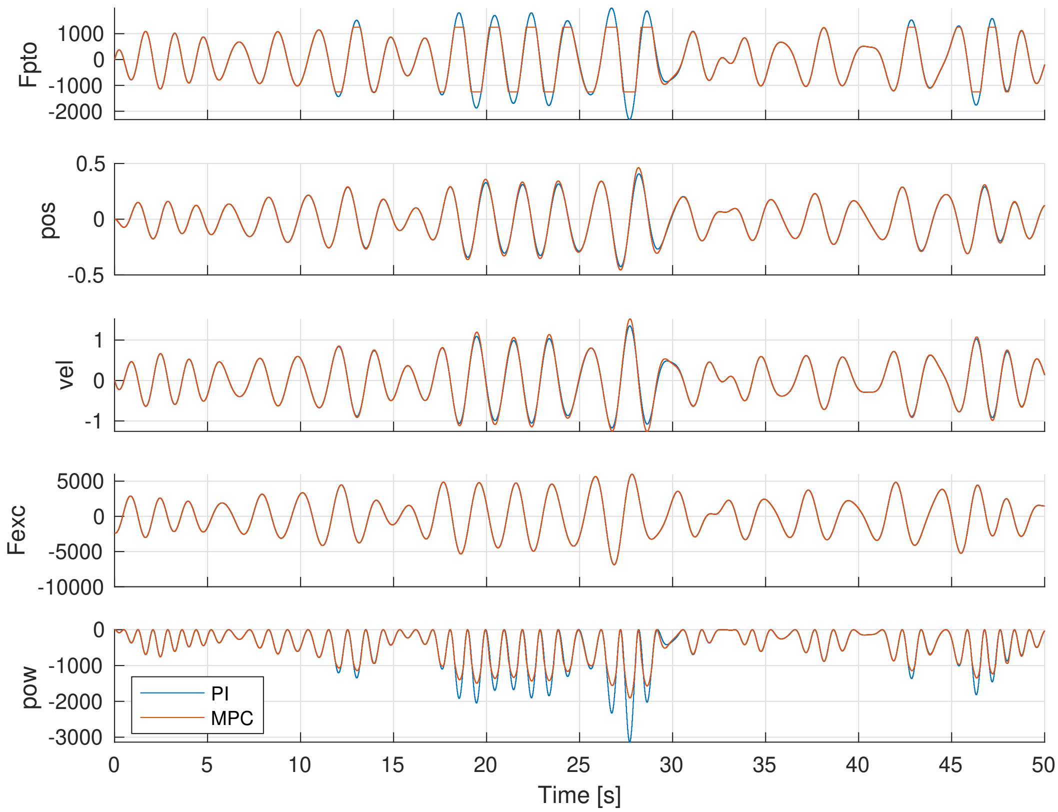

Figure D-4. Sample Simulink results from demonstration code.

B. CODE LISTINGS

Listings for the demonstration code are provided in the subsequent sections. Note that these `.m` files along with the Simulink file for simulating the controllers can be obtained from `https://mhkdr.openei.org`.

B.1. fbCntrlDes_demo.m

```
% Copyright 2019 NTESS
%
% Licensed under the Apache License, Version 2.0 (the "License");
% you may not use this file except in compliance with the License.
% You may obtain a copy of the License at
%
%     http://www.apache.org/licenses/LICENSE-2.0
%
% Unless required by applicable law or agreed to in writing, software
% distributed under the License is distributed on an "AS IS" BASIS,
% WITHOUT WARRANTIES OR CONDITIONS OF ANY KIND, either express or implied.
% See the License for the specific language governing permissions and
% limitations under the License.
%
%%%%%%%%%%%%%%%%%%%%%%%%%%%%%%%%%%%%%%%%%%%%%%%%%%%%%%%%%%%%%%%%%%%%%%%%%%%


clc
clear
close all

%% User input

IDs = 1:13;
Tps = [1.5800, 1.5800, 2.5000, 2.5000, 2.5000, 2.5000, 3.5000, 3.5000,...
    3.5000, 3.5000, 3.5000, 2.5000, 1.5800];
Hss = [0.127, 0.127, 0.127, 0.127, 0.254, 0.254, 0.127, 0.127, 0.254,...
    0.254, 0.381, 0.381, 0.254];
gammas = [1, 3.3, 1, 3.3, 1, 3.3, 1, 3.3, 1, 3.3, 3.3, 3.3, 3.3];

fprintf('Sea state')
fprintf('\n----------------------------------------------------------------------------------------------------')
fprintf('\nID:\t')
fprintf('%7i',IDs)
fprintf('\n----------------------------------------------------------------------------------------------------')
fprintf('\nHs [m]:\t')
fprintf('%7.3f',Hss)
fprintf('\nTp [s]:\t')
fprintf('%7.1f',Tps)
fprintf('\ngamma:\t')
fprintf('%7.1f',gammas)
fprintf('\n----------------------------------------------------------------------------------------------------')
fprintf('\n')
pID = input('Sea state ID: ');
ind = find(pID == IDs);
if isempty(ind)
    error('Sea state selection not found')
end
Hm0 = Hss(ind);
Tp = Tps(ind);
gamma = gammas(ind);

fprintf('\nMPC design parameters\n')
fprintf('---------------------\n')
predHor = input('Prediction horizon (default: 2) [s]: ');
Umax = input('PTO force limit (default: 1e10) [N]: ');
Zmax = input('Position limit (default: 1e10) [m]: ');
Rmax = input('PTO force slew rate limit (default: 1e10) [N/s]: ');
ITERmax = input('Max solver iterations (default: no limit): ');

%% Initial set up

% Load WEC model
mf = matfile('WaveBot_heaveModel.mat');
f = mf.f;               % frequency vector
H_frf = mf.H_frf;       % wave-body impedance FRF
Zi_frf = mf.Zi_frf;     % wave excitation FRF

% Create wave spectrum
Spect = jonswap(2*pi*f,[Hm0, Tp, gamma]);

%% PI tuning

[gains,pow] = fbCntrlDes(f,Zi_frf,H_frf,Spect,[],1);
```

```
Kp = gains(1);
Ki = gains(2);

%% MPC Design

if isempty(Umax)
    Umax = 1e10;
end
if isempty(Zmax)
    Zmax = 1e10;
end
if isempty(Rmax)
    Rmax = 1e10;
end
if isempty(predHor)
    predHor = 2;
end

[MPCobj,Plant,Sf] = mpcCntrlDes(f,Zi_frf,H_frf,...
    Spect,Kp,Ki,Umax,Zmax,Rmax,predHor,ITERmax);

%% Create Wave time series

% calculate excitation force time series
exc_mag = H_frf.*sqrt(Spect.S);

% add zero'd higher frequency components to this spectra to increase
% time-domain resolution, make symmetric about zero freq for ifft
f_2pow(:,1) = linspace(0,100*max(f),2^nextpow2(100*length(f)));
[~,ftozero] = min(abs(min(f)-f_2pow));
exc_mag = [zeros(ftozero,1); exc_mag; ...
    zeros(length(f_2pow)-length(exc_mag)-ftozero,1)];
rng(1);

% default randomizes phase of each freq component, but allows specification
phaseSeed = 2*pi*rand(length(f_2pow),1);

% complex-value representation
exc_comp = exc_mag .* exp(1i.* phaseSeed);

% conjugate symmetric exc_comp;
exc_comp = [flipud(exc_comp); 0 ;exc_comp];

% excitation time-series
exc_TS = ifft(ifftshift(exc_comp),'symmetric').*length(exc_mag);
dt = 1/(2*(max(f_2pow)));
t_vec = [dt:dt:(length(exc_TS)-1) * dt];

% create structure for simulink input
exc_TS_sim = struct();
exc_TS_sim.time = t_vec;
exc_TS_sim.signals.values = exc_TS(1:end-1);
exc_TS_sim.signals.dimensions = [1];

%% Simulate w/ Simulink

open('fbCntrlDes_model')
VSS_NONE = Simulink.Variant('VSS_MODE==0');
VSS_PI = Simulink.Variant('VSS_MODE==1');
VSS_MPC = Simulink.Variant('VSS_MODE==2');

x0=zeros(1,2);
r=zeros(1,4);

for ii = [1, 2]
    VSS_MODE = ii;
    simout{ii} = sim('fbCntrlDes_model',...
        'StopTime', num2str(50),...
        'ReturnWorkspaceOutputs','on');
end

%%

figure('name','Simulink results')
N = simout{1}.logsout.numElements;
ax = [];
for ii = 1:N
    ax(ii) = subplot(N,1,ii);
    hold on
    grid on
    for jj = 1:length(simout)
        plot(simout{jj}.logsout.getElement(ii).Values)
    end
    ylabel(simout{1}.logsout.getElement(ii).Name)
    title('')
    if ii ~=N
        set(ax(ii),'XTickLabel',[])
        xlabel('')
    end
end
xlabel('Time [s]')
linkaxes(ax,'x')
```

```
xlim([0, simout{1}.SimulationMetadata.ModelInfo.StopTime])
l1 = legend('PI','MPC');
set(l1,'location','southwest')
```

B.2. fbCntrlDes.m

```
function [gains, pow] = fbCntrlDes(f,Zi,H,S,motorSpecs,plotflag)
% [gains, pow] = fbCntrlDes(f,Zi,H,S,motorSpecs,plotflag)
%
% Finds optimal PI controller gains (designed for WaveBot).
%
% Inputs
%   f            frequency vector [Hz]
%   Zi           wave-body impedance FRF
%   H            excitation FRF
%   S            wave spectrum (same formatting as WAFO)
%   motorSpecs   structure with motor parameters (see below)
%   plotflag     1 to produce plots
%
% Outputs
%   gains        [Kp, Ki]
%   pow          power [w]
%
% Copyright 2019 NTESS
%
% Licensed under the Apache License, Version 2.0 (the "License");
% you may not use this file except in compliance with the License.
% You may obtain a copy of the License at
%
%     http://www.apache.org/licenses/LICENSE-2.0
%
% Unless required by applicable law or agreed to in writing, software
% distributed under the License is distributed on an "AS IS" BASIS,
% WITHOUT WARRANTIES OR CONDITIONS OF ANY KIND, either express or implied.
% See the License for the specific language governing permissions and
% limitations under the License.
%
%%%%%%%%%%%%%%%%%%%%%%%%%%%%%%%%%%%%%%%%%%%%%%%%%%%%%%%%%%%%%%%%%%%%%%%%%%%%%
%%

if nargin < 5
    plotflag = 0;
end

if nargin < 4 || isempty(motorSpecs)
    Kt = 6.1745;     % WaveBot motor torque constant
    R = 0.5;         % WaveBot motor electrical winding resistance
    N = 12.4666;     % WaveBot heave gear ratio
else
    Kt = motorSpecs.Kt;
    R = motorSpecs.R;
    N = motorSpecs.N;
end

w = 2*pi*f;
n = length(f);

%% Wave spectrum and excitation

Hm0 = spec2char(S,1);
Tp = spec2char(S,11);
Te = spec2char(S,5);

% amplitude spectrum
dw = S.w(2) - S.w(1);
ampSpect = sqrt(2*S.S*dw) .* exp(1i*rand(n,1));

% complex excitation spectrum
Fe = H .* ampSpect;

%% Controllers

% define PI feedback controller FRF
piControlFrf = @(Kp,Ki) Kp - 1i*Ki./w;

% define P feedback (resistive damping) controller FRF
pControlFrf = @(Kp,Ki) Kp;

%% Objective functions

% define objective functions (power will be negative)
powObj_pi_e = @(x) WaveBot_fbPow(Zi,Fe,piControlFrf(x(1),x(2)),Kt,R,N);
powObj_pi_m = @(x) WaveBot_fbPow(Zi,Fe,piControlFrf(x(1),x(2)),Kt,0,N);
powObj_p_e = @(x) WaveBot_fbPow(Zi,Fe,pControlFrf(x(1),x(2)),Kt,R,N);

%% Optimization solution

x0 = [0,0];
```

```
opts = optimoptions('fminunc');
opts.Display = 'off';
[x_pi_e,fval_pi_e] = fminunc(powObj_pi_e,x0,opts);
[x_pi_m,fval_pi_m] = fminunc(powObj_pi_m,x0,opts);
[x_p_e,fval_p_e] = fminunc(powObj_p_e,x0,opts);

%% frequency dependent power

% PI controller tuner for electrical power electrical power
[~,pow_pi_e_f,pow_ub_f] = WaveBot_fbPow(Zi,Fe,piControlFrf(x_pi_e(1),x_pi_e(2)),Kt,R,N);

% PI controller tuned for mechanical power mechanical power
[~,pow_pi_m_f,~] = WaveBot_fbPow(Zi,Fe,piControlFrf(x_pi_m(1),x_pi_m(2)),Kt,0,N);

% PI contorller tunded for mechanical power electrical power
[fval_pi_me,pow_me_f,~] = WaveBot_fbPow(Zi,Fe,piControlFrf(x_pi_m(1),x_pi_m(2)),Kt,R,N);

% P controller tuned for electrical power electrical
[~,pow_p_e_f,~] = WaveBot_fbPow(Zi,Fe,pControlFrf(x_p_e(1),x_p_e(2)),Kt,R,N);

gains = [x_pi_e(1), x_pi_e(2)];
pow = fval_pi_e;



% Electrical power if you use gains from mechanical optimum




fprintf('\n----------------------------------------------------\n')
fprintf('Sig. wave height [m]:\t\t%.2f\n',Hm0)
fprintf('Peak period [s]:\t\t%.2f\n',Tp)
fprintf('Energy frequency [Hz]:\t\t%.3f\n',1/Te)
fprintf('Optimal gains (Kp, Ki):\t\t(%.1e, %.1e)\n',x_pi_e(1),x_pi_e(2))
fprintf('----------------------------------------------------\n')
fprintf('Theoretical power limit [W]:\t%.2e\n',sum(pow_ub_f))
fprintf('Optimal avg. power, elec. [W]:\t%.2e\n',fval_pi_e)
fprintf('\tPercent capture:\t%.1f%%\n',sum(pow_pi_e_f)/sum(pow_ub_f)*100)
fprintf('Optimal avg. power, mech. [W]:\t%.2e\n',fval_pi_m)
fprintf('\tPercent capture:\t%.1f%%\n\n',sum(pow_pi_m_f)/sum(pow_ub_f)*100)



%% Plotting

if plotflag


    %-----------------------------------
    figure('name','Zi Bode')

    ax(1) = subplot(2,1,1);
    semilogx(f,mag2db(abs(Zi)))
    hold on
    grid on
    ylabel('$\left\| Z_i \right\|$ [dB]','interpreter','latex')

    ax(2) = subplot(2,1,2);
    semilogx(f,unwrap(angle(Zi)))
    hold on
    grid on
    ylabel('$\angle Z_i$ [rad]','interpreter','latex')

    %-----------------------------------
    figure('name','Zi real & imag.')

    ax(1) = subplot(2,1,1);
    semilogx(f,real(Zi))
    hold on
    grid on
    ylabel('Re$\left\{ Z_i \right\}$','interpreter','latex')

    ax(2) = subplot(2,1,2);
    semilogx(f,imag(Zi))
    hold on
    grid on
    ylabel('Im$\left\{ Z_i \right\}$','interpreter','latex')

    linkaxes(ax,'x')
    clear ax

    %-----------------------------------
    figure('name','H real & imag.')

    ax(1) = subplot(2,1,1);
    semilogx(f,real(H))
    hold on
    grid on
    ylabel('Re$\left\{ H \right\}$','interpreter','latex')

    ax(2) = subplot(2,1,2);
```

```
    semilogx(f,imag(H))
    hold on
    grid on
    ylabel('Im$\left\{ H \right\}$','interpreter','latex')

    linkaxes(ax,'x')
    clear ax

    %-------------------------------------
    figure('name','H Bode')

    ax(1) = subplot(2,1,1);
    semilogx(f,mag2db(abs(H)))
    hold on
    grid on
    ylabel('$\left\| H \right\|$ [dB]','interpreter','latex')

    ax(2) = subplot(2,1,2);
    semilogx(f,unwrap(angle(H)))
    hold on
    grid on
    ylabel('$\angle H$ [rad]','interpreter','latex')

    xlabel('Freq. [Hz]','interpreter','latex')

    linkaxes(ax,'x')

    %-------------------------------------
    figure('name','Wave spectrum')
    hold on
    grid on
    plot(f,S.S*2*pi)
    ylabel('Spect. density [m$^2$/Hz]','interpreter','latex')
    xlabel('Freq. [Hz]','interpreter','latex')



    %-------------------------------------
    Kps = linspace(x_pi_e(1)*2.5,0,20);
    Kis = linspace(-1.25*abs(x_pi_m(2)),1.25*abs(x_pi_m(2)),20);

    for ii = 1:length(Kps)
        for jj = 1:length(Kis)
            powm(ii,jj) = powObj_pi_e([Kps(ii),Kis(jj)]);
        end
    end

    [mgKp, mgKi] = meshgrid(Kps,Kis);

    pn = powm'./pow;
    minds = pn>0;
    mmask = nan(size(pn));
    mmask(minds) = 1;

    figure('name','Optimal power contour')
    title('$P^{elec}/P^{elec}_{max}$','interpreter','latex')
    hold on
    grid on
    ct = contourf(Kps,Kis,pn.*mmask,20);
    pl(1) = plot(x_pi_e(1),x_pi_e(2),'k*');
    pl(2) = plot(x_pi_m(1),x_pi_m(2),'k+');
    lg = legend(pl,...
        sprintf('Electrical optimal, $P^{elec}/P^{elec}_{max}=%.2f$',fval_pi_e/fval_pi_e),...
        sprintf('Mechanical optimal, $P^{elec}/P^{elec}_{max}=%.2f$',fval_pi_me/fval_pi_e));
    set(lg,'interpreter','latex')
    set(lg,'location','southeast')
    colormap('cool')
    cb = colorbar();
    caxis([0,1])
%     zlim([0,1])
    xlabel('$K_P$','interpreter','latex')
    ylabel('$K_I$','interpreter','latex')

    %-------------------------------------
    Sn = S.S/S.w;
    Sn = Sn/max(Sn);
%     pow_e_fn = pow_e_f ./ pow_ub_f;
%     pow_m_fn = pow_m_f ./ pow_ub_f;
    pow_e_fn = pow_pi_e_f / min(pow_ub_f);
    pow_m_fn = pow_pi_m_f / min(pow_ub_f);
    pow_p_e_fn = pow_p_e_f / min(pow_ub_f);
    pow_ub_fn = pow_ub_f / min(pow_ub_f);
    pow_e_fn(isnan(pow_e_fn)) = 0;
    pow_m_fn(isnan(pow_m_fn)) = 0;
    figure('name','Capture efficiency')
    hold on
    grid on
    plot(f, Sn,'k--')
    plot(f,pow_ub_fn)
    plot(f, pow_m_fn)
    plot(f, pow_e_fn)
    plot(f, pow_p_e_fn)
```

```
    l1 = legend('$J / J_{max}$',...
        '$P^{mech}_{CC}/P^{mech,\,max}_{CC}$',...
        '$P^{mech}_{PI}/P^{mech,\,max}_{CC}$',...
        '$P^{elec}_{PI}/P^{mech,\,max}_{CC}$',...
        '$P^{elec}_{P}/P^{mech,\,max}_{CC}$');
    set(l1,'interpreter','latex')
    set(l1,'fontsize',12)
    xlabel('Freq. [Hz]','interpreter','latex')

end
```

B.3. WaveBot_fbPow.m

```
function [P, P_f, Pub_f] = WaveBot_fbPow(Zi, Fe, C, Kt, R, N)
% [P, Omega] = WaveBot_fbPow(Zi, Fe, C, Kt, R, gear_ratio)
%
% Calculates average power for the WaveBot based on a feedback controller.
%
% Inputs
%
%   Zi      impedance FRF
%   Fe      excitation FRF
%   C       controller FRF
%   Kt      torque constant [Nm/A]
%   R       winding resistance [Ohms]
%   N       gear ratio
%
%--------------------------------------------------------------------------

% electrical constant for three-phase PMS motor
Ke = Kt*2/3;

Omega = Fe ./ (Zi - C);
P_f =  3/4*real(conj((Ke*N + C*R/(N*Kt)).*Omega) .* C/(N*Kt) .* Omega);

P = sum(P_f);

% upper-bound based on "complex conjugate control"
% (perfect impedance matching)
Pub_f = -1 * abs(Fe).^2 ./ (8 * real(Zi));
```

B.4. mpcCntrlDes.m

```
function [MPCobj,Plant,Sf] = mpcCntrlDes(f,Zi_frf,H_frf,Spect,Kp,Ki,Umax,Zmax,Rmax,predHoriz,maxIter)
% [MPCobj,Plant,Sf] = mpcCntrlDes(f,Zi_frf,H_frf,Spect,Kp,Ki,Umax,Zmax,Rmax,predHoriz,maxIter)
%
% Creates a feedback tuned MPC.
%
% Inputs:
%   f           frequency vector
%   Zi_frf      impedance freq. response function
%   H_frf       excitation freq. response function
%   Spect       spectrum (WAFO format)
%   Kp          proportional gain
%   Ki          integral gain
%   Umax        max PTO force [N]
%   Zmax        max stroke position [m]
%   Rmax        max PTO force slew rate [N/s]
%   predHoriz   prediction horizon [s]
%   maxIter     max MPC solver iterations
%
% Outputs:
%   MPCobj      Matlab MPC Toolbox object
%   Plant       2nd order plant used for MPC model
%   Sf          Scaling factor applied for optimization
%
% Copyright 2019 NTESS
%
% Licensed under the Apache License, Version 2.0 (the "License");
% you may not use this file except in compliance with the License.
% You may obtain a copy of the License at
%
%     http://www.apache.org/licenses/LICENSE-2.0
%
% Unless required by applicable law or agreed to in writing, software
% distributed under the License is distributed on an "AS IS" BASIS,
% WITHOUT WARRANTIES OR CONDITIONS OF ANY KIND, either express or implied.
% See the License for the specific language governing permissions and
% limitations under the License.
%
%%%%%%%%%%%%%%%%%%%%%%%%%%%%%%%%%%%%%%%%%%%%%%%%%%%%%%%%%%%%%%%%%%%%%%%%%%%
```

```
Ts = 0.02;
predHoriz = floor(predHoriz/Ts);

%%

exc = H_frf(:).*sqrt(Spect.S(:));

opt = tfestOptions('WeightingFilter', 1e-3+(exc/max(exc)) );
G_par = tfest(inv(frd(Zi_frf*1i*2*pi.*f, 2*pi*f)), 2,0, opt);

% figure('name','Reduced system Bode')
% bode(G_par, inv(frd(Zi_frf.*(1i*2*pi*f), 2*pi*f)))



[num2,den2] = tfdata(G_par,'v');
b0 = num2(3);
a1 = den2(2); a0 = den2(3);

sysA = [0 1;-a0 -a1];
sysB = [0;b0];
sysC = eye(2);
sysD = zeros(2,1);
SYS = ss(sysA,sysB,sysC,sysD);
Plant = c2d(SYS,Ts,'zoh');

%% Scaling

Sf = 20000; % Scaling factor
G = Plant*Sf;
Kp = Kp/Sf;
Ki = Ki/Sf;
Umax = Umax/Sf;
Rmax = Rmax/Sf*Ts;

%%

Kpi=[Ki Kp];
sigma=1e-5;

np=predHoriz;
nc=np;

[QMIN,RMIN,PMIN,~,~,~,~,~,~] = MPC_Cairano_YALMIP_PI_General(sigma,G.A,G.B,Kpi,np)

%%

NewPlant = G;
L = chol(PMIN);

set(NewPlant,'C',[G.C;L],'D',[G.D;zeros(2,1)], 'OutputName', '', 'OutputUnit', '' )
NewPlant.InputGroup.MV = 1;
NewPlant.OutputGroup.MO = [1 2];
NewPlant.OutputGroup.UO = [3 4];

% MPC_verbosity = mpcverbosity('off');
MPCobj = mpc(NewPlant,G.Ts,np,nc);

MPCobj.MV.Min = -Umax;
MPCobj.MV.Max = Umax;
MPCobj.MV.MinECR = 0;
MPCobj.MV.MaxECR = 0;
MPCobj.MV.RateMin = -Rmax;
MPCobj.MV.RateMax =  Rmax;

% MPCobj.MV.RateMinECR = 0.1;
% MPCobj.MV.RateMaxECR = 0.1;
MPCobj.OV(1).Min = -Zmax;
MPCobj.OV(1).Max = Zmax;
MPCobj.OV(1).MinECR = 2e-6;
MPCobj.OV(1).MaxECR = 2e-6;

ywt = sqrt(diag(QMIN))';
uwt = sqrt(diag(RMIN))';
MPCobj.Weights.OV = [ywt 0 0];
MPCobj.Weights.MV = uwt;
MPCobj.Weights.ManipulatedVariablesRate = 0.01;
MPCobj.Weights.ECR = 1e+4;
MPCobj.Model.Noise = ss(0*eye(2));

% see page 4-68 in toolbox manual (user's guide)
U = struct('Weight',uwt);
Y = struct('Weight',[0 0 1 1]);
setterminal(MPCobj,Y,U)

setoutdist(MPCobj,'model',ss(zeros(4,1)))
setEstimator(MPCobj,[],G.C);

mpcgain = dcgain(ss(MPCobj));
fprintf('\nMPC  : K = [%6.6g,%6.6g]',mpcgain(1),mpcgain(2));
fprintf('\nPI   : K = [%6.6g,%6.6g]',Ki,Kp);
fprintf('\nError: e = [%6.6g,%6.6g] (%%)\n', ...
```

```
    abs((mpcgain(1)-Ki)*100/Ki),abs((mpcgain(2)-Kp)*100/Kp));

if nargin > 7 && ~isempty(maxIter)
    MPCobj.Optimizer.UseSuboptimalSolution = true;
    MPCobj.Optimizer.MaxIter = maxIter;
end

end

function [QMIN,RMIN,PMIN,H,Fp,K_,S_,T_,Q_p] = MPC_Cairano_YALMIP_PI_General(sigma,A,B,K,np)

% This functions solves Lemma 3 in Di Cairano & Bemporad (IEEE 2010).
% To run this function, YALMIP must be installed in the computer.

nQ = size(A,1);
nR = size(B,2);
nK = size(K,2);

% Define decision variables
P = sdpvar(nQ,nQ);
Q = diag(sdpvar(nQ,1));
R = sdpvar(nR,nR);

Q_ = double2sdpvar(zeros(np*nQ,np*nQ));
K_ = zeros(np,nK);
T_ = zeros(np*nQ,nQ);
S_ = zeros(np*nQ,np);

K_(1,:) = K;
T_(1:2,1:2) = A;
S_(1:2,1) = B;
Q_(1:2,1:2) = Q;

for i = 2:np
    % K_(i,:) = K_(i-1,:)*1;
    K_(i,:) = K*(A+B*K)^(i-1);
%     if i == np
%         K_(i,:) = K*0;
%     end
    T_(2*i-1:2*i,:) = T_(2*i-3:2*i-2,:)*A;
    S_(2*i-1:2*i,1) = A*S_(2*i-3:2*i-2,1);
    for k = 2:np
        S_(2*k-1:2*k,1) = A*S_(2*k-3:2*k-2,1);
        S_(2*k-1:2*k,i) = A*S_(2*k-3:2*k-2,i);
    end
    S_(:,i) = circshift(S_(:,i-1),nQ);
    S_(1:(i-1)*nQ,i) = zeros((i-1)*nQ,1);
end

for j = 2:np
    if j < np
        Q_(1:2*j,1:2*j) = blkdiag(Q_(1:2*(j-1),1:2*(j-1)),Q);
    else
        Q_(1:2*j,1:2*j) = blkdiag(Q_(1:2*(j-1),1:2*(j-1)),P);
    end
end

% R_ = R*eye(np);
% H_ = R_+S_'*Q_*S_;
% F_ = S_'*Q_*T_;

% Define constraints
F = [P>=0,R-sigma>=0];

% Define objective function
N_ = S_'*Q_*(T_+S_*K_)+R*K_;
h = norm(N_,2);

% Solve the optimization problem
% ops = sdpsettings('solver', 'sedumi', 'sedumi.eps', 1e-8);
ops = sdpsettings('solver', 'sedumi');
optimize(F,h,ops);

% Display the solutions
QMIN = value(Q);
RMIN = value(R);
PMIN = value(P);

Q_p = zeros(np*nQ,np*nQ);
Q_p(1:2,1:2) = QMIN;

for j = 2:np
    if j < np
        Q_p(1:2*j,1:2*j) = blkdiag(Q_p(1:2*(j-1),1:2*(j-1)),QMIN);
    else
        Q_p(1:2*j,1:2*j) = blkdiag(Q_p(1:2*(j-1),1:2*(j-1)),PMIN);
    end
end

R_p = RMIN*eye(np);
H = R_p+S_'*Q_p*S_;
Fp = S_'*Q_p*T_;
```

```
end
```

B.5. fbCntrlDes_model.slx

Figure D-5 shows the Simulink model for simulating both the PI controller and MPC (through a variant subsystem).

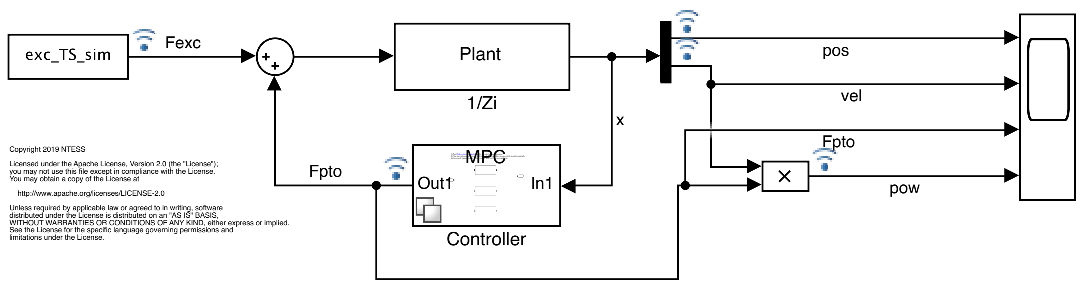

Figure D-5. Simulink model for demonstration code.

REFERENCES

[1] Giorgio Bacelli and Ryan G. Coe. WEC system identification and model validation. In *Marine Energy Technology Symposium (METS2017)*, Washington, D.C., 2017.

[2] Giorgio Bacelli, Ryan G. Coe, David Patterson, and David Wilson. System identification of a heaving point absorber: Design of experiment and device modeling. *Energies*, 10(10):472, 2017.

[3] Giorgio Bacelli, Steven J. Spencer, David C. Patterson, and Ryan G. Coe. Wave tank and bench-top control testing of a wave energy converter. *Applied Ocean Research*, 86:351 – 366, 2019.

[4] Hancheol Cho, Giorgio Bacelli, and Ryan G Coe. Linear and nonlinear system identification of a wave energy converter. In *Proceedings of the 6th Marine Energy Technology Symposium (METS)*, Washington, D.C., 2018.

[5] Hancheol Cho, Giorgio Bacelli, and Ryan G. Coe. Model predictive control tuning by inverse matching for a wave energy converter. *Energies*, 12(21):4158, Oct 2019.

[6] Ryan G. Coe, Giorgio Bacelli, Victor Nevarez, Hancheol Cho, and Felipe Wilches-Bernal. A comparative study on wave prediction for WECs. Technical Report SAND2018-10945, Sandia National Laboratories, 2018.

[7] Ryan G. Coe, Giorgio Bacelli, David Patterson, and David G. Wilson. Advanced WEC Dynamics & Controls FY16 testing report. Technical Report SAND2016-10094, Sandia National Labs, Albuquerque, NM, October 2016.

[8] Ryan G. Coe, Giorgio Bacelli, Steven J. Spencer, and Hancheol Cho. Initial results from wave tank test of closed-loop WEC control, 2018.

[9] Rik Pintelon and Johan Schoukens. *System identification: A frequency domain approach*. John Wiley & Sons, 2012.

DISTRIBUTION

Hardcopy—External

Number of Copies	Name(s)	Company Name and Company Mailing Address
1	Naval Surface Warfare Center, Carderock (NSWCCD)	

Hardcopy—Internal

Number of Copies	Name	Org.	Mailstop

Email—Internal (encrypt for OUO)

Name	Org.	Sandia Email Address
Technical Library	01177	libref@sandia.gov

Sandia National Laboratories

Sandia National Laboratories is a multimission laboratory managed and operated by National Technology & Engineering Solutions of Sandia LLC, a wholly owned subsidiary of Honeywell International Inc., for the U.S. Department of Energy's National Nuclear Security Administration under contract DE-NA0003525.